UNIVERSITY OF CALIFORNIA

Los Angeles

Transcranial ultrasound stimulation: promises and challenges

A dissertation submitted in partial satisfaction of the requirements for the degree

Doctor of Philosophy

in Neuroscience

by

Ian Szwast Heimbuch

2021

ABSTRACT OF THE DISSERTATION

Transcranial ultrasound stimulation: promises and challenges

by

Ian Szwast Heimbuch

Doctor of Philosophy in Neuroscience

University of California, Los Angeles, 2021

Professor Andrew Charles, Co-Chair

Professor Marco Iacoboni, Co-Chair

Transcranial focused ultrasound stimulation (tUS) is an emerging technique for non-invasive brain stimulation (NIBS). tUS offers the option of higher spatial resolution and modulation of deeper neural structures, compared to other NIBS techniques. However, the neuromodulatory effects of tUS are still poorly understood, and the few experiments published thus far have shown variable outcomes between regions and studies.

To better understand the strengths, weakness, and feasibility prospects of tUS for use in humans, I compared tUS to an established NIBS technique, transcranial magnetic stimulation (TMS), in a cortical region with previously unclear tUS results but established TMS results: primary motor cortex (M1). I found no change in ongoing muscle activity concurrent with tUS stimulation. I also found no significant change in M1 cortical excitability due to tUS exposure.

To explore causes of variability in tUS, I performed acoustic simulations that replicated conditions of the M1 experiments. Specifically, I used participant-specific magnetic resonances images (MRI) to find where in the brain tUS pressure fields landed and how strong those pressure fields were. With this simulation data, I explored the spatial precision and volume of tUS, the accuracy of tUS device

placement in my own data, and whether there was a correlation between tUS exposure and M1 excitability. I found that tUS produced a narrow ellipsoid intracranial pressure field with a full width at half maximum roughly 4 mm wide. While the simulations showed that tUS exposure levels varied, I found no clear correlation between tUS exposure and M1 excitability from these data.

Lastly, acoustic simulations provide significant insight for any tUS experiment, since it provides investigators estimates of the location and intensity of the intracranial ultrasonic field. However, implementing such simulations is challenging and time-consuming, which may explain why many published tUS studies do not perform acoustic simulations. To make acoustic simulation more accessible for tUS investigators, I built an open-source MATLAB toolbox that integrates medical imaging and neuronavigation with acoustic simulation. An increased adoption of acoustic simulation in tUS experiments should accelerate collective progress within the field.

The dissertation of Ian Szwast Heimbuch is approved.

Nanthia Suthana

Nader Pouratian

Martin M. Monti

Marco Iacoboni, Committee Co-Chair

Andrew C. Charles, Committee Co-Chair

University of California, Los Angeles

2021

TABLE OF CONTENTS

TABLE OF FIGURES

ACKNOWLEDGEMENTS

I would like to give thanks to all members of my committee:

Dr. Andrew Charles for taking me into his lab despite my lack of experience in human research.
Dr. Marco Iacoboni for his significant mentorship. Dr. Iacoboni always finds times for his lab members, and I sincerely appreciate it. He is an empathetic and enthusiastic person, and it was nice to be a part of his lab.
Dr. Martin Monti for always providing helpful and valuable insight. Ultrasound stimulation is such a small field, so I was lucky to have such an engaging ultrasound collaborator on campus in Dr. Monti.
Dr. Nader Pouratian for bringing me into his fMRI DBS project, which had a strong influence on my career goals. He always made me feel listened to in meetings, which was very impactful as a young graduate student. I am also appreciative for him wholeheartedly agreeing to stay on my committee as a remote contributor.
Dr. Nanthia Suthana for kindly allowing me to work with her lab on the development on my EEG project. I always felt welcomed. She is also an inspiring investigator. Through her research and organization of the Center for NeuroTechnology, she has heavily impacted my career goals.

I would also like to express my sincere gratitude to **Dr. Alapakkam Sampath** for providing so much help in finding a new lab early in my graduate career. I genuinely may have not been able to continue with graduate school had it not been for him facilitating that transition. He is one of the most genuinely good people I have ever had the chance to know in academia.

I would also like to acknowledge the contributions of Dr. Guido Faas, who started the ultrasound research journey for the Andrew Charles lab. He joined me in brainstorming solutions for many of the technical problems that came about developing this project. I would also like to thank Dr. Allan Wu, who had an especially strong influence on the cSP component of my work.

I also want to thank my various friends and colleagues in the Brain Mapping Center who provided me so much help over the years. Among them, I want to note:

Yeun Kim, whose immense computational insight over the years was a huge technical and emotional boon throughout my time in the Brain Mapping Center.
Dr. Mayank Jog for his enthusiastic and generous insight about various topics, from MRI to physics simulations to manuscripts. His feedback on an early form of my manuscript that became Part 3 of this dissertation was immensely helpful and is very much appreciated.
Shakthi Visagan, who was always happy to share his incredible talents with me, including during the many times we compared notes on acoustic simulations. Certain insights of his were transformative in terms of progress on my acoustic simulation work, which at times was an otherwise frustrating endeavor, and for that I am forever grateful.
Antoni Kubicki, whose impressive knowledge regarding MRI, etc. meant he was helping me almost as soon as he joined the Brain Mapping Center. I was very lucky to have him as an office neighbor.

This project was also only possible through the collaboration and help of many additional people. For all their support and friendship, I sincerely appreciate it:

Sonja Hiller
Vaughan Greer
Nguyen Do
Darin Williams
Mary Susselman
Dr. Tiffany Fan
Alessandra Dallavecchia
Dr. Mahsa Malekmohammadi
Jessica Martinez
Dr. Dan Ennis

I also want to thank my partner, **Yi-Ching Chiu**, for being so supportive—especially during the stressful months of the final dissertation push. She is an immensely intelligent and empathetic person whose involvement in my life begets insight, diversity, and fulfilment. I am continuously struck how lucky I am to have her as a partner and friend.

I also want to thank my parents, **Scott Heimbuch** and **Susan Szwast Heimbuch**, for cultivating my sense of curiosity from a young age. I consider myself an open-minded and empathetic person, and I believe that is the case thanks to them. They are two incredible people, both independently and together, and I am very appreciative to have them as parents.

VITA

EDUCATION

• *University of California, Los Angeles*	*Los Angeles, CA*	*2014-2021*
• *Boston University*	*Boston, MA*	*2010-2014*

RESEARCH

• *Andrew Charles Laboratory* *Marco Iacoboni Laboratory*	*UCLA*	*Summer 2016-Present*
• *Alapakkam Sampath Laboratory*	*UCLA*	*Fall 2015 – Winter 2016*
• *Howard Eichenbaum Laboratory* Research Assistant	*Boston University*	*2013-2014*
• *Michael Kilgard Laboratory* Research Assistant	*University of Texas at Dallas*	*Summer 2012*

RESEARCH PAPERS

- **Heimbuch, I.S.**, Fan, T.K., Wu, A., Faas, G.C., Charles, A.C., Iacoboni, M., Ultrasound Stimulation of the Motor Cortex during Tonic Muscle Contraction. *bioRxiv*; doi:10.1101/2021.05.03.442483 [Preprint]
- **Heimbuch, I.S.**, Faas, G.C., Iacoboni, M., Charles, A.C., TUSX: an accessible toolbox for transcranial ultrasound simulation. *bioRxiv*: https://doi.org/10.1101/2021.06.03.446963 [Preprint]
- Rangel, L.M., Rueckemann, J.W., Rivière, P.D., Keefe, K.R., Porter, B.S., **Heimbuch, I.S.**, Budlong, C. H., Eichenbaum, H., Hippocampal Rhythmic Coordination During Associative Memory Processing, *eLife*, 2016 Jan 11; doi:10.7554/eLife.09849

CONFERENCE ABSTRACTS

- **Heimbuch, I.S.**, Iacoboni, M., Charles, A.C., TUSX: an accessible toolbox for transcranial ultrasound simulation, *Organization for Human Brain Mapping Annual Meeting 2021* [Accepted]
- **Heimbuch, I.S.**, Faas, G.C., Fan, T., Iacoboni, M., Charles, A.C., Acoustic Simulation to Understand Variability in Transcranial Ultrasound of Motor Cortex, *Organization for Human Brain Mapping Annual Meeting 2020*
- Rangel, L.M., Rosen, J.S., Chawla, K.V., Ferreri, B.J., Porter, B.S., **Heimbuch, I.S.**, Eichenbaum, H., Persistent Increases in Beta Frequency Oscillatory Activity in the Dentate Gyrus of the Hippocampus During Object-Context Association Intervals, *Society for Neuroscience Conference 2014*

AWARDS AND FELLOWSHIPS

- Gordon Hein Scholarship
- Will Rogers Scholarship

1 INTRODUCTION

Ultrasonic waves are acoustic waves above the frequency range of human hearing (>20 kHz). Ultrasonic waves mechanically propagate through a medium, with alternating periods of compression and rarefaction (stretching) as the pressure wave passes. Ultrasound (US) can be produced with a transducer, which consists of a piezoelectric material that resonates within a narrowly tuned frequency range (Figure 1-1). Along with being constrained to a narrow frequency, transducers are constructed to produce a set focal pattern, converging their waves to a focal point or as a unified column.

Ultrasound in the 1 to 15 kHz range has long been used in medicine as a diagnostic imaging tool in soft tissues (*The Safe Use of Ultrasound in Medical Diagnosis*, 2012). In the last few decades, there has also been substantial research in the use of high-intensity ultrasound for targeted brain lesions (~650 kHz). However, only recently has ultrasound received extensive attention for its neuromodulation capabilities.

1.1 EXISTING LITERATURE

1.1.1 Historical Findings

As far back as the late 1920s, it was known that ultrasound could have an effect on neural and muscle tissue, as investigated on amphibian muscle tissue (Harvey, 1929). Central nervous system modulation began with 1950s experiments that demonstrated focused US stimulation of the LGN could suppress light-evoked potentials in the visual cortex of cats (Fry, Ades, & Fry, 1958). As for ultrasound stimulation in humans, in the 1970s ultrasound was shown to be capable of generating somatosensations (touch sensations) from exposure of human peripheral nerves (Gavrilov et al., 1976; Gavrilov & Tsirulnikov, 2012).

1.1.2 Early Renaissance

An increasing wave of interest in ultrasound as a non-invasive brain stimulation tool began in the 2000s. With this wave and the discoveries that came before, a few underlying capabilities of basic neural US effects have been established. At a local circuit level, US is able to both excite (Bachtold, Rinaldi, Jones, Reines, & Price, 1998) and suppress neural activity *in vitro* (Bachtold et al., 1998; Rinaldi, Jones, Reines, & Price, 1991). At a systems level, US is able to both excite (Lee, Kim, et al., 2016; Yang et al., 2018) and suppress local activity *in vivo* (Fry et al., 1958; Legon et al., 2014; Yoo et al., 2011). It has also been shown that US can generate action potentials both *in vitro* (Tyler et al., 2008) and *in vivo* (Lee, Kim, et al., 2016).

Human transcranial ultrasound stimulation (tUS)[*] studies began around 2014, with multiple investigations that demonstrated ultrasound can modulate human cortical activity. The first of these studies to use a purpose-built transducer (rather than a diagnostic imaging device) showed that time-locked tUS stimulation of somatosensory cortex can modulate sensory perception, improving subject performance in two-point and frequency discrimination tasks (Legon et al., 2014). In this study and others, tUS was also shown to affect EEG signals, altering somatosensory evoked potentials and oscillatory frequency dynamics (Lee et al., 2015; Legon et al., 2014; J. Mueller, Legon, Opitz, Sato, & Tyler, 2014). tUS is also capable of generating sensory phenomena, with the generation of somatosensations and phosphenes from stimulating somatosensory and visual cortex, respectively (Lee et al., 2015; Lee, Kim, et al., 2016). tUS-generated phosphenes were also associated with BOLD contrast responses that mirrored responses to real visual stimuli (Lee, Kim, et al., 2016). However, there are only

[*] As a novel field, the acronyms and terminology for the use of ultrasound as a non-invasive brain stimulation (or neuromodulation) technique have not been unified. Acronym variations include: tFUS (transcranial focused ultrasound), fUS (focused ultrasound), FUS (focused ultrasound), TUS (transcranial ultrasound stimulation), LIFU (low-intensity transcranial focused ultrasound), and LIFUP (low-intensity focused ultrasound pulsation). For this dissertation, I chose to go with a middle ground: tUS (transcranial ultrasound stimulation).

slightly over a dozen peer-reviewed tUS papers in humans thus far (T. Kim et al., 2021; Wang, Zhang, Yu, Smith, & Feng, 2019). A detailed list of every human and animal study between 2008 and mid-2020 is available in a review compiled by Wang and colleagues and its follow-up article (T. Kim et al., 2021; Wang et al., 2019).

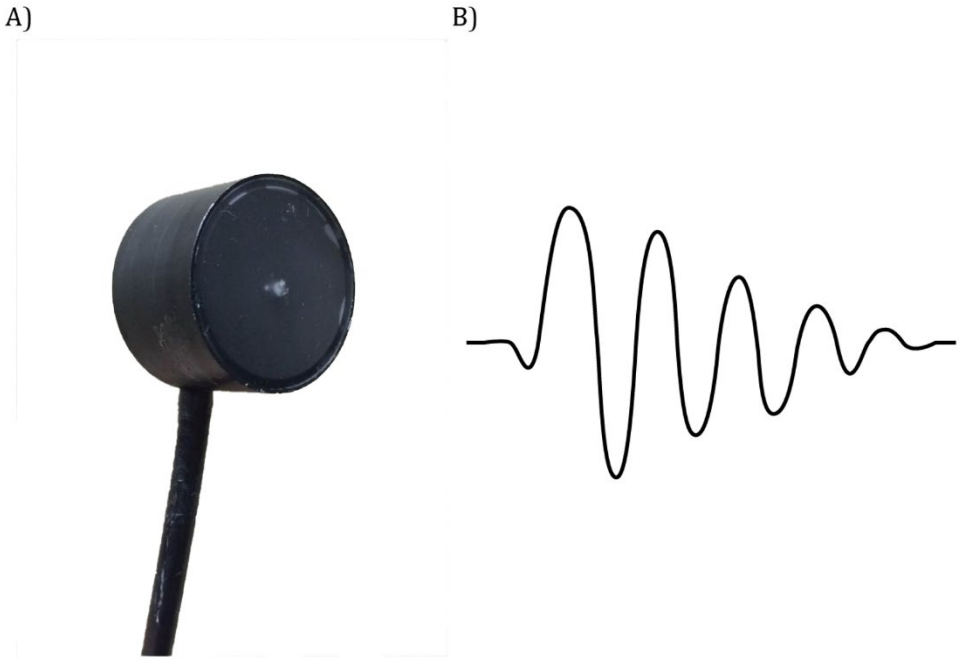

Figure 1-1. Transducer and waveform. A) An example of a focused ultrasound transducer, capable of tUS. B) An illustration of the ultrasound amplitudes emitted when a short voltage pulse is delivered to an ultrasound transducer. Voltage pulses are repeated to produce longer-lasting bursts.

1.2 Mechanism

The precise physiological roots of US neural effects (<~5 W/cm^2) are still being investigated. Currently, the consensus is that US waves can mechanically increase membrane conductance in neurons, glia, and non-neural cells (Chapman, MacNally, & Tucker, 1980; Mortimer & Dyson, 1988; Tyler et al., 2008), likely through mechanically sensitive ion channels.

1.2.1 Mechanosensitive Ion Channels

Certain families of ion channels undergo protein conformation changes due to changes in the surrounding environment, i.e. physiologically relevant mechanical forces or the voltage potential across

the membrane, that alter the channel's ion conductance. It is reasonable to assume that the artificially induced mechanical forces of ultrasonic waves could cause these conformational changes as well, thereby modulating channel conductance. This is the most supported theory underlying neural modulation by ultrasound (Heureaux, Chen, Murray, Deng, & Liu, 2014; Kubanek, 2018; Kubanek et al., 2016; Tufail, Yoshihiro, Pati, Li, & Tyler, 2011; Tyler, 2011, 2012; Tyler et al., 2008; Wahab et al., 2012).

Channels explicitly involved in mechanosensation are understandably robustly affected by ultrasonic waves (Gavrilov & Tsirulnikov, 2012; Ibsen, Tong, Schutt, Esener, & Chalasani, 2015; Kubanek et al., 2016; Kubanek, Shukla, Das, Baccus, & Goodman, 2018; Prieto, Firouzi, Khuri-Yakub, & Maduke, 2018).

While most of the research on these mechanosensitive channels have been in the peripheral nervous system, there is evidence some families of mechanosensitive channels are present in the brain—with examples in both neurons (Hervieu et al., 2001; Kubanek et al., 2016; Maingret, Patel, Lesage, Lazdunski, & Honoré, 1999; Sukharev & Corey, 2004; Tyler, 2012) and glia (Bowman, Ding, Sachs, & Sokabe, 1992; Ostrow & Sachs, 2005; Ostrow, Suchyna, & Sachs, 2011). However, it is unlikely the extent of their CNS presence is ubiquitous enough to explain all US neural effects. That leaves voltage-gated channels (VGCs) as the putative key player in the neural effects of US. *In vitro* studies have shown there is indeed evidence that some VGCs are modulated by ultrasound (Kubanek et al., 2016; Morris, 2011; Tyler et al., 2008). Among the VGCs with US effects confirmed *in vitro* are Ca^{2+} channels (Tyler et al., 2008), Na^{+} channels (Kubanek et al., 2016; Tyler et al., 2008), and K^{+} channels (Kubanek et al., 2016). However, a thorough catalogue of US-sensitive VGCs and variants has not been established—an endeavor complicated by the challenge of performing whole-cell electrophysiology during US and by the fact that US-sensitivity likely varies by acoustic frequency (Ye, Brown, & Pauly, 2017).

For further discussion of mechanisms underlying US neural effects, see reviews by Naor and colleagues and Tyler and colleagues (Naor, Krupa, & Shoham, 2016; Tyler, Lani, & Hwang, 2018).

1.2.2 Refuted Mechanism Theories

Mechanisms other than the opening of mechanically sensitive ion channels have been investigated and, largely, ruled out. For example, US does not appear to cause aberrant fusion of synaptic vesicles or other disruptive synaptic effects such as synaptic damage. This consideration came out of evidence that high-intensity US (>~100 W/cm^2) can generate such effects, including vesicle depletion and loss in synaptic density (Borrelli, Bailey, & Dunn, 1981). However, quantitative electron microscopy following low-intensity US has shown excitatory synapses, postsynaptic densities, and vesicle pools remain intact (Tufail et al., 2010). Also, cleaving of SNARE protein complexes with botulinum toxin ceases US-evoked neurotransmitter release *in vitro*, which would not be the case if US waves were mechanically forcing vesicles to merge (Tyler et al., 2008).

1.3 Accuracy and Precision

1.3.1 Precision

A major draw of ultrasound over other neuromodulation techniques, such as transcranial magnetic stimulation (TMS) and transcranial direct current stimulation (tDCS), is its superior spatial precision and tissue penetration. The theoretical limit of focal specificity of ultrasound is its acoustic wavelength. Assuming one had an ideal spherical array of transducers, the constructive interference would create a spherical hotspot at the center of the sphere. This concept is leveraged in the neurosurgical technique of high-intensity focused ultrasound (HIFU), in which an array of US transducers is used to make precise MR-guided ablations of small areas such as thalamic nuclei (Ernst Martin, Jeanmonod, Morel, Zadicario, & Werner, 2009; P. J. J. White, 2006). In the case of tUS, which so far has been approached with only a single ultrasound transducer fabricated to focus to a focal point, the transducer creates an ellipsoid hotspot—the width of which is contingent on the acoustic frequency. Specifically, tUS focal diameters range from 4 to 7 mm for devices used in humans and non-human primates and ~3 mm in mice

(Deffieux et al., 2013; Lee et al., 2015; Legon et al., 2014; Tufail et al., 2010). This far surpasses the wider ~12 mm diameter focal zones of figure-8 TMS coils (Wagner, Valero-Cabre, & Pascual-Leone, 2007). In terms of depth, small single-element transducers are capable of penetrating 18 to 47 mm past dura (Deffieux et al., 2013; Lee et al., 2015; Legon et al., 2014)—far surpassing the ~15-mm limit of a figure-8 TMS coil (Roth, Amir, Levkovitz, & Zangen, 2007). With a larger single-element transducer, tUS can target subcortical structures while still maintaining narrow ellipsoid hotspots (Cain, Spivak, et al., 2021; Cain, Visagan, et al., 2021; Monti, Schnakers, Korb, Bystritsky, & Vespa, 2016). This combination of precision and depth allows for the stimulation of more targeted cortical regions, regardless of their position along gyral-sulcal anatomy.

1.3.2 Acoustic Attenuation

The challenges of tUS delivery revolve around two effects on acoustic waves: attenuation and impedance transitions. Attenuation is the loss of energy as waves pass through tissue. Attenuation is dependent on both US frequency and the material involved (Goss, Johnston, & Dunn, 1978; Pichardo, Sin, & Hynynen, 2010; *The Safe Use of Ultrasound in Medical Diagnosis*, 2012; Tufail et al., 2010). Attenuation consists of two components: absorption of energy into the tissue and scattering of the waves. In soft tissues, these components make up ~90% and ~10% of attenuation, respectively (at ~1 MHz) (The Safe Use of Ultrasound in Medical Diagnosis, 2012). In bone, scattering plays a larger role in attenuation (Pinton et al., 2012).

While overall attenuation is relatively low in fluids and soft tissues, it is relatively high in bone. As such, tUS transmission is heavily attenuated by the skull (Goss et al., 1978; G. T. C. and K. Hynynen, 2002; Pichardo et al., 2010; *The Safe Use of Ultrasound in Medical Diagnosis*, 2012). Since attenuation increases with higher frequencies, tUS stimulation is only feasible within certain frequency constraints. As a result, tUS transmission above ~1.4 MHz is almost entirely attenuated by the skull (K. Hynynen &

Jolesz, 1998; O'Brien, 2007; Pichardo et al., 2010; P. J. White, Clement, & Hynynen, 2006). Thus, all transcranial ultrasound studies in humans have used acoustic frequencies no higher than 860 kHz (T. Kim et al., 2021; Wang et al., 2019), except for the two studies that have used diagnostic ultrasound imaging devices (Gibson et al., 2018; Hameroff et al., 2013).

1.3.3 Impedance Mismatches

Much like in electrical systems, impedance transitions must be carefully considered in acoustic applications. The rate at which a material opposes the flow of acoustic motion is its specific impedance. As an acoustic wave reaches the border between material types, a portion of the energy is reflected due to the impedance mismatch of the materials. The remaining energy passes into the second material. While the degree of reflection is minor in transitions between soft tissues and fluids, roughly half of US energy is reflected at transitions between bone and soft tissue (*The Safe Use of Ultrasound in Medical Diagnosis*, 2012).

1.3.4 Accuracy for tUS Experiments

Given that much of the acoustic energy can be lost with tUS stimulation, it is critical to have a reliable estimate of the true intensity and location of tUS sonication. Ideally, these estimates should be done for each subject and skull location individually. Significant skull thickness variations exist across subjects, ranging from 5 to 10 mm above the postcentral gyrus (Lee et al., 2015). Additionally, skull bone composition is not uniform, containing varying thicknesses of compact cortical bone and spongy trabecular bone depending on the area and individual (Pichardo et al., 2010). Because of their differing densities and geometries, these bone types have separate attenuation coefficients and specific impedances (Pichardo et al., 2010). Furthermore, acoustic diffraction by the skull causes significant shifts in acoustic focus. Normally on the order of 0 to 3 mm, offsets as high as 13 mm can occur in some individuals (K. Hynynen & Jolesz, 1998; Lee et al., 2015). These factors should also be taken into account

to create subject-specific intensity profiles, consisting of simulated acoustic propagation through subject-specific magnetic resonance (MR) imagery (Kyriakou et al., 2014; Lee et al., 2015).

1.4 SAFETY

The deposition of energy into tissue that occurs with US can have hazardous physiological consequences. Hence, strict procedures should be used with tUS. For all US exposure, this energy transfer has two types of effects on tissue: mechanical and thermal (*The Safe Use of Ultrasound in Medical Diagnosis* 2012, pg. 13).

1.4.1 Mechanical Effects

Since ultrasonic waves are mechanical, the effect of mechanical forces on tissue is a primary safety concern. Most importantly, the alternating compression and rarefaction of US generates the potential for cavitation. Even at relatively low US intensities, cavitation can occur when gas bodies in tissue vibrate (stable cavitation). At higher intensities, these gas bodies can expand and eventually collapse (inertial cavitation). The ensuing shockwave causes damage to the surrounding tissue (M. W. Miller, Miller, & Brayman, 1996; O'Brien, 2007). While such gas bodies are not significantly present in human tissues outside the lungs and intestines (O'Brien, 2007; *The Safe Use of Ultrasound in Medical Diagnosis*, 2012), inertial cavitation is still possible in non-gaseous tissues at ~1000 W/cm^2, which is three orders of magnitude greater than intensities used in low-intensity tUS (Frizzell, 1988).

The peak rarefaction pressure of the acoustic waves directly relates to cavitation risk (*The Safe Use of Ultrasound in Medical Diagnosis*, 2012). Since it is obviously not possible to measure intracranial US pressures directly, tUS device pressures must be measured in a water tank, and peak rarefaction pressure *in situ* can be deduced either through detailed acoustic simulation or a simpler estimate—either of which rely on the frequency-specific attenuation coefficient for the tissue (O'Brien, 2007; *The Safe Use of Ultrasound in Medical Diagnosis*, 2012). With an estimate of *in situ* pressure, risks of inertial

cavitation damage can be approximated with the Mechanical Index (MI), a unit-less rating based on cavitation thresholds (Apfel & Holland, 1991; Holland & Apfel, 1989).

Cavitation risks are higher at lower US frequencies (*The Safe Use of Ultrasound in Medical Diagnosis* 2012, p. 23). Perhaps for this reason, recent tUS studies have not gone below 250 kHz. Frequencies below 250 kHz could be investigated, given it is done with intensities low enough to prevent damage (lessening peak rarefaction pressures and MI). While likely safe, this could potentially drop intensities below those needed to generate physiological effects.

Another safety concern is the reflection of US waves within the skull, potentially creating standing waves. Such interference patterns can cause dangerous increases in intensity at their antinodes (Baron, Aubry, Tanter, Meairs, & Fink, 2009; Daffertshofer et al., 2005; *The Safe Use of Ultrasound in Medical Diagnosis*, 2012). The likelihood of generating standing waves with small focused US transducers to cortical targeting in humans is relatively low, given that any energy from small-diameter transducers is attenuated long before reaching the opposing end of a human skull (Lee et al., 2015; Legon et al., 2014; J. Mueller et al., 2014). The risk of standing waves is also assuaged by emitting US waves in pulses.

It should also be noted: ophthalmic tissue is significantly more prone to acoustically induced damage than other soft tissues (O'Brien, 2007). As such, caution should be taken when performing any US research near the orbits.

1.4.2 Thermal Effects

Heating is the other physical effect of US energy absorption. The amount of heat deposited depends directly on the time-averaged energy output of the transducer, along with the acoustic absorption properties of the tissue. These frequency-specific properties are quantified as an absorption coefficient, one of the two components of the aforementioned attenuation coefficient (*The Safe Use of Ultrasound in Medical Diagnosis*, 2012). Just as denser, harder materials have higher attenuation coefficients,

harder tissues have higher absorption coefficients. This increased absorption results in greater heat production. For instance, US passed through the skull produces roughly 50 times as much heat as in brain tissue, with absorption coefficients of 10 dB cm^{-1} MHz^{-1} and 0.2 dB cm^{-1} MHz^{-1} respectively (Duck, 1990). Therefore, the vast majority of temperature increase with tUS occurs at the skull, with some of this heat diffusing to surrounding soft tissue (*The Safe Use of Ultrasound in Medical Diagnosis*, 2012).

Much like mechanical effects, thermal effects on tissue have historically been estimated with a Thermal Index (TI) for diagnostic ultrasound use. The TI for a protocol depends on the power output of the transducer and the acoustic heating susceptibility of the tissue—specifically the power necessary to heat the tissue by 1 °C (O'Brien, 2007). Recent transcranial US experiments in mice and humans showed no significant temperature increases, staying below an estimated 0.03 °C (Lee et al., 2015; Tufail et al., 2010). Thermal estimates can also be derived from acoustic simulations (Constans, Mateo, Tanter, & Aubry, 2018). If real-world measurements are desired, the thermal production of tUS protocols can be measured using tissue-mimicking phantoms and a digital thermometer or even MR thermometry (Eames et al., 2015; Farrer et al., 2015).

In any case, the use of low-intensity transducers and short pulse durations allows for the modulation of neural tissue without significant temperature elevations.

1.4.3 Overall Safety

Overall, as in other forms of transcranial neurostimulation like TMS or tDCS, the safety of US is entirely dependent on the parameters of the protocol. For tUS, the parameters that matter are the ultrasound intensity, acoustic frequency, protocol duration, and duty cycle (i.e. pulses) used. Under proper protocols, tUS should be safe in both animal models and humans. This expectation has been corroborated by histological analyses in mice (Mehić et al., 2014; Tufail et al., 2010), rats (Min et al.,

2011), rabbits (Yoo et al., 2011), and monkeys (Gaur et al., 2020) which showed no structural damage or cell death after US. It should be noted that a 2016 histology study that found very minor presence of extravascular red blood cells (RBCs) in sheep following tUS (Lee, Lee, et al., 2016) could not be replicated (Gaur et al., 2020). Since Gaur and colleagues found extravascular RBCs in control animals and only outside the tUS field, they concluded the minor extravascular RBCs found by Lee and colleagues were post-mortem artifacts from the extraction processes. As such, the histological evidence for tUS remains promising. Behaviorally, no severe medical side effects from tUS have been reported in humans or animals (Lee et al., 2015; Lee, Kim, et al., 2016; Lee, Lee, et al., 2016; Legon et al., 2014, 2020; J. Mueller et al., 2014; Tufail et al., 2010). A review of ultrasound safety, including a synthesis of histological results with their respective US protocols, is available from Blackmore and colleagues (Blackmore, Shrivastava, Sallet, Butler, & Cleveland, 2019).

1.5 DISSERTATION AIMS

1.5.1 Summary

Transcranial focused ultrasound stimulation (tUS) is emerging as a novel technique for non-invasive brain stimulation (NIBS) in humans. However, the neuromodulatory effects of tUS are poorly understood, and the few results so far have shown variable outcomes between regions and studies.

To better understand the strengths, weakness, and feasibility prospects of tUS for use in humans, I compared tUS to an established NIBS technique, transcranial magnetic stimulation (TMS), in a cortical region with unclear tUS results but established TMS results: primary motor cortex (M1) (see **Aim 1**).

To explore causes of variability in tUS, I performed acoustic simulations that matched Aim 1 experiment conditions. Specifically, I used participant-specific MRI to find where in the brain tUS pressure fields landed and how strong those pressure fields were. With this simulation data, I explored the spatial precision and volume of tUS, the accuracy of our neuronavigated protocol, and whether there was a correlation between tUS exposure and M1 excitability (see **Aim 2**).

Lastly, acoustic simulations like those in Aim 2 can bring a lot of insight to tUS experiments. However, implementing such simulations is a challenging, time-consuming task, which may be why many published tUS studies do not report performing acoustic simulations of their experiments. To bridge this gap, I built an open-source MATLAB toolbox that integrates medical imaging (MRI or CT) and neuronavigation with acoustic simulation (see **Aim 3**).

1.5.2 Aim 1

Examined modulatory tUS effects in M1 compared to known TMS effects

1A) Determine whether single-trial tUS is capable of exciting primary motor cortex (M1)

1B) Investigate the capability of single-trial tUS and single-trial TMS to inhibit tonic, voluntary motor activity

1C) Investigate if repeated tUS trials affects M1 excitability

1.5.3 Aim 2

Examined if variations in tUS exposure can explain tUS outcome variability

Use subject-specific MRI to perform acoustic simulations that match tUS experiments. Explore whether there is a correlation between tUS exposure and M1 excitability

1.5.4 Aim 3

Constructed an open-source toolbox that integrates medical images and acoustic simulation for tUS experiments

Integrate MRI and CT with a general-use acoustic simulation package, k-Wave. Validate performance with comparisons to condition-matched pressure field measurements in a water tank.

2 ULTRASOUND STIMULATION OF THE MOTOR CORTEX DURING TONIC MUSCLE CONTRACTION

2.1 ABSTRACT

Transcranial ultrasound stimulation (tUS) shows potential as a noninvasive brain stimulation (NIBS) technique, offering increased spatial precision compared to other NIBS techniques. However, its reported effects on primary motor cortex (M1) are limited. We aimed to better understand tUS effects in human M1 by performing tUS of the hand area of M1 ($M1_{hand}$) during tonic muscle contraction of the index finger. Stimulation during muscle contraction was chosen because of the transcranial magnetic stimulation-induced phenomenon known as cortical silent period (cSP), in which transcranial magnetic stimulation (TMS) of $M1_{hand}$ involuntarily suppresses voluntary motor activity. Since cSP is widely considered an inhibitory phenomenon, it presents an ideal parallel for tUS, which has often been proposed to preferentially influence inhibitory interneurons. Recording electromyography (EMG) of the first dorsal interosseous (FDI) muscle, we investigated effects on muscle activity both during and after tUS. We found no change in FDI EMG activity concurrent with tUS stimulation. Using single-pulse TMS, we found no difference in M1 excitability before versus after sparsely repetitive tUS exposure. Using acoustic simulations in models made from structural MRI of the participants that matched the experimental setups, we estimated in-brain pressures and generated an estimate of cumulative tUS exposure experienced by $M1_{hand}$ for each subject. We were unable to find any correlation between cumulative $M1_{hand}$ exposure and M1 excitability change. We also present data that suggest a TMS-induced MEP always preceded a near-threshold cSP.

2.2 INTRODUCTION

Transcranial ultrasound stimulation (tUS) has gained attention in the past years as a potential new tool for noninvasive brain stimulation (NIBS). tUS has higher spatial precision compared to other NIBS techniques such as transcranial magnetic stimulation (TMS) and transcranial electric stimulation (TES), which presents a possibility of improved targeting (Deffieux et al., 2013; Lee et al., 2015; Legon et al., 2014; Roth et al., 2007; Wagner et al., 2007). Furthermore, tUS can deliver its energy much deeper while maintaining focal precision—deeper than TMS or TES (Legon, Ai, Bansal, & Mueller, 2018).

Previous studies have demonstrated that ultrasound is capable of stimulating central structures in animals (Fry et al., 1958), peripheral nerve pathways in animals and humans (Gavrilov et al., 1976; Gavrilov, Tsirulnikov, & Davies, 1996), the retina (Menz, Oralkan, Khuri-Yakub, & Baccus, 2013), and intact brain circuits in animals (Tufail et al., 2010). However, the number of human tUS studies thus far is limited. In primary somatosensory cortex, tUS has been shown to modulate touch discrimination (Legon et al., 2014), induce localized somatosensations when targeting the cortical hand representation (Lee et al., 2015, 2017), and induce changes in intrinsic and evoked EEG dynamics (J. Mueller et al., 2014). In primary visual cortex, tUS can induce individual visual phosphenes, percepts of a flash of light, that were accompanied with an evoked potential and blood-oxygenation-level-dependent (BOLD) contrast similar to those seen with photic stimulation (Lee, Kim, et al., 2016). However, the effects of tUS in primary motor cortex (M1) have been less clear.

Much of our understanding of motor cortex stimulation comes from TMS investigations, where it has been the standard for noninvasive M1 perturbation for decades (Chen et al., 1997; Hess, Mills, & Murray, 1987; Hess, Mills, Murray, & Schriefer, 1987; Y.-Z. Huang, Edwards, Rounis, Bhatia, & Rothwell, 2005; Oberman, Edwards, Eldaief, & Pascual-Leone, 2011; Priori, Berardelli, Rona, Accornero, & Manfredi, 1998). Suprathreshold single-pulse TMS of M1 induces contraction in the corresponding

muscles, and electromyography (EMG) allows for the quantification of these motor evoked potentials (MEPs). Since MEP size increases as a sigmoidal function of TMS intensity above motor threshold (Hess, Mills, & Murray, 1987; Möller, Arai, Lücke, & Ziemann, 2009), MEP strength is frequently used as an indicator of corticospinal excitability, both in neuromodulatory and behavioral interventions (Chen et al., 1997; Christov-Moore, Sugiyama, Grigaityte, & Iacoboni, 2016; Fitzgerald, Fountain, & Daskalakis, 2006; Hess, Mills, & Murray, 1987; Hess, Mills, Murray, et al., 1987; Y.-Z. Huang et al., 2005; Liebetanz et al., 2003; Oberman et al., 2011; Priori et al., 1998; Thut & Miniussi, 2009). This is supported by pharmacological evidence that shows motor threshold, the TMS intensity needed to elicit an MEP, is a proxy for the within-subject excitability of the cortico-cortical axons affected by the induced current of TMS pulse (Ziemann et al., 2015). We investigated the neuromodulatory effects of tUS on M1 by analyzing its effect on TMS-evoked MEP.

Cortical silent periods (cSP) are a phenomenon of suppressed EMG activity during tonic contraction following single-pulse TMS of the corresponding M1 motor representation. cSPs typically last from 100-300 ms. Importantly, cSPs are considered to be driven predominantly by cortical inhibition from ~50 ms after instigation (Wolters, Ziemann, & Benecke, 2012). Specifically, pharmacological evidence suggests that the cSP effect is mediated by GABA receptor-dependent postsynaptic inhibition (Werhahn, Kunesch, Noachtar, Benecke, & Classen, 1999; Ziemann et al., 2015). When elicited during tonic contraction of the contralateral hand, cSPs are reported to be observable either following an MEP or without inducing an MEP, at subthreshold TMS intensities (Classen & Benecke, 1995; Davey, Romaiguère, Maskill, & Ellaway, 1994). As such, cSP provides a valuable method of investigation of inhibitory mechanism in motor cortex.

As a whole, the field is still building its understanding of what, if anything, tUS can affect via M1 stimulation. To date, no tUS study has been able to induce motor contraction through human M1 stimulation. Previous animal model studies suggest that tUS-induced MEPs may only be producible at

acoustic intensities above human-safe levels (H. Kim, Chiu, Lee, Fischer, & Yoo, 2014; King, Brown, Newsome, & Pauly, 2013; Krasovitski, Frenkel, Shoham, & Kimmel, 2011; Tufail et al., 2010; Ye et al., 2017; Yoo et al., 2011). Given that change in motor contraction strength has been the benchmark for M1 modulation studies, the established capabilities of TMS have been leveraged to investigate tUS effects on M1. For example, tUS of the hand area reduced the size of motor evoked potentials (MEPs) evoked by concurrent and concentric TMS (Fomenko et al., 2020; Legon, Bansal, Tyshynsky, Ai, & Mueller, 2018). A separate study reported a lasting increase in the size of MEPs after exposure to an ultrasound imaging device (Gibson et al., 2018). Additionally, tUS of M1 alone was shown to affect reaction time in a motor task(Legon, Bansal, et al., 2018).

Because of its physiological underpinnings, the cSP is in a unique position to be leveraged as an externally detectable phenomenon to better understand tUS effects on M1. Specifically, tUS has been proposed to preferentially affect inhibitory interneurons (H. Kim et al., 2014; Legon et al., 2014; Nguyen, Berisha, Konofagou, & Dmochowski, 2020; Plaksin, Kimmel, & Shoham, 2016; Rinaldi et al., 1991), feeding well into cSP's existence as a interneuron-facilitated phenomenon. Additionally, since cSPs have been reported to occur without a preceding MEP (Cantello, Gianelli, Civardi, & Mutani, 1992; Classen & Benecke, 1995; Davey et al., 1994; Wassermann et al., 1993; Wolters et al., 2012), tUS' apparent inability to instigate an MEP does not preclude its use to attempt induction of cSPs. But as of yet, it is unknown if tUS can engage the necessary inhibitory circuits to instigate a cSP. We addressed this by performing tUS of M1 on participants executing voluntary muscle contraction and analyzing the EMG data from the contracted muscle.

2.3 METHODS

Two experiments were performed in this study. In Experiment 1, we measured how tonically contracted hand muscles respond to single-pulse TMS and single-burst tUS of M1. We performed separate trials

using tUS and TMS. In Experiment 2, we measured how cortical excitability is affected by tUS exposure. Excitability was gauged using single-pulse TMS.

2.3.1 Data acquisition

2.3.1.1 Participant Demographics

Research participants were right-handed with no neurological conditions. Due to TMS use, subjects with an increased risk of seizure were excluded (Figure 2-22). Due to MRI use, subjects with MR-incompatible implants were excluded. Participants were 18 to 42 years old, A subset of Experiment 1 participants (n = 10; mean: 25.9 years) participated in Experiment 2 (n = 8; mean: 26.75 years). Note that subject ID numbers are not sequential since other recruited subjects were used in a different study.

2.3.1.2 EMG and NIBS Placement

Electrode sites were cleaned with abrasive skin prep gel (Nuprep) and alcohol wipes. A surface EMG electrode (two 10 x 1 mm contacts; 10 mm spacing) measured the right first dorsal interosseous (FDI) muscle activity, and the signal was amplified (x1000) (Delsys Inc., Boston, MA) and sampled at 5000 Hz. The surface electrode was additionally secured to the finger with medical tape. A wide ground electrode was placed on the back of the hand. EMG was recorded for 1-second epochs around NIBS (both TMS and tUS) onset. A structural MRI (T1-weighted; 0.8 x 0.8 x 0.8 mm voxels) was acquired in a previous visit, and each structural MRI was registered to standard space for NIBS targeting of standard-space coordinates (Montreal Neurological Institute, MNI; 1-mm atlas). Registration was performed in FSL (the FMRIB Software Library) on brain volumes extracted using the optiBET tool for FSL's BET (Jenkinson, Beckmann, Behrens, Woolrich, & Smith, 2012; Lutkenhoff et al., 2014). NIBS position with respect to the subject's head was tracked using neuronavigation software (Brainsight, Rogue Research, Montreal, QC) loaded with the subject's MRI. The neuronavigation software was prepared with pre-determined trajectories, which were the shortest Euclidean distance from the scalp to a set voxel as determined by a

custom MATLAB script (Mathworks, Inc., Natick, MA). At the beginning of each NIBS session, five single TMS pulses were given at each target of a 6-target grid over the left motor cortex using MNI space (Figure 2-20). The grid's origin was placed at MNI coordinates that correspond to $M1_{hand}$ as based on a meta-analysis of fMRI motor experiments: x = −39, y = −24, z = 57 (Mayka, Corcos, Leurgans, & Vaillancourt, 2006). This coordinate corresponds morphologically to the cortical 'hand knob' (Yousry et al., 1997). The other five targets on the grid were in a 12 voxel-width grid (9.6 mm grid interval) anterior, posterior, and medial, anteromedial, and posteromedial from the $M1_{hand}$ coordinate in subject space. The targets that elicited the largest, second-largest, and third-largest average MEPs were used as placement points for the NIBS devices. These three positions are referred to below as "TMS target", "2nd-best", and "3rd-best" targets respectively. For all TMS trials, the TMS coil was oriented with the handle pointed backwards and angled 45° from midline.

2.3.1.3 Experiment 1, cSPs

Participants moved their index finger laterally during trials to maintain consistent FDI contraction across trials, as monitored by a digital scale (20-40% maximum voluntary contraction, depending on the subject). NIBS was delivered during contraction. Percent maximum contraction varied between subjects so that every subject maintained a comparable level of EMG activity (~150-200 peaks per second). 20 trials were performed at each of three TMS intensity levels: 90%, 100%, and 110% of % active motor threshold (aMT) (60 TMS trials total per subject). 20 tUS trials were performed for each of the following four parameters: 300-ms burst duration at the TMS target, 300-ms burst duration at the 2nd-best target, 300-ms burst duration at the 3rd-best target, and 500-ms burst duration at the TMS target. Subjects were told to use the feedback of the digital scale display to maintain their target FDI contraction force, and subjects were cued to relax between trials to avoid fatigue. Subjects monitoring their contraction level also had the benefit of keeping subject attention constant across trials in Experiment 1, since

attention can affect EMG measurements (Vance, Wulf, Töllner, McNevin, & Mercer, 2004; Zachry, Wulf, Mercer, & Bezodis, 2005). Trials had a jittered intertrial interval of 10 ± 2 s.

2.3.1.4 Experiment 2, Cortical Excitability

MEPs were measured with the subject's hand relaxed. TMS was delivered at the same suprathreshold intensity for both "before" and "after" conditions within subjects. TMS was set to 110-120 %rMT (percent resting motor threshold), (110%: n = 1; 115%: n = 4; 120% n = 3). %rMT was varied across subjects to assure that each subject had consistent MEP sizes. 20 MEPs were acquired before exposure to tUS and 20 MEPs were acquired after exposure to tUS. tUS exposure protocol was the same as described in "Experiment 1, cSPs:" (20 trials each: 300 ms at TMS target, 300 ms at 2nd-best, 300 ms at 3rd-best, 500 ms at TMS target). Trials had a jittered intertrial interval of 10 ± 2 s.

2.3.1.5 tUS Equipment

The tUS device used was a 500-kHz focused piezoelectric transducer (Blatek Industries, Inc., State College, PA). The transducer had a face width of 3 cm and a focal point of 3 cm. The transducer was housed in a custom 3D-printed handle, and an infrared tracker was mounted to the housing for neuronavigation (Figure 2-1). The transducer was driven by 500-kHz sine-wave voltage pulses from a waveform generator (33500B Series, Keysight Technologies, Santa Rosa, CA) and voltage pulses were amplified by a 50-dB radio frequency amplifier (Model 5048, Ophir RF, Los Angeles, CA). A 3-dB fixed attenuator was attached in line following the amplifier.

tUS bursts were pulsed with a 1-kHz pulse repetition frequency and a duty cycle of 36% (Figure 2-2). Each burst lasted either 300 or 500 ms (tUS on for 108 or 180 ms total). Transducer output was confirmed via measurements made via hydrophone in degassed water (1 mm, Precision Acoustics Ltd, Dorchester, UK). Transducer output was set to produce an intensity of 15.48 W/cm^2 in degassed water (spatial peak, pulse average; I_{sppa}). These parameters were chosen to not exceed an in-tissue estimate of 4.9 W/cm^2. This is within safe levels (max Mechanical Index: 0.8) (ter Haar et al., 2011) and is within intensities of previous human tUS studies (Ai, Mueller, Grant, Eryaman, & Legon, 2016; Lee et al., 2015; Lee, Kim, et al., 2016; Legon et al., 2014; J. Mueller et al., 2014).

Figure 2-1. tUS transducer in housing

2.3.1.6 TMS Equipment

Single-trial, monophasic TMS was applied using a figure-eight coil (70 mm diameter) via a Magstim 200^2 magnetic stimulator (Magstim, Whitland, Dyfed, UK). An infrared tracker was mounted to the TMS coil for neuronavigation. Individual resting and active motor thresholds were determined using simple adaptive PEST (SA-PEST) (Adaptive PEST TMS threshold assessment tool, Brain stimulation laboratory, Department of Psychiatry, Medical University of South Carolina). Trials had a jittered intertrial interval of 10 ± 2 s.

2.3.2 EMG data analysis

2.3.2.1 EMG Post-processing

EMG traces were high-pass filtered with a 10-Hz cutoff (filter transition: 5-10 Hz), unless noted as unfiltered. This high-pass filter

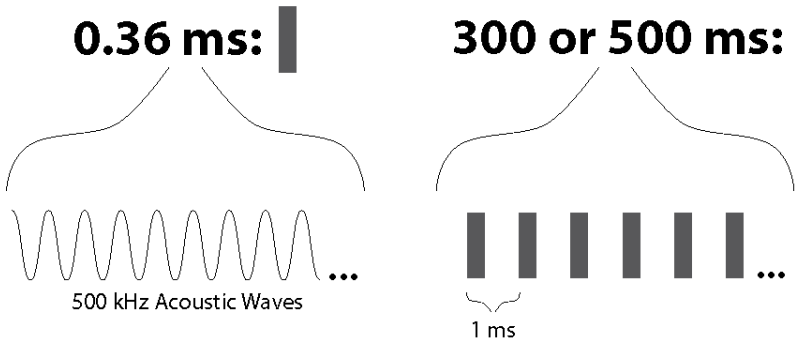

Figure 2-2. tUS Protocol. Illustration of a single trial of tUS.

was applied to remove voltage shift and low-frequency noise. All EMG post-processing was performed using MATLAB.

2.3.2.2 cSP Measurement

cSPs were measured using an automated script written in MATLAB, which used a rolling standard deviation (STD) to see when EMG activity quieted below a threshold (Figure 2-9). The rolling STD window had a width of 3 ms. The cSP threshold was set using the baseline EMG variability—specifically ½ STD of the rolling STD trace the 200-ms period before TMS onset. cSP onset was set to the timepoint the rolling STD first fell below threshold after the MEP peak. cSP starts were also contingent on the raw EMG being near or below zero (specifically, below the same threshold value). In rare cases in which no cSP onset point was found within the first 15 ms, the onset was set to the first rising EMG value.

cSP offset was set where the rolling STD first rose back above threshold. A 15-ms 'amnesty period' was included for offset auto-detection to correct for trials with large MEPs, which have large STD values in their valleys after the MEP peak. If the rolling STD reached threshold from 0-15 ms after cSP onset, the window from 15-30 ms after cSP onset would be checked ('post-amnesty period'). If the rolling STD trace stayed below threshold during the entire 15-ms post-amnesty period, the amnesty period transgression would be ignored (i.e. a silent period >30 ms). If not, the first threshold breach is used (i.e. a silent period <15 ms).

2.3.2.3 MEP Measurement, Resting

To quantify the size of MEPs Experiment 2, we used the area of the MEPs. The area under the curve (AUC) of the rectified MEP waveform from 20 to 120 ms after the TMS pulse was estimated via the trapezoidal method in MATLAB. AUC was not used in Experiment 1 (voluntary contractions) because of surrounding EMG activity.

2.3.2.4 MEP Measurement, Voluntary Contraction

MEP peak-to-peak measurements were measured by the absolute height from the peak to the mean of the two flanking valleys of the peak. To improve accuracy of automated MEP detection during tonic contraction, MEP search was constrained using per-subject exemplar data from trials with overt MEPs. A 10-ms search window was centered around the expected MEP timepoint. Expected MEP timepoint was the median MEP timepoint during resting TMS MEP trials (Experiment 2 TMS MEP data). For the two subjects who did not participate in Experiment 2, trials with visually overt MEPs during tonic contraction were used instead (Experiment 1 TMS MEP data). This search approach was used both for the positive MEP peak and its two flanking negative valleys.

Candidate peaks and valleys in the EMG data were found using the *findpeaks* MATLAB function. To avoid minor, extraneous peaks from being selected, only peaks with a prominence and width above the 50th percentile were eligible.

TMS cSP trials were categorized into three labels: *MEP*, *stub*, and *none*. Overt MEPs (*MEP*) occurred within the 10-ms search window and had a peak-to-peak height above 0.5 mV. Potential-but-short MEPs (*stubs*) occurred within the 10-ms search window and had a peak-to-peak height below 0.5 mV. Trials with no peak that met conditions (50th percentile prominence, width) within the 10-ms search window were labeled *none*.

2.3.2.5 EMG Characteristics

Additional characteristics of the EMG traces were calculated to contrast TMS and tUS effects on the FDI EMG signal during voluntary contraction, as well compare within different periods of tUS trials. First, spectral components were determined by estimating the short-term, time-localized power spectrum of each trial and then taking the mean to get separate average spectrograms for TMS trials and tUS trials. Second, lengths of silences in the EMG signal were calculated with a sliding window approach.

Specifically, the cSP algorithm (see cSP Measurement) searched for a silence duration from a window centered at 0.001-second intervals from 0.05 to 0.95 s. The first and last 0.05 s were excluded to avoid edge artifacts. The results were then averaged within their respective groups to get mean silence traces.

Two additional characteristics were calculated to investigate possible EMG responses time-locked to tUS exposure: the height of the EMG (AUC) and the rate of EMG peaks. AUC was calculated as described above (MEP Measurement, Resting) for two 150-ms epochs: from 200 to 50 ms before tUS onset and from 50 to 200 ms after tUS onset. This provides two 150-ms epochs wholly covered by 'off' and 'on' periods of tUS. Rate of EMG peaks was calculated using findpeaks() function in MATLAB on each EMG trace, binning peaks by time for the tUS-off or tUS-on periods (i.e. both the pre- and post-tUS periods were included together for tUS-off). All EMG characteristics processing was performed in MATLAB.

2.3.3 Acoustic simulation

2.3.3.1 Skull Mask Processing

For acoustic simulations and skull thickness measurements, binary skull masks were produced in BrainSuite using its "Cortical Surface Extraction Sequence" (Shattuck & Leahy, 2002). Skull masks were corrected by hand with the mask brush tool in BrainSuite. In MATLAB, skull masks were linearly interpolated to increase resolution to 0.2-mm-width voxels, and they were rotated such that the tUS trajectory was in line with the computational grid. Masks were also smoothed via morphological image processing both before and after transformation. Masks were cropped to the area of interest, creating a 484 x 484 x 484 volume.

2.3.3.2 k-Wave Simulations

Acoustic simulations were performed using k-Wave, an open-source acoustics toolbox for MATLAB (Treeby & Cox, 2010). Each skull mask was imported into k-Wave, providing a computational grid spacing of 0.2 mm. To simulate the transducer, we set a curved disc pressure source (k-Wave function:

makeBowl) with a curvature radius of 30 mm and aperture of 30 mm to mirror the focal length and width of the real transducer, respectively. The pressure source emitted a 0.5 MHz sine wave, resulting in a grid points per wavelength (PPW) of 14.8. Simulations were performed at a temporal interval of 285 temporal points per period (PPP) for a Courant-Friedreichs-Lewy (CFL) number of 0.0519. Perfectly matched layers (PML) of 14 grid points were added for a total grid size of 512 x 512 x 512.

To allow comparison to real-world pressure measurements in the water tank, each tUS trajectory was simulated twice: once to simulate propagation through the skull and once to simulate propagation through water. For skull simulations, the same acoustic properties were given for all points within the skull mask: density of 1732 kg/m^3, a sound speed of 2850 m/s, and an alpha coefficient of 8.83 [dB/(MHz^y cm)] (Treeby & Cox, 2014). The use of homogenous skull acoustic properties has been shown to be effective in simulations within the frequencies used here (Jones & Hynynen, 2016; G. W. Miller, Eames, Snell, & Aubry, 2015; J. L. B. Robertson, Cox, Jaros, & Treeby, 2017). All values not within the skull mask were given bulk acoustic values of brain: 1546.3 kg/m^3, a sound speed of 1035 m/s, and an alpha coefficient of 0.646 [dB/(MHz^y cm)] (Duck, 1990). Homogenous water simulations were given acoustic properties of water at 20 °C: a density of 998 kg/m^3, a sound speed of 1482 m/s, and an attenuation constant of 2.88 × 10^{-4} [Np / m] (Duck, 1990). An alpha power of 1.43 was used for all simulations.

To estimate in-brain pressures experienced by participants for a given tUS trajectory, we used a ratio of pressures from the skull and water simulations. The estimated pressure ($P_{est.}$) at a given location was calculated as

$$P_{est.} = \frac{P_{skull\ sim.}}{P_{water\ sim.}} \times P_{water,real}$$

Where $P_{skull\ sim.}$ is the temporal maximum pressure value at that same location in the skull simulation for the specific subject and trajectory. $P_{water\ sim.}$ is the temporal maximum pressure value at the focal point of the water simulation. $P_{water,real}$ is the temporal maximum pressure value at the focal point measured in a water tank of degassed water using the same parameters as used in the experiment (see tUS Equipment). To avoid any potential outliers in the simulated data, spatial averaging was performed on $P_{skull\ sim.}$ and $P_{water\ sim.}$ by taking the mean within a 0.6-mm radius sphere. $P_{water,real}$ was 1.40 MPa for all subjects except one (sbj11), whose $P_{water,real}$ was 1.13 MPa due to the lower waveform generator setting used for that session (user error).

Simulations were performed on the Ahmanson-Lovelace Brain Mapping Center computational cluster. Each simulation instance was allocated 24 CPU cores and took approximately 2.5 hours with the C++ implementation of k-Wave (kspaceFirstOrder3D-OMP) (Treeby, Jaros, Rendell, & Cox, 2012).

2.3.3.3 Target Registration

NIBS targets and the location of $M1_{hand}$ were determined via registration to standardized stereotactic space (Montreal Neurological Institute, MNI). Registration was performed with FSL's FNIRT/FLIRT tools (Jenkinson, Bannister, Brady, & Smith, 2002; Jenkinson & Smith, 2001). $M1_{hand}$ was set to the voxel closest to the MNI coordinates x = −39, y = −24, z = 57 (Mayka et al., 2006).

2.3.3.4 Exposure

An estimate of cumulative $M1_{hand}$ exposure was made by multiplying the individual peak pressure at the $M1_{hand}$ voxel for each of the three tUS trajectories by the time the tUS device was on for that location. Specifically, exposure was defined as

$$\sum_{traj\,=\,1}^{n} P_{traj} \times Time_{traj}$$

for $\boldsymbol{n}$ number of tUS trajectories, where $\boldsymbol{P_{traj}}$ is the pressure at the $M1_{hand}$ voxel for that trajectory, and $\boldsymbol{Time_{traj}}$ is time tUS was on for that trajectory. We display these values in the form Pascal-hours (Pa·hr).

2.3.4 Statistics

2.3.4.1 Experiment 1, cSPs

TMS cSP durations vs. aMT was analyzed with a one-way repeated-measures ANOVA. For post-hoc tests, Welch's t-tests were performed on the group distribution pairs (90 & 100, 90 & 110, 100 & 110) using the cSP durations demeaned to their respective subject mean (*Duration – Subject Mean*).

EMG spike rate on vs. off was analyzed using a paired t-test, with the rates 'on' rate and the 'off' rate for each trial paired.

2.3.4.2 Experiment 2, Cortical Excitability

$M1_{hand}$ excitability was analyzed with a paired ranked non-parametric t-test since the distribution was non-gaussian. We performed this using resampling using a script in R (R Core Team, 2021). For null hypothesis testing, permutation was used to create a null distribution of all permutations of before- and after-tUS values swapped within subjects (256 permutations). All 16 medians of each permutation (8 subjects, 2 conditions) were then ranked against one another. The difference of the means of the permuted group ranks for each permutation was used as the values of the null distribution. The value of p equaled the number of permutations in which the absolute difference of the mean ranks was greater than the real absolute difference of the mean ranks.

Confidence intervals were calculated using the bootstrap method (10,000 bootstrap samples). Each bootstrap sample was made by sampling with replacement the 16 real median MEP sizes (8 subjects, 2 conditions). The 95% confidence intervals were set as the 2.5^{th} and 97.5^{th} percentiles of the bootstrap samples' differences of the group means.

To investigate any association between cortical excitability change and total tUS exposure of $M1_{hand}$, an estimate of total tUS exposure for a participant was calculated with the following formula:

$$\sum_{traj=1}^{n} P_{traj} \times Time_{traj}$$

Where $\boldsymbol{n}$ is the number of tUS trajectories used with that participant, $\boldsymbol{P_{traj}}$ is the pressure (estimated) at $M1_{hand}$ voxel for that trajectory, and $\boldsymbol{Time_{traj}}$ is the time the tUS device was on for that trajectory. Determination of $\boldsymbol{P_{traj}}$ is outlined in k-Wave Simulations. The spearman correlation coefficient (r_s) was calculated for these values.

2.3.4.3 cSP Null Distribution

To bootstrap a null distribution of cSP lengths our automated cSP algorithm would find if applied to null, non-cSP data, we used a sliding window approach on non-cSP data. This data was real EMG traces collected during tonic contraction by the same subjects and sessions as Experiments 1 and 2—specifically, the one-second tonic contraction trials collected during tUS exposure. tUS trials were deemed valid as null EMG traces since we saw no change in EMG traces between tUS on vs. tUS off (Figure 2-4, Figure 2-5, Figure 2-10, Figure 2-11, Figure 2-12). For every null trial, the cSP algorithm searched for a silence duration from a window centered from each 0.001-second interval from 0.05 to 0.95 s. The first and last 0.05 s were excluded to avoid edge artifacts. All trials, subjects, and sliding-window increments were grouped into a single distribution (686,457 sliding window samples).

2.4 RESULTS

2.4.1 Experiment 1

2.4.1.1 TMS cSPs

Single-pulse TMS was performed over left $M1_{hand}$ during tonic contraction of the FDI muscle (n = 10). TMS was delivered at 90%, 100%, and 110% aMT. cSP duration increased with TMS intensity (ANOVA: $F_{2,16}$: 26.31, $p < 0.001$; Welch's t-tests: $p < 0.001$, all pairs) (Figure 2-3, Figure 2-16, Figure 2-17). The aMT threshold for one subject (sbj11) was set mistakenly low, resulting in TMS intensities lower than intended and therefore elicited very few cSPs.

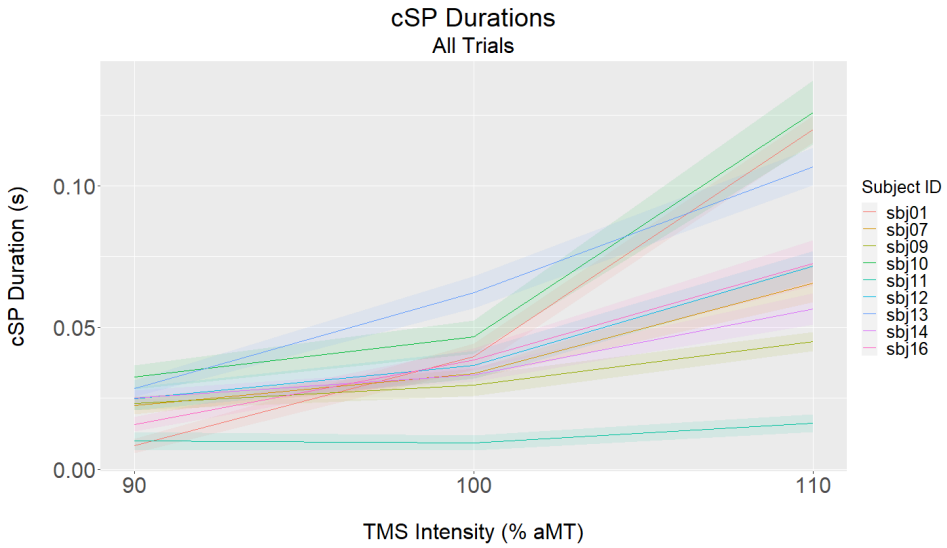

Figure 2-3. cSP length for each TMS intensity, per subject. Line: median. Ribbon: standard error of the mean. One subject (sbj08) with whom resting motor threshold was used is not shown here (see Figure 2-16).

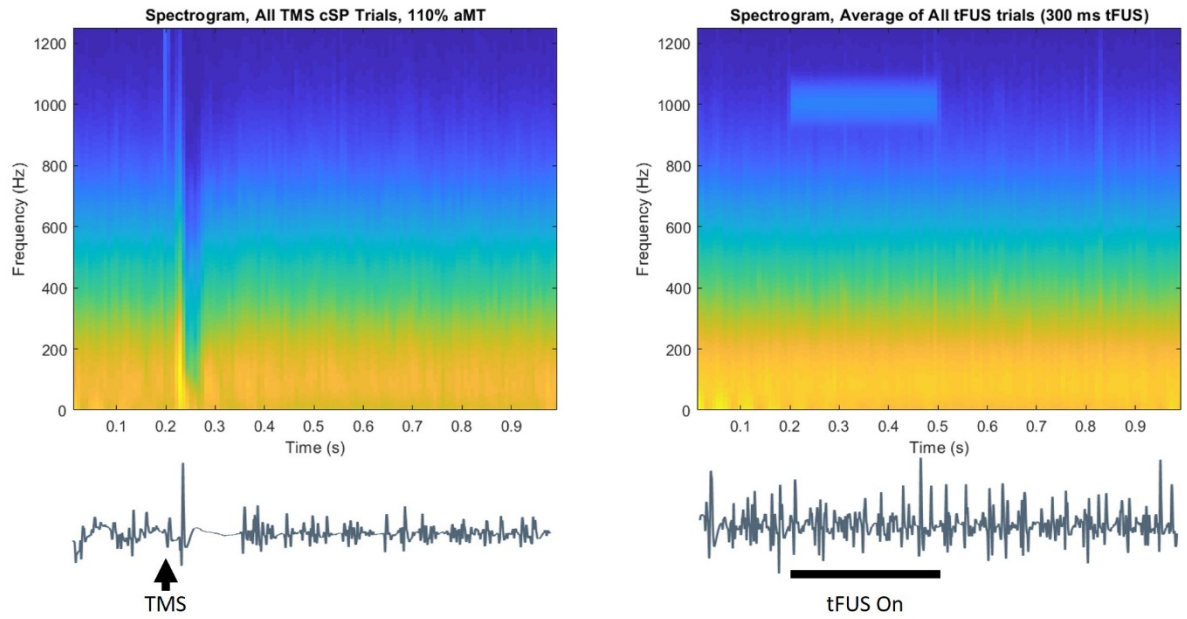

Figure 2-4. Average spectrograms during tonic contraction. Left) TMS trials. Right) tUS trials (300-ms tUS duration trials only). Signal around the 1000-Hz range from 0.2-0.5 s during tUS trials is noise recorded from the amplifier. This frequency component matches the pulse repetition frequency. Example EMG traces placed below the spectrograms illustrate timing.

We also examined the size and presence of MEPs preceding cSPs. For trials with overt MEPs, the lengths of the subsequent silent periods were noticeably longer than would be seen by chance (Figure 2-13). Among trials with a peak within the expected 10-ms time window, trials with a peak smaller than the standard MEP peak-to-peak amplitude threshold of 0.5-mV, henceforth referred to as "stub" trials (Figure 2-18), mostly showed silences within lengths that would be seen by chance (Figure 2-13). However, some "stub" trials did show long silence durations on par with those of overt MEP cSPs. Lastly, trials in which there was *no* peak within the 10-ms time window showed silence durations within what would be seen by chance, with only one of these trials showing a silence above the 95th percentile of the null distribution.

2.4.1.2 tUS

Single-burst tUS was performed over left $M1_{hand}$ during tonic contraction of the FDI muscle (n = 10). The 300-ms or 500-ms bursts were delivered at three trajectories per subject, one of which was also the trajectory for TMS.

No overt silent periods were visible during single trials of tUS stimulation. To investigate whether tUS caused any suppression of the EMG trace, we investigated the height of the EMG traces (area-under-the-curve, AUC) (Figure 2-10), the lengths of the intermittent contraction silences, the rate of EMG peaks (Figure 2-11), and the spectral components of the EMG signals. While a drop in signal power of the spectral components occurs due to TMS-induced cSP, no spectral changes are visible during tUS trials (Figure 2-4). The same disparity is seen comparing the length of silences in the EMG signal, with a clear rise in mean silence period in response to TMS-induced cSP but no change in response to tUS (Figure 2-5),

For comparisons performed within tUS trials, the height of the EMG traces showed no difference directly before versus after tUS onset (150-ms epochs before vs. after tUS) (Figure 2-10). The rate of EMG peaks while tUS was on vs. off also showed no significant difference (Figure 2-11, Figure 2-12), with a confirming there was only a small but statistically insignificant tUS effect on rate of EMG peaks (Delta: -0.91 Hz; 95% CI: -1.99, 0.16 Hz; p = 0.095) (Figure 2-15).

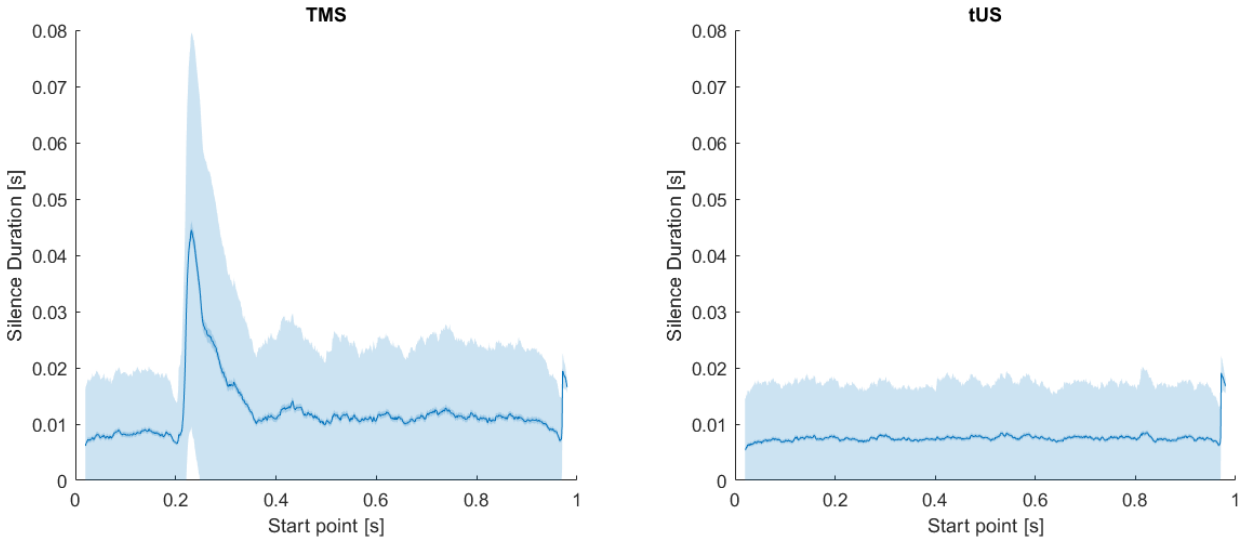

Figure 2-5. Silence durations across trials, using a sliding window. Duration is as measured from the start point of a given sliding window iteration. Left) TMS; Right) tUS. X-axis: Timepoint measured from. Middle Trace: Mean silence duration. Inner Margin: SEM. Outer Margin: STD

2.4.2 Experiment 2

2.4.2.1 Cortical Excitability

Cortical excitability was gauged before and after exposure to tUS by recording MEPs from single-pulse TMS over $M1_{hand}$ (n = 8). Both the pre-tUS and post-tUS measurements (1-min post-tUS) consisted of 20 suprathreshold TMS trials with an intertrial interval of 10 ± 2 s. The size of TMS-induced MEPs did not vary between before- and after-tUS conditions, according to a ranked paired non-parametric t-test (Figure 2-8) (Delta: -0.64 mV-ms; 95% CI: -2.39, 0.84 mV-ms; p = 0.51).

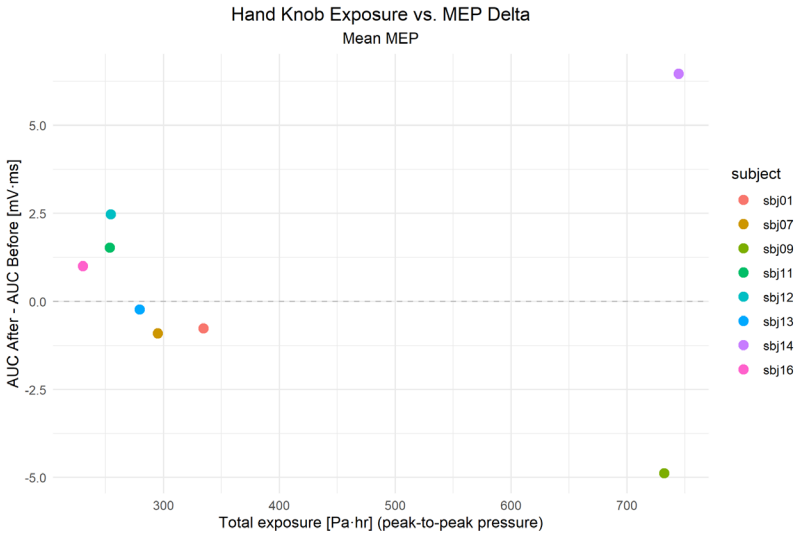

Figure 2-6. M1 excitability vs. Exposure. Estimate of total exposure of $M1_{hand}$ to tUS cumulatively during the session (horizontal axis) compared to the change in cortical excitability, as measured by TMS-evoked MEP (vertical

2.4.2.2 Exposure vs. Excitability

To investigate the variability that was present among cortical excitability responses, we compared subjects' cortical excitability change to total estimated tUS exposure in the session. tUS exposure estimates were made using acoustic simulations in models that matched each experimental setup, with skull data computed from structural MRI of the tUS participants. These data showed no obvious correlation between $M1_{hand}$ exposure and cortical excitability change (n = 8), with a spearman correlation coefficient of -0.21 (Figure 2-6).

2.4.3 Acoustic Simulation

Acoustic simulation results suggest we very accurately 'hit' targets we were aiming at (Figure 2-7). tUS produced pressures in an ellipsoid focus, with a mean FWHM with of 4.5 mm (Figure 2-21).

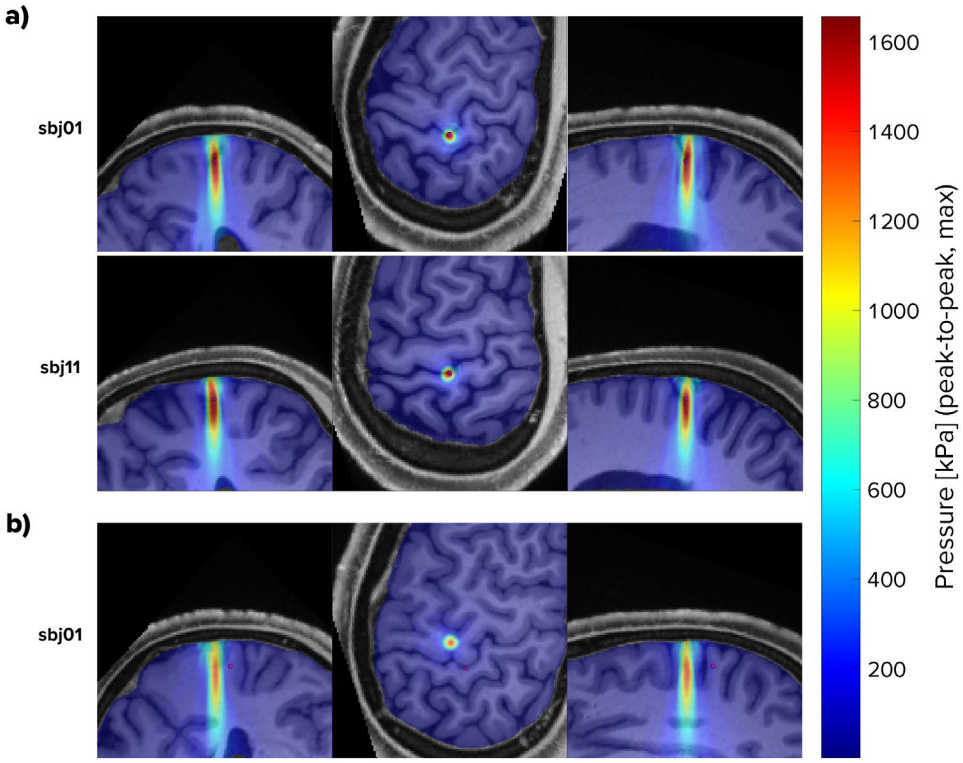

Figure 2-7. Simulated pressures (examples). a) Two example trajectories that were aimed at the respective subject's $M1_{hand}$. b) One example trajectory that was aimed at the respective subject's $M1_{hand}$.

2.5 Discussion

2.5.1.1 Experiment 1

2.5.1.2 No tUS-MEPs

We were unable to elicit tUS-induced MEPs at safe intensities. This was the expected outcome, given the lack of MEPs in previous human tUS studies (Ai, Bansal, Mueller, & Legon, 2018). Recent animal model work suggests that motor activation via ultrasound stimulation of motor cortex may not be feasible, proposing that previously reported motor contractions in anesthetized animals likely relied on auditory mechanisms (Guo et al., 2018; Sato, Shapiro, & Tsao, 2018). We did not investigate for potential tUS-MEPs during rest beyond a single pilot subject (data not shown). No tUS-induced MEPs appeared during active contraction trials either.

2.5.1.3 Cortical Silent Period, TMS

Our data found no cSPs that occurred without a preceding TMS-evoked MEP (Figure 2-6), despite structuring the study to facilitate a high prevalence of near-threshold MEPs. As such, this contradicts claims in the literature that TMS-induced cSPs can occur without an MEP (Classen & Benecke, 1995; Davey et al., 1994; Hupfeld, Swanson, Fling, & Seidler, 2020). One explanation for this difference is that a small "stub" MEP could precede reported "MEP-less" cSPs, with its amplitude not surpassing the amplitude of tonic contraction. This is supported in these data by the consistent appearance of an EMG peak within the latency window expected for TMS-evoked MEPs.

If this MEP-cSP dependency is true, this could suggest that cortical silent period is dependent on the recruitment of M1 motor units. TMS preferentially depolarizes axons (Lazzaro, Ziemann, & Lemon, 2008; Lefaucheur et al., 2014; McIntyre & Grill, 2002; Nowak & Bullier, 1998), while tUS has been proposed to preferentially affect inhibitory neurons (H. Kim et al., 2014; Legon et al., 2014; Nguyen et al., 2020; Plaksin et al., 2016; Rinaldi et al., 1991). If these assumptions are true, this could explain why tUS struggled to silence corticospinal output.

To be clear regarding the notion of "stub" trials within our TMS data, we do not believe all TMS trials classified as a "stub" by the algorithm are MEPs. Rather, we believe there are two underlying distributions that fall under the "stub" designation. The first: trials in which there is a TMS-evoked MEP that is shorter than the standard threshold (0.5 mV). The second: trials in which there was an EMG peak produced *by chance*—created by a peak in tonic muscle EMG activity that fell within the expected time window (Figure 2-18).

We must also note: For cSP length determination, we took a conservative approach on brief EMG activity flanked by periods of silence, referred to in the literature as late excitatory potentials (LEPs) (Butler, Petersen, Herbert, Gandevia, & Taylor, 2012; Kallioniemi et al., 2015; Wilson, Thickbroom, &

Mastaglia, 1995). Of the two silent periods flanking an LEP, we included only the first silent period when measuring cSP duration. Since these LEPs appear heuristically as short EMG disruptions of a longer cSP, a visual inspection of the data suggests that ignoring these LEPs would have resulted in less variable cSP durations within blocks (Figure 2-14). For comparison, these LEPs have at times been ignored in past by-hand cSP measurements (Hupfeld et al., 2020).

2.5.1.4 Cortical Silent Period, tUS

Single-burst tUS of the hand area of left motor cortex did not affect tonic muscle contraction of the FDI muscle. Specifically, there were no deviations in gap duration between tonic muscle spikes (Figure 2-5), spectral components (Figure 2-4), or prevalence of EMG peaks (Figure 2-11, Figure 2-12). This is in sharp contrast to the lengthy silent periods from single-pulse TMS.

Since these data revealed no time-locked tUS effects, this leaves open the question whether tUS affects cortical motor circuitry *at these parameters*. Looking to the TMS literature for insight, we know that it *is* possible to induce detectable excitation of motor cortex without a measurable peripheral effect. Specifically, electroencephalography (EEG) recordings during subthreshold single-pulse TMS show significant TMS-evoked potentials, despite a lack of a peripheral MEP (Gordon, Desideri, Belardinelli, Zrenner, & Ziemann, 2018). Given this, it is possible there were tUS effects that did not interact with corticospinal projections—making them undetectable by EMG and therefore undetectable by our experiment. While EEG is not necessarily a more sensitive readout to study all mechanisms, such as for certain corticospinal excitability experiments (Desideri, Zrenner, Gordon, Ziemann, & Belardinelli, 2018), methods like EEG and fMRI that record cortical effects directly could provide a more complete picture of time-locked tUS effects in future investigations.

2.5.2 Experiment 2

2.5.2.1 Cortical Excitability

Our data showed no group difference in M1 excitability in response to tUS, as indicated by no change in MEPs evoked by TMS at the same M1 trajectory. Our data differ from data by Gibson and colleagues that showed increased excitability of M1 after ultrasound exposure (Gibson et al., 2018). There are study design differences that could have driven this disparity. The first is the tUS device used. While we used a 500-kHz single-element focused transducer, *Gibson et. al 2018* used an imaging ultrasound device, which consisted of an array of 80 transducer elements emitting frequencies in a range between 1.53 and 3.13 MHz. This frequency range is noteworthy because acoustic attenuation increases as a function of acoustic frequency (Hayner & Hynynen, 2001; *The Safe Use of Ultrasound in Medical Diagnosis*, 2012; P. J. White et al., 2006). *Gibson et al. 2018* cited papers that used ultrasound imaging

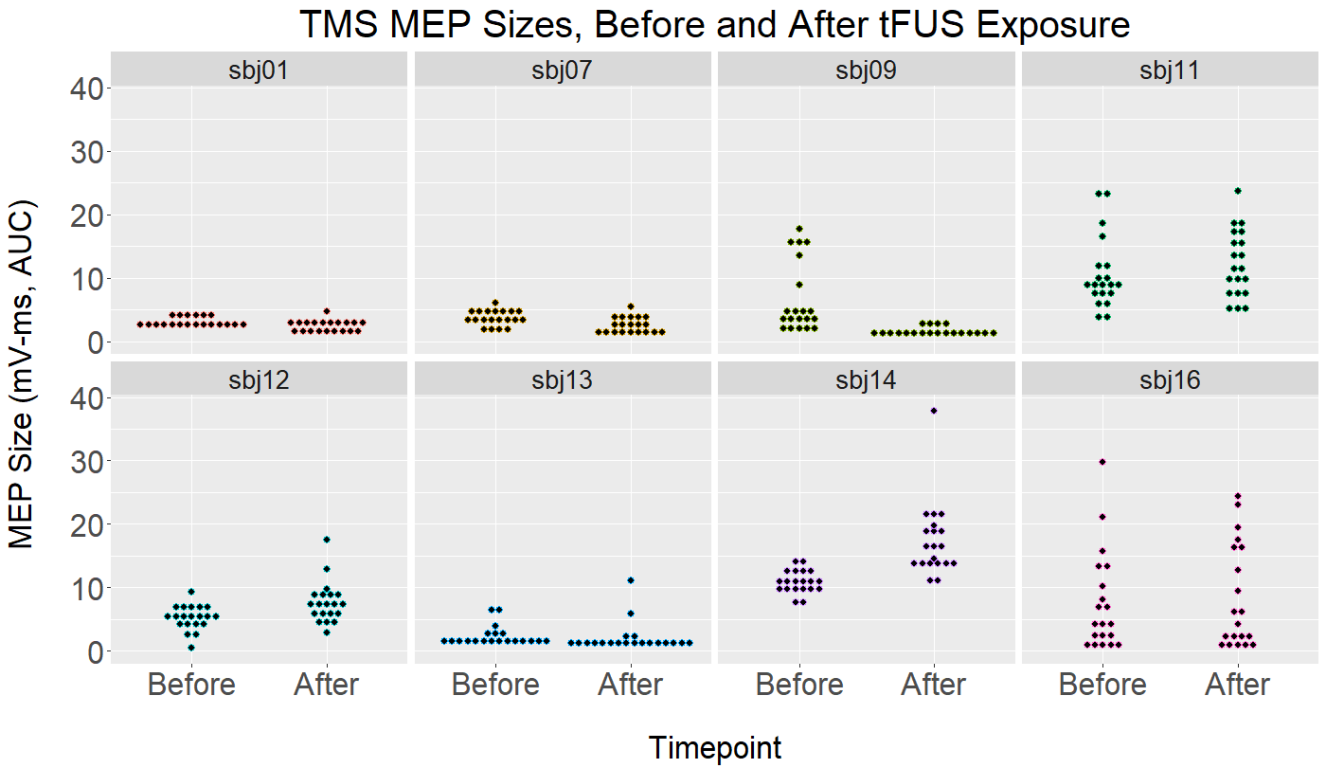

Figure 2-8. TMS MEP sizes, before and after tUS. Each subplot contains data from one subject: trials before and after tUS on the left and right, respectively. Each point marks the size of one MEP (area under the curve, mV-ms). Points are organized into vertical-axis bins to aid in visualization.

devices to image through the skull as evidence of the device's validity for use over M1. However, all studies they cited placed the device over the temporal window—an area of the skull that is significantly thinner than that over M1 (temporal window: ~3 mm; parietal bone: ~6 mm) (Kwon, Kim, Kang, Bae, & Kwon, 2006; Mahinda & Murty, 2009). In fact, measurement of ultrasound propagation through ex-vivo human parietal skull shows that little to no energy is transmitted at frequencies above ~1.5 MHz (K. Hynynen & Jolesz, 1998; O'Brien, 2007; Pichardo et al., 2010; P. J. White et al., 2006).

The second noticeable difference between the two studies is the stimulation protocol. While *Gibson et al.* delivered constant exposure to an ultrasound imaging protocol for 2 minutes, we delivered separate bursts of ultrasound (duration: 300-500 ms each) with long gaps between bursts (8-12 s inter-burst interval)—an interval that was chosen to support the primary aim of this study: investigation for silent periods. Our ~10-second interval is very slow compared to repetitive TMS protocols used to modulate cortical excitability, and it ventures into the intertrial interval range suggested for use to avoid central habituation effect in sensory stimulation studies.(Baumgärtner, Greffrath, & Treede, 2012; Greffrath, Baumgärtner, & Treede, 2007; Warbrick, Derbyshire, & Bagshaw, 2009) If neuromodulation is the aim, future tUS studies may want to use more compressed protocols with shorter inter-burst intervals. A compressed approach was shown to successfully affect tUS targets in non-human primates, as shown by the reduction of resting-state fMRI connectivity following a 40-s tUS protocol (pulse repetition frequency: 10 Hz; pulse length: 30 ms) (Folloni et al., 2019; Verhagen et al., 2019). These non-human primate studies showed effects lasting up to two hours after stimulation. However, they also used tUS intensities, 24.1-31.7 W/cm^2, that were significantly higher than the levels used here or any other human tUS study (human max.: 4.9 W/cm^2 in *Legon et al. 2014*). While histological examination in these studies revealed no microstructure damage, the protocol in question still corresponds to a mechanical index of ~3.6—higher than the 1.9 maximum allowed by the FDA for diagnostic imaging (Şen, Tüfekçioğlu, & Koza, 2015; *The Safe Use of Ultrasound in Medical Diagnosis*, 2012). Given that the most

robust tUS effects seem to occur at high intensity levels, future studies will need to carefully explore whether consistent, behaviorally relevant tUS effects are feasible at intensities safe for human exposure. Replication of repetitive tUS protocols, at lower intensities, will likely be the first step.

2.5.2.2 Exposure vs. Excitability

With this small sample size (n = 8), we saw no correlation between $M1_{hand}$ exposure and cortical excitability change, though the calculation of this correlation was also low-powered. This conclusion is to be expected since this study was not designed to investigate such a correlation, with $M1_{hand}$ exposure effectively stratified into two levels depending on whether the $M1_{hand}$ target was used once or twice (i.e. whether it was the primary NIBS target, "TMS target"). Studies that wish to investigate potential correlation effects of exposure levels would need to expose participants at a variety of different levels and have a larger sample size than used here to increase statistical power compared.

While we performed acoustic simulation on 907 cm^3 volumes (~300-350 cm^3 of which were grey or white matter), we still chose to tabulate cumulative exposure for a single location: $M1_{hand}$. $M1_{hand}$ was chosen because it is the most reasonable small-volume, easily identifiable cortical area that is known to play a direct role in hand muscle contraction. It is, however, possible that directly targeting $M1_{hand}$ may not be the ideal choice for modulating voluntary muscle contraction with tUS. This notion of placement is especially important given the spatially precise nature of tUS compared to a TMS or transcranial electrical stimulation—especially with a small, focused ultrasound transducer as used here.

2.5.3 tUS and M1

While there could be multiple causes, one potential explanation could lie in cytoarchitectural differences between brain regions. Crucially, motor cortex has significantly lower neuronal density compared to somatosensory and visual cortex (Atapour et al., 2019; Beaulieu & Colonnier, 1989; Collins, 2011; Collins, Airey, Young, Leitch, & Kaas, 2010). As such, for a tUS pressure field of a given size, the number of

individual neurons that fall within the focus would be lower in M1 compared to primary somatosensory (S1) or primary visual cortex (V1). This disparity could leave M1 neurons at a relative disadvantage for reaching thresholds to create detectable systems-level effects from tUS exposure. Additionally, the inherent cytoarchitectural and circuitry differences between 'output' cortical regions, like M1, compared to 'input' cortical regions, like S1 and V1, could likely have a significant role.

2.6 Conclusion

We performed neuronavigated tUS and TMS of primary motor cortex (M1) in healthy volunteers. We found no concurrent change in finger EMG activity from tUS of M1 during voluntary muscle contraction. We also did not find any consistent effect of tUS M1 exposure on motor cortex excitability, as measured by single-pulse TMS of M1. We performed acoustic simulations using structural MRI of the study participants to estimate the degree and location of ultrasound intracranially. Using these simulations, we were unable to find any correlation between cumulative ultrasound exposure of the M1 hand area and M1 excitability change.

Within the TMS-only data, our data suggest that cortical silent periods (cSP) may be contingent on a motor evoked potential (MEP) occurring at cSP onset, though at times the MEP may elude visual detection due to a small amplitude that does not rise above the level of tonic muscle activity. This finding questions previous reports of cSPs without MEPs (Classen & Benecke, 1995; Davey et al., 1994; Hupfeld et al., 2020).

While the negative tUS results reported here mirror struggles other investigators have shown when attempting to elicit measurable modulation of M1 by tUS, this was also a pilot study with small sample sizes (n = 8; n = 10). As such, clearer results may emerge with larger datasets or changes in methodology.

2.7 Additional Figures

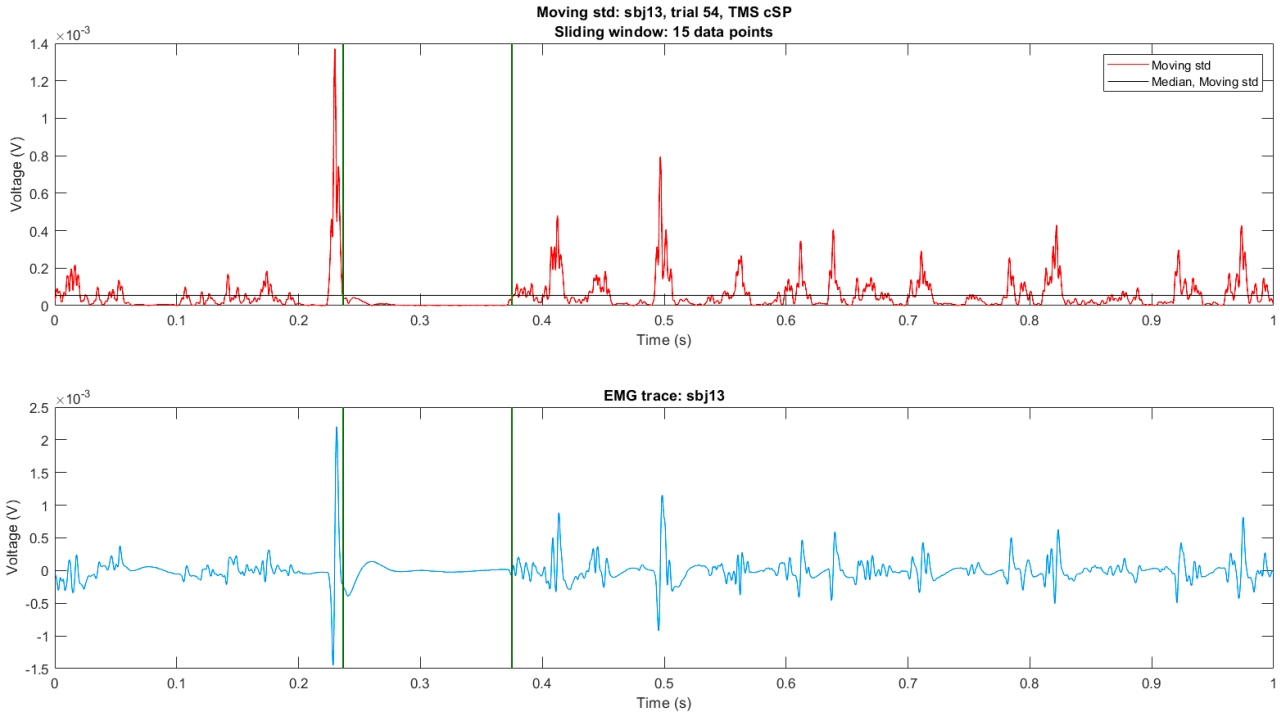

Figure 2-9 Visualization of the automated cSP detection method. Top) Sliding window standard deviation trace of a single trial EMG trace. The black horizontal line marks the detection threshold. The vertical green lines mark the beginning and end of the detected cSP. Bottom) The original high-pass filtered EMG trace.

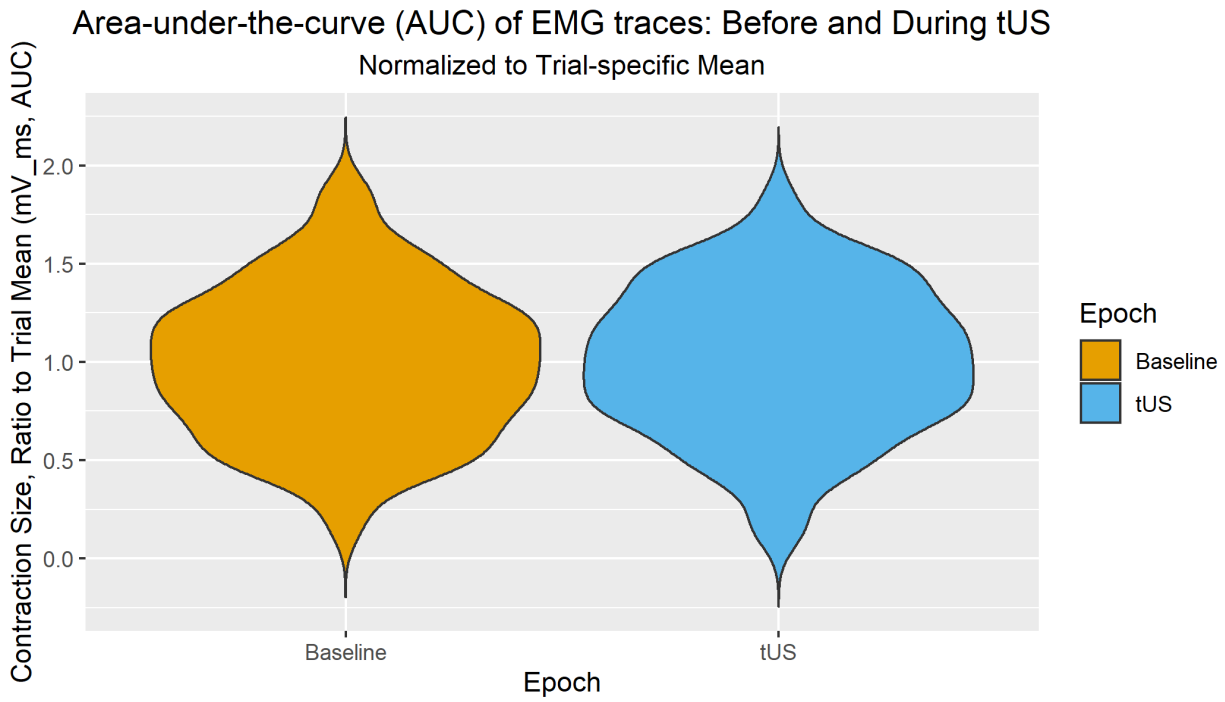

Figure 2-10. Area-under-the-curve of tUS traces. Level of EMG activity during different sections of tUS trials. Left) Baseline, -200 to -50 ms before onset. Right) 0 to 150 ms after tUS onset (first 150 ms of tUS exposure). Values were normalized via dividing by the trial mean.

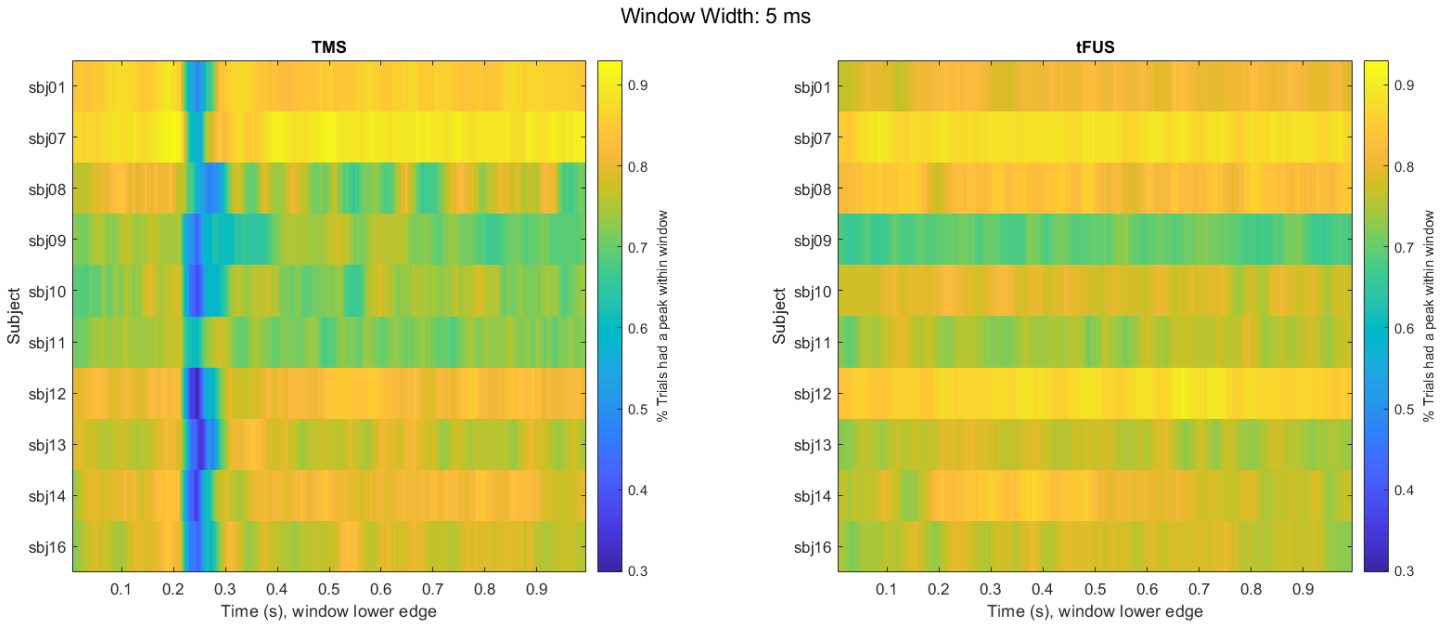

Figure 2-11. Prevalence of EMG peaks. A sliding window approach (1-ms steps) checked if an EMG peak occurred during a 5-ms time window following that point. Peaks were detected using findpeaks() function in MATLAB. Each row contains data for all trials per subject. Color shows percentage of trials that had a peak during that time window. Percentage data was smoothed with a moving mean (~6-ms window). Left) TMS trials. Right) tUS trials. EMG traces were high pass filtered at 10 Hz.

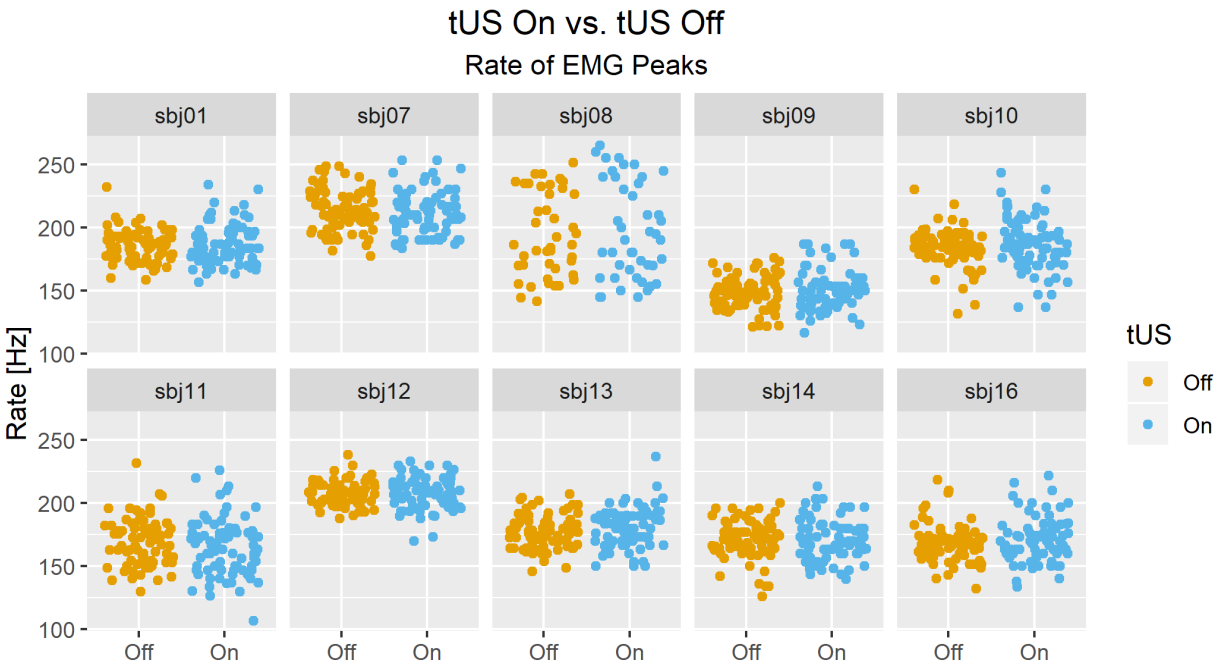

Figure 2-12. Rate of EMG peaks during a single tUS trial. One dot per trial per condition ('Off' and 'On'). EMG traces were bandpass filtered to 10-800 Hz.

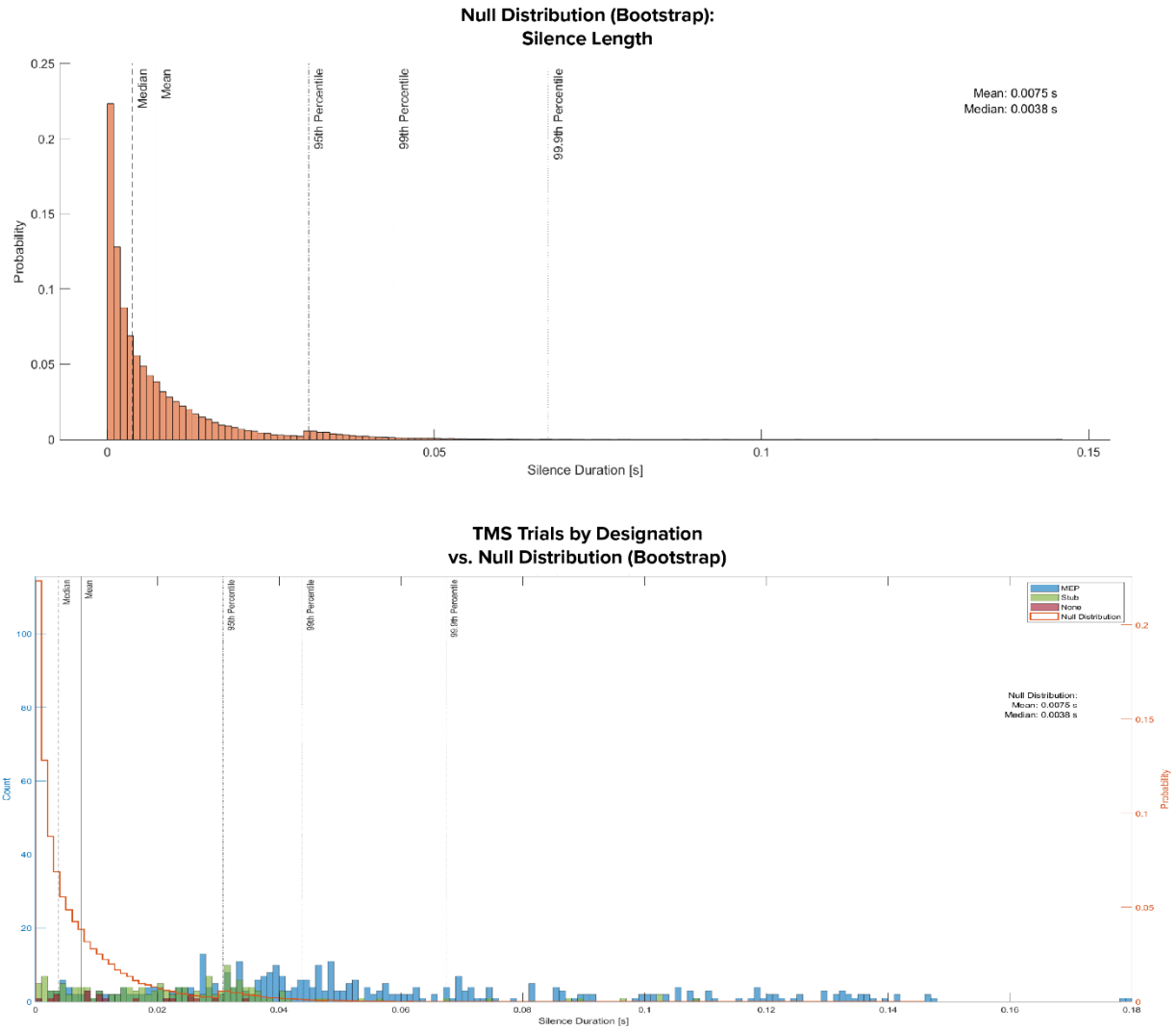

Figure 2-13. Bootstrapping a null distribution for silence duration. ***Top:*** *Distribution of silence lengths when cSP length algorithm is run from different time points along each EMG from a contracting finger. Sliding window approach was used to bootstrap these values, with a sliding window step size of 0.001 seconds. Histogram bin width 0.001 seconds. "Null" data were the one-second tonic contraction trials during tUS exposure. tUS trials were deemed valid as null EMG traces since we saw no change in EMG traces between tUS on vs. tUS off (Figure 2-4, Figure 2-5, Figure 2-12). The first and last 50 ms were removed to avoid boundary effects. 686,457 sliding window samples.* ***Bottom:*** *Lengths of silent periods for trials grouped into three categories: a clear MEP was present ("MEP", blue), a small peak that may have been an MEP was present ("Stub", green), and no detectable peak was present ("None", red). Null distribution (see Top) overlayed in orange. MEP: 361. Stub: 151. None: 18.*

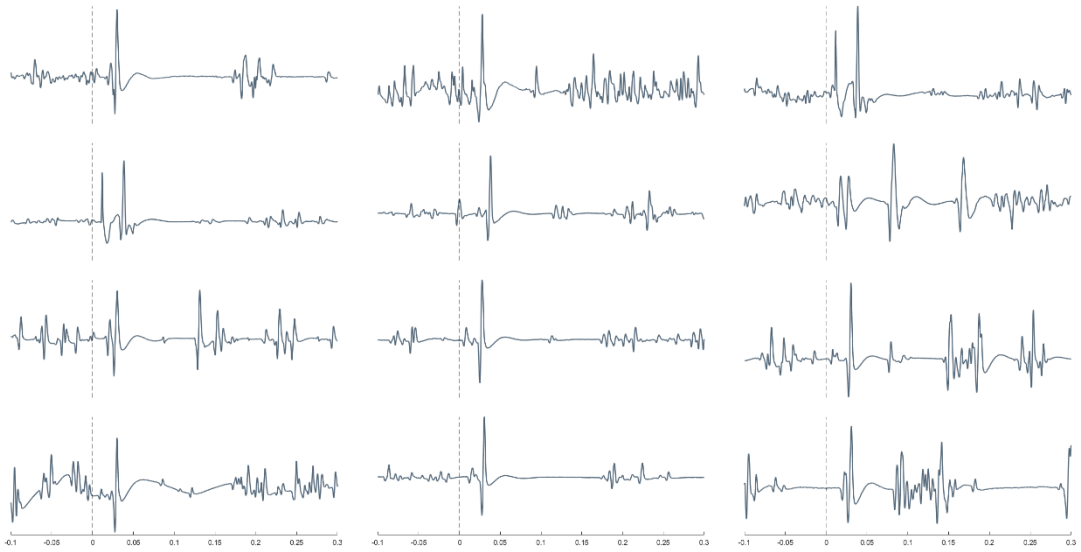

Figure 2-14. Examples of cSPs with late excitatory potentials (LEPs). X-axis: Time [s]. TMS onset at 0 s. Examples are from multiple subjects.

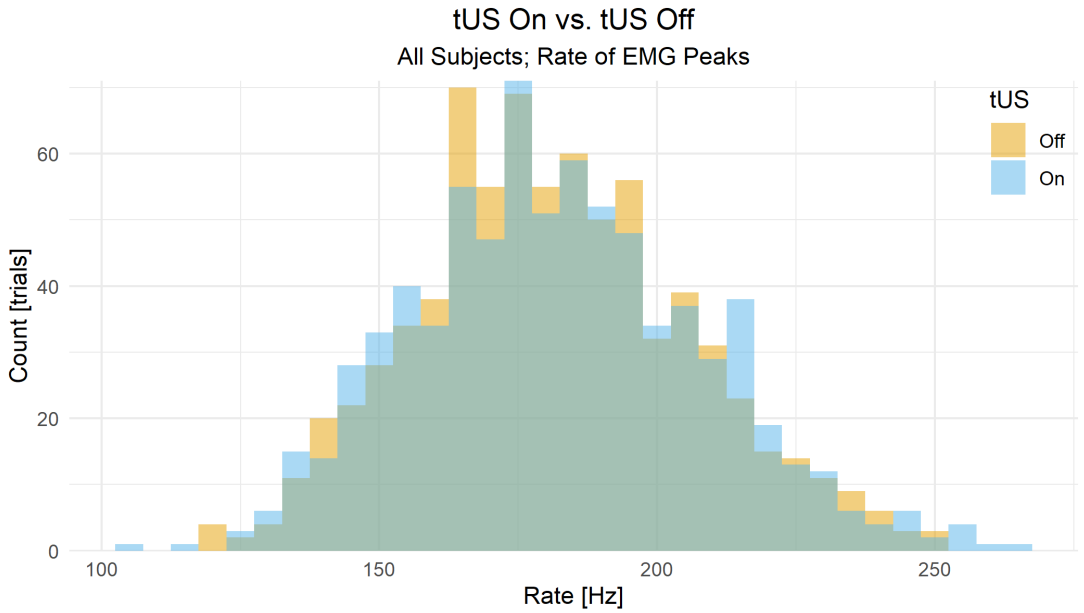

Figure 2-15. Distributions of rate of EMG peaks during a single tUS trial. All subjects; all trials. EMG traces were bandpass filtered to 10-800 Hz. Same data as shown per subject in Figure 2-12. Difference of the mean rates of EMG peaks were only marginally lower for tUS 'On' vs. tUS 'Off' (Delta: -0.91 Hz; 95% CI: -1.99, 0.16 Hz; p = 0.095; paired t-test).

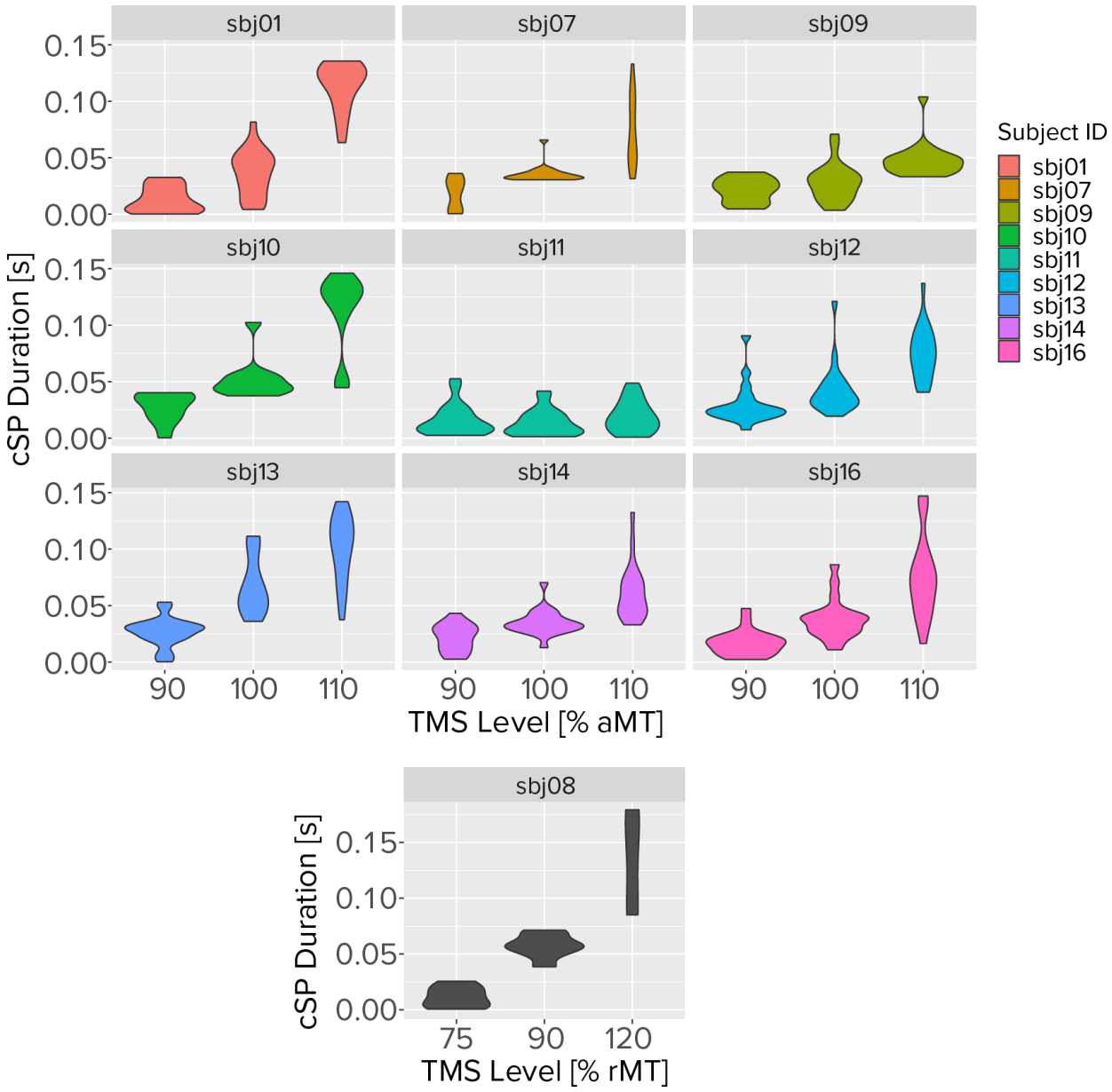

Figure 2-16. Violin plots of TMS-evoked cSP durations separated by research participant ("Subject ID"). Same data as shown in Figure 2-3. sbj08 subject was excluded from Figure 2-3 since their cSP trials were not used in analysis (due to use of different TMS levels). Non-zero silence durations were recorded for 90% aMT for two reasons. First, there are inherent gaps between EMG peaks during tonic contraction, which average ~7.5 ms with our algorithm and our data (Figure 2-13, Top). Second, TMS of M1 results in a distribution of responses, with some trials reaching MEP and cSP threshold while other trials do not (i.e. motor thresholds are never hard cutoffs).

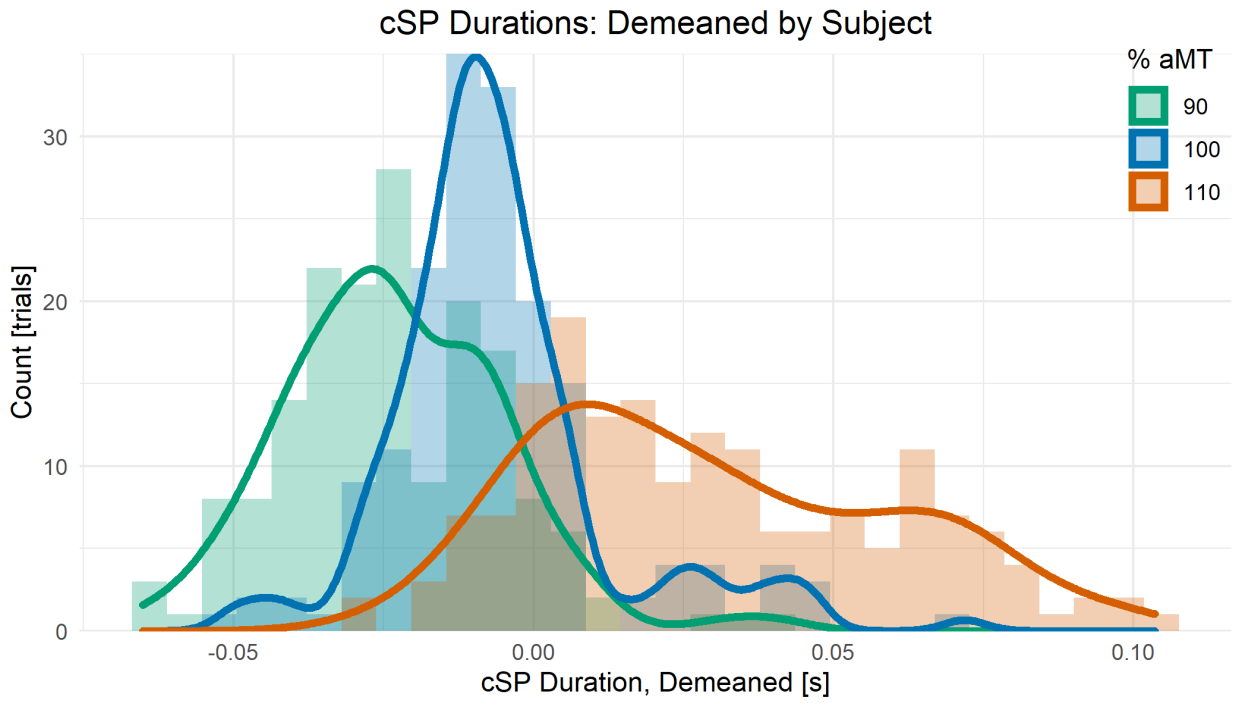

Figure 2-17. cSP durations demeaned by subject mean. Histograms and density plots shown by % aMT. Welch's t-tests performed as post-hoc tests confirmed cSP duration increased by % aMT ($p < 0.001$, all pairs). For non-demeaned data see Figure 2-3 and Figure 2-16. One subject (sbj08) with whom resting motor threshold was used is not shown here (see Figure 2-16).

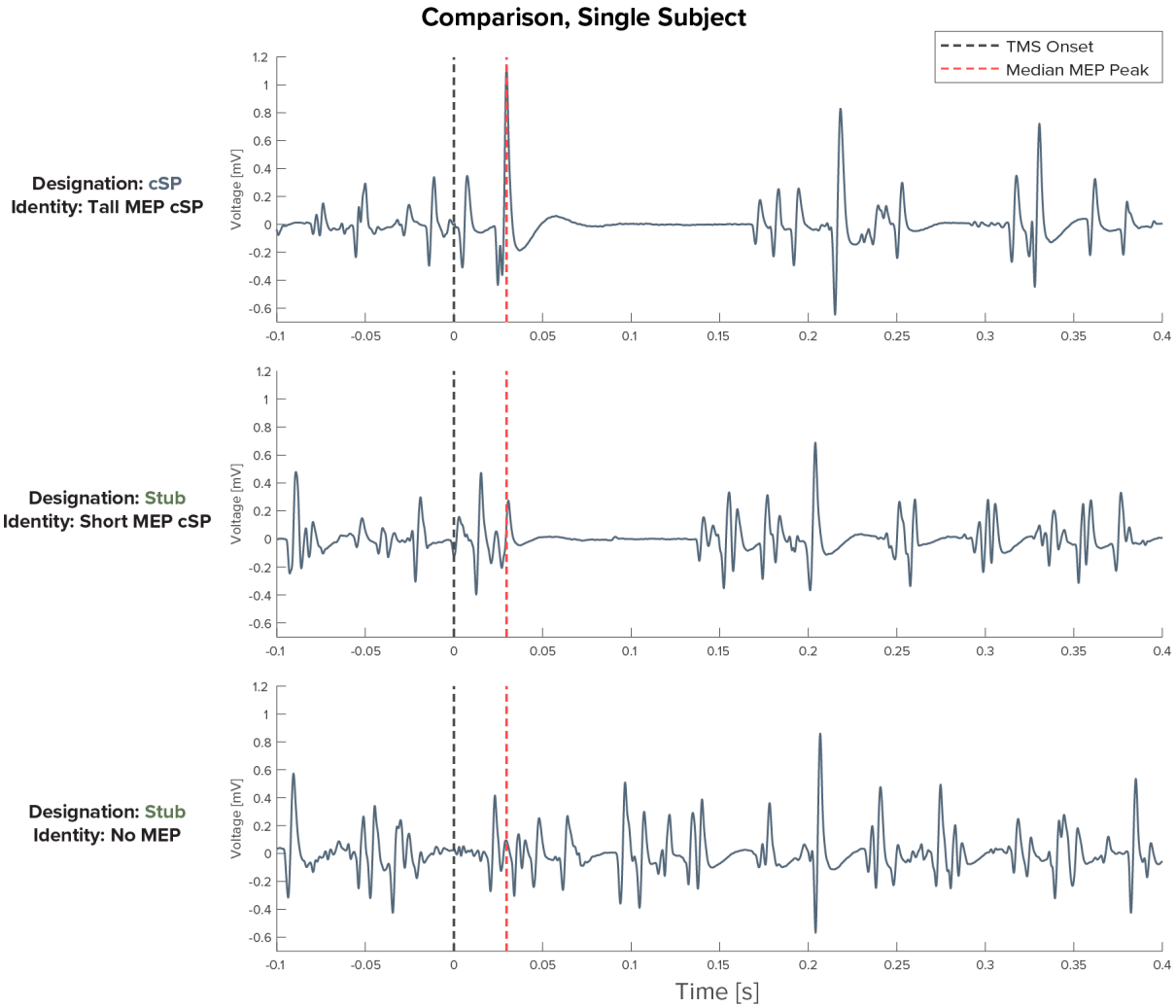

*Figure 2-18. Comparison of three different results from single-pulse TMS during tonic contraction. All three trials are from the same subject. The automated trial designation classified each trial (**Top**, **Middle**, **Bottom**) as: "cSP", "Stub", "Stub". These two distinct examples of scenarios that fall under the "Stub" designation, as determined by the algorithm. This illustrates that there are likely two main distributions of trials that fall under the "Stub" designation. The first: trials in which there is a TMS-evoked MEP that is shorter than the standard threshold (0.5 mV). The second: trials in which there was by chance an EMG peak produced by tonic muscle contraction that fell within the expected time window.*

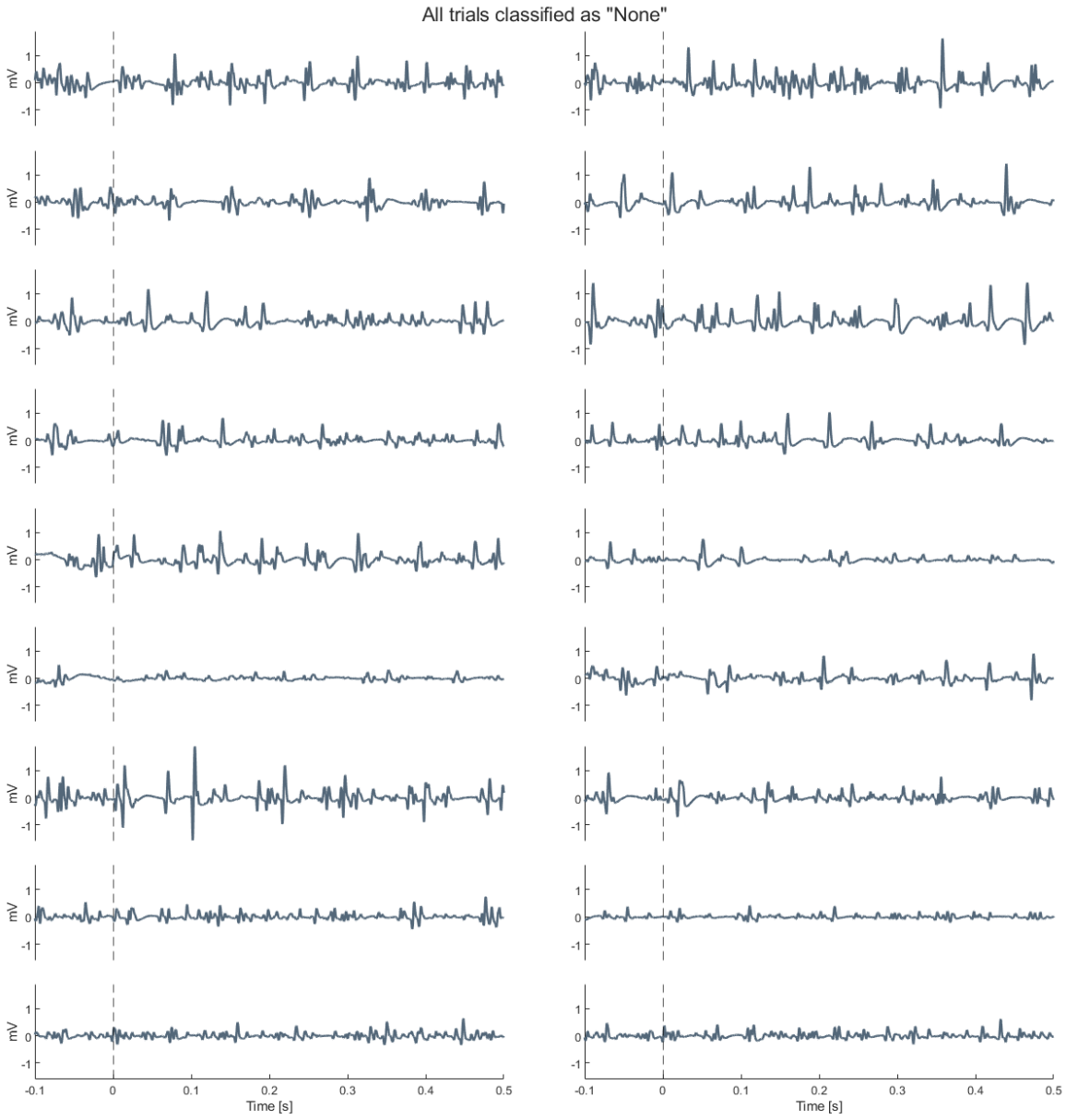

Figure 2-19. All tonic contraction TMS trials designated as "None". TMS onset at 0 s. "None" trials had no prominent EMG peak within the 10-ms search window. Peaks had to be above the 50th percentile for peak prominence and above the 50th percentile for peak width (for EMG peaks within the 1-second trial).

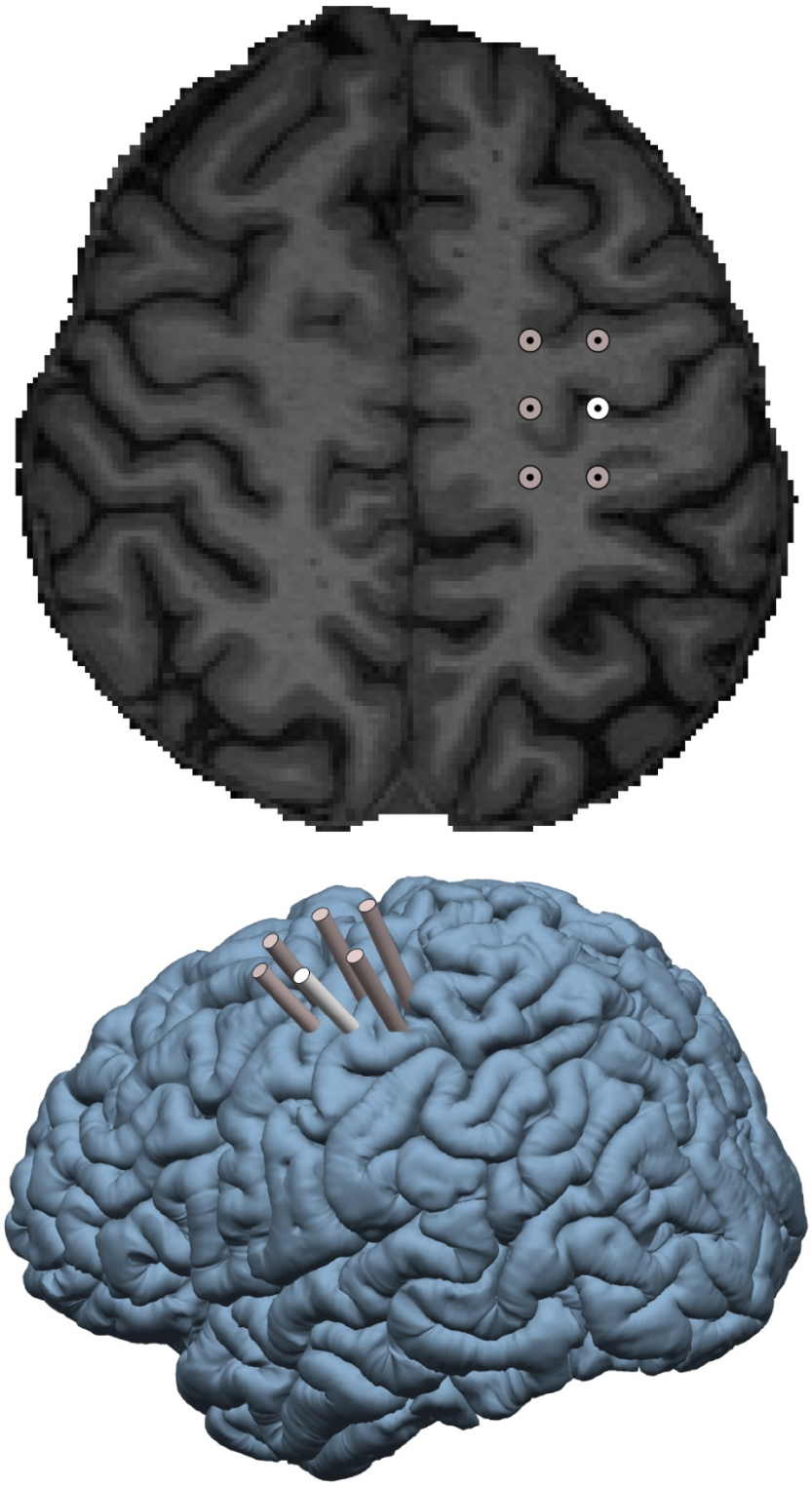

Figure 2-20. TMS search grid and trajectories. Illustration of the TMS search grid used in both 2D and 3D. The grid's origin (white) was placed at MNI coordinates that correspond to $M1_{hand}$ as based on a meta-analysis of fMRI motor experiments: x = −39, y = −24, z = 57 (Mayka et al., 2006). The other five targets on the grid (grey) were in a 12 voxel-width grid (9.6 mm grid interval) around $M1_{hand}$ in subject space. See EMG and NIBS Placement.

Subject	FWHM [mm]			Pressure$_{Peak\text{-}to\text{-}Peak}$ [kPa]			Target
	Average	Dim. 1	Dim. 2	Anywhere	$M1_{hand}$	Target	
sbj01	4.4	4.4	4.4	470	441	441	$M1_{hand}$
sbj01	4.6	4.8	4.4	441	37	399	other
sbj01	4.9	5.0	4.8	406	19	378	other
sbj07	4.5	4.4	4.6	428	386	386	$M1_{hand}$
sbj07	4.3	4.4	4.2	451	23	375	other
sbj07	4.5	4.6	4.4	423	42	376	other
sbj08	4.2	4.0	4.4	418	18	357	other
sbj08	4.0	3.8	4.2	441	21	306	other
sbj09	4.5	4.6	4.4	463	438	446	$M1_{hand}$
sbj09	4.9	5.0	4.8	434	41	414	other
sbj09	4.9	4.6	5.2	414	13	343	other
sbj10	4.4	4.0	4.8	430	15	280	other
sbj10	4.2	4.2	4.2	456	34	326	other
sbj10	3.9	3.6	4.2	439	13	316	other
sbj11	4.6	4.6	4.6	374	361	361	$M1_{hand}$
sbj11	5.5	5.0	6.0	302	33	252	other
sbj11	5.6	5.8	5.4	292	11	266	other
sbj12	3.7	3.4	4.0	397	348	348	$M1_{hand}$
sbj12	4.4	4.4	4.4	362	25	268	other
sbj12	4.6	4.8	4.4	367	10	274	other
sbj13	4.4	4.2	4.6	430	395	395	$M1_{hand}$
sbj13	5.3	5.8	4.8	343	23	272	other
sbj13	5.0	5.2	4.8	361	14	280	other
sbj14	5.1	4.6	5.6	396	26	386	other
sbj14	4.3	4.4	4.2	452	449	449	$M1_{hand}$
sbj14	5.0	5.0	5.0	412	18	372	other
sbj16	5.2	4.4	6.0	386	314	314	$M1_{hand}$
sbj16	4.4	3.8	5.0	379	18	362	other
sbj16	3.2	3.4	3.0	386	22	317	other

Figure 2-21. Table of simulated pressure values for each trajectory used with ultrasound. Data for both experiments included. Included are full width half maximum (FWHM) values [mm] of width of the ellipsoid focus of the focused ultrasound beam. The maximum pressures for three key locations for the simulation are also shown: the maximum pressure anywhere, at $M1_{hand}$, and at the target coordinate used to aim the trajectory. In some cases, the trajectory coordinate and the $M1_{hand}$ coordinate are the same ('Target' column).

Neurological screening questionnaire

- Do you have any active medical, neurological, or psychiatric diagnosis (such as depression, schizophrenia, or bipolar disorder)?
- Do you have a pacemaker, deep brain stimulator, or other implanted electrical device (including intrauterine devices or braces)?
- Do you have, or have you ever had, a significant head injury or neurological disorder (such as a concussion or seizure disorder)?
- Do you have, or have you ever had, any seizures within the past six months?
- Do you have a family history of seizures?
- Do you have, or have you ever had, a history of alcohol or substance dependence?
- Do you have, or have you ever had, any cognitive impairments?
- Do you take any antidepressant medications (such as Prozac, Zoloft, or tricyclic antidepressants)?
- Do you take any antipsychotic medications?
- Do you take any antiviral medications?
- Do you take any amphetamines (such as Adderall)?
- Do you have a history of fainting?
- Do you have a history of migraines?
- Do you have a chronic pain disorder?
- Are you pregnant, or is there a chance you could become pregnant?

Figure 2-22. Full screening neurological health questionnaire used for recruitment. A 'Yes' to any question prevented inclusion in the study.

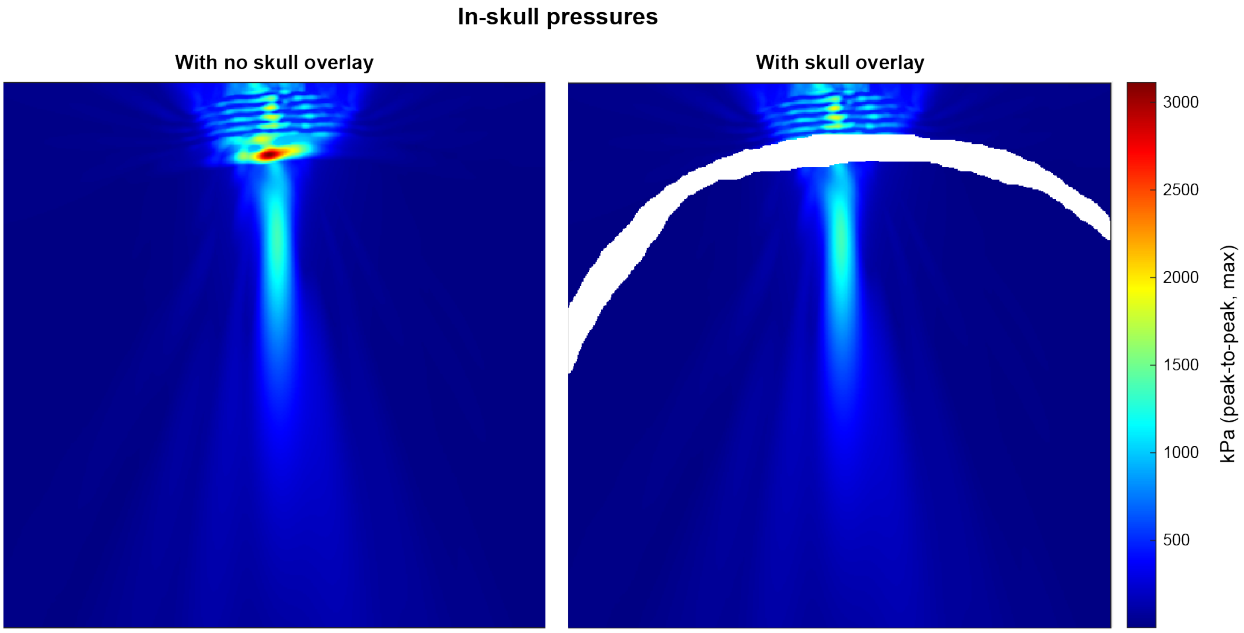

Figure 2-23. In-skull pressures. Figure shows how the highest pressures during transcranial ultrasound simulation occur inside the skull. This disparity is why only in-brain pressures are shown in other figures in this dissertation, since excluding in-skull pressures allows for a larger range of the colormap to be designated to in-brain pressures.

2.7.1 Exposure Formula

$$\sum_{traj\,=\,1}^{n} P_{traj} \times Time_{traj}$$

$\boldsymbol{n}$: Number of tUS trajectories

$\boldsymbol{P_{traj}}$: Pressure (est.) at $M1_{hand}$ voxel

$\boldsymbol{Time_{traj}}$: tUs-on time for that trajectory

2.7.2 k-Wave Parameters

2.7.2.1 Medium Properties

	Density [kg/m3]	Speed of Sound [m/s]	Alpha Coefficient [dB/(MHz^{y} cm)]
Skull	1732	2850	8.83
Brain	1546.3	1035	0.645946
Water	998	1482	6.7403×10^{-5}

Alpha Power (y): 1.43

3 TUSX: AN ACCESSIBLE TOOLBOX FOR TRANSCRANIAL ULTRASOUND SIMULATION

3.1 ABSTRACT

Normally, the complicated nature of acoustic simulation makes it infeasible for most research groups doing individual transcranial ultrasound studies, hindering interpretation of results and complicating the determination of safety limits. We present here an open-source MATLAB toolbox to perform acoustic simulations using subject-specific medical images for transcranial ultrasound experiments. This toolbox, Transcranial Ultrasound Simulation Toolbox (TUSX), consists of an integrated processing pipeline that takes in structural MR or CT images, processes them for accurate simulation, and runs the simulations using k-Wave, an existing open-source acoustics package. We describe here the processing TUSX performs, along with its reasoning. We also validate its output using real-world pressure measurements in a water tank.

3.2 INTRODUCTION

The use of ultrasound for non-invasive brain stimulation (NIBS) has been gaining increased attention in recent years, in part due to it offering increased spatial precision compared to other NIBS techniques. For example, a small single-element transducer produces an ellipsoid intracranial focus with a full width half maximum focus of 4 to 7 mm (Deffieux et al., 2013; Lee et al., 2015; Legon et al., 2014; Tufail et al., 2010). Since transcranial ultrasound can be so precise, accurate understanding of where its energy lands is crucial for interpretation of results. Reasonable success with tUS placement can be made with simple geometric targeting. However, skull bone significantly affects tUS pressure fields, sometimes leading to

resulting pressure focuses deviating over a centimeter from the intended target (K. Hynynen & Jolesz, 1998; Lee et al., 2015).

Ultrasonic waves are acoustic waves above the frequency range of human hearing (>20 kHz). Ultrasonic waves mechanically propagate through a medium, with alternating periods of compression and rarefaction (stretching) as the pressure wave passes. The precise nature of this propagation depends on the characteristics of the medium, mainly the speed of sound, density, and attenuation coefficient (α), and the acoustic frequencies involved (Ono, 2020).

The mathematical nature of the interaction of particles interacting in an acoustic wave are well understood (Feynman, Leighton, Sands, & Hafner, 1965). It is this understanding that allows for imaging uses of ultrasound such as sonography and non-destructive ultrasonic testing. As such, the large-scale nature of acoustic waves passing through materials can be modeled with various methods (Cox, Kara, Arridge, & Beard, 2007; Treeby & Cox, 2009). However, the options to perform such simulations are either commercial (e.g. multiphysics engineering simulation software) or accurate and open-source but with a learning curve. An example of the latter is k-Wave, a powerful open-source tool to perform computationally efficient acoustic simulations using a k-space corrected pseudospectral time domain (PSTD) scheme (Treeby & Cox, 2010). Since k-Wave is robust and flexible, it also leaves a novice user open to mistakes that can make implementation challenging or, worse, lead to erroneous results.

Here we present a toolbox that streamlines the process. Using this toolbox, TUSX (Transcranial Ultrasound Simulation Toolbox), simulations can be performed using conventional MRI or CT images with subject-specific precision. First, we outline the primary processing pipeline within the toolbox and discuss the reasoning for key features. Second, we show validation experiments that demonstrate the simulation results predict ultrasound pressure fields with sufficient accuracy. Finally, we discuss applications for this toolbox for transcranial ultrasound research in human participants.

3.3 METHODS

3.3.1 Toolbox Overview

TUSX, which the authors pronounce as “tusks”, takes in a 3D head volume (MR or CT) and isolates the skull using SPM12 (Friston, Ashburner, Kiebel, Nichols, & Penny, 2007) and ROAST (Y. Huang, Datta, Bikson, & Parra, 2019). The skull volume is then scaled using interpolation to a higher resolution, which is necessary for accurate simulation. The location, trajectory, and other parameters of the ultrasound transducer is set by the user. The volume is then rotated such that the transducer trajectory is in line with the computational grid. This rotation improves accuracy by reducing the effect of ‘staircasing’ along the skull edge, which would otherwise cause aberrant interference patterns (J. L. B. Robertson et al., 2017). The skull volume is smoothed at multiple steps (before and after rotation) using morphological image processing (Figure 3-1).

The proper acoustic parameters are then applied to each part of the volume. For MR images, a homogenous skull medium is used. For CT images, a homogenous skull medium or a heterogeneous skull medium derived from the apparent bone density is used (Connor, Clement, & Hynynen, 2002). Additional k-Wave parameters are then set at proper values for the given volume. TUSX then executes the time domain 3D acoustic simulation via k-Wave (Treeby & Cox, 2010), which uses a k-space pseudospectral method. TUSX can execute the simulation via k-Wave’s MATLAB (Mathworks, Inc., Natick, MA) implementation or export it for use in k-Wave’s compiled C++ version for improved performance (Treeby et al., 2012).

3.3.1.1 Scaling

Due to the nature of the numerical methods used to perform the acoustic simulations, final accuracy depends on the spatial resolution of the simulation grid—specifically the ratio of simulation grid points per acoustic wavelength (PPW). Ideally, simulations would be performed at ~10 PPW or greater to

assure no significant loss of accuracy (J. L. B. Robertson et al., 2017). But even for a high-resolution Human Connectome Project T1-weighted structural MRI (voxel width: 0.8 mm), simulating from the untouched volume gives a PPW of ~3.9 (using a tUS-typical 500 kHz source). However, by increasing the spatial resolution of the computational grid through interpolation of the volume, the PPW is raised to ~7.8 and ~15.6 for a 2X and 4X increase, respectively. TUSX uses nearest-neighbor interpolation when scaling skull masks (i.e. binary volumes) and linear interpolation when scaling CT bone density values.

Increasing the resolution used also has the benefit of allowing for more accurate representations of curved (or otherwise non-orthogonal) acoustic sources within the grid, which is also crucial for simulation accuracy (Wise, Cox, Jaros, & Treeby, 2019).

3.3.1.2 Smoothing

The binary skull masks are smoothed by TUSX via morphological image processing in a multi-step process. First, morphological closing (i.e. dilation then erosion) is performed using a spherical structuring elements of radius 4 times the scaling factor (see Scaling). This fills in staircasing effects introduced by the nearest-neighbors interpolation of the initial binary skull mask. Second, morphological opening (i.e. erosion then dilation) is performed using a spherical structuring element of radius 1 times the scaling factor. This removes extraneous jagged protrusions from the skull mask, which are likely not present on the skull.

TUSX also has the option of performing an initial smoothing step before any other skull processing. This option involves morphological closing followed by opening with spherical structuring elements (radius: 1 grid point). While a relatively minor effect, this option is of particular use when reorientation is desired since the step smooths out minor protrusions and divots that could be accentuated by the linear transformation process.

As a whole, the smoothing process serves to assure an accurate representation of a human skull, since the curves of a typical cranium is fairly smooth. The process improves simulation accuracy since smoothing the scaled skull masks reduces the amount of staircasing along the curves of the skull, and such staircasing is a significant cause of simulation error (J. L. B. Robertson et al., 2017).

3.3.2 Skull Mask Creation

3.3.2.1 Skull

TUSX creates a simulation volume by importing a medical image and applying the appropriate acoustic values to each part of the volume. NIfTI-formatted MR or CT volumes are supported for importation. For MRI, users can either import a binary skull mask in which skull voxels have already been selected by a separate tissue segmentation program (e.g. BrainSuite or FSL BET). Alternatively, users with SPM12 installed can feed in a T1-weighted image, and the skull mask will be created automatically using a specific extraction pipeline for skull from the open-source transcranial electric simulation pipeline ROAST (Y. Huang et al., 2019).

For skull masks, the acoustic properties for bulk skull are applied to all points within the skull (i.e. no differentiation between compact and spongy bone). This approach allows for use of structural MRI for simulation, even though it does not have the same detail of bone density as CT. Importantly, the use of skull masks with homogenous skull acoustic properties has been shown to be effective in simulations within the frequencies used for transcranial ultrasound stimulation (Jones & Hynynen, 2016; G. W. Miller et al., 2015; J. Robertson, Martin, Cox, & Treeby, 2017). The acoustic properties to be used for bulk skull can be set by the user or kept to default TUSX values.

3.3.2.2 Brain

TUSX models the entire intracranial space as a homogenous medium, using the bulk acoustic properties of brain tissue. We chose this approach because it has been shown that modeling brain morphology

does not significantly impact intracranial results (J. K. Mueller, Ai, Bansal, & Legon, 2016), due to the relatively minor differences in acoustic properties between intracranial media (i.e. grey matter, white matter, cerebrospinal fluid). As with skull, the user can set desired acoustic properties to be used for brain tissue or use default TUSX values.

3.3.2.3 Volume Dimensions

TUSX crops the simulation volume down to the region of interest to improve performance. Due to the spatially precise nature of tUS, many tUS experiments involve stimulation volumes significantly smaller than the full intracranial space. As such, TUSX can restrict the simulation to the area surrounding the tUS trajectory.

TUSX will also choose precise dimensions integers for best performance. Specifically, the computations performed by k-Wave involve fast Fourier transforms, which works best on powers of two or other integers with low prime factors (Treeby & Cox, 2010). TUSX executes this through a combination of removal of single slices to avoid odd integers, cropping, and the selection of the thickness for the perfectly matched layer (PML), which surrounds the volume to prevent waves from wrapping to the other side of the volume.

3.3.3 Transducer Creation

Placement of the ultrasound transducer within the simulation grid is straightforward with TUSX. The user provides two coordinates in NIfTI voxel space: one for the center of the transducer face and one to set where the transducer is facing. The use of NIfTI voxel space significantly streamlines the process of placement for researchers, who are likely already working with NIfTI coordinates for other aspects of their projects.

An example workflow is as follows. 1) A researcher chooses a cortical ROI in their preferred imaging software (e.g. an fMRI hotspot or anatomical marker). 2) The researcher uses their preferred software to

select a point on the scalp such that the transducer would face the ROI. 3) The scalp coordinate is placed into TUSX as the 'transducer' coordinate, and the ROI coordinate is input as the targeting coordinate.

Transducer size, shape, focal length, and acoustic frequency are also set by parameters provided by the user. TUSX creates the single-element transducer pressure source as a disc or curved spherical cap within the simulation grid (k-Wave function: *makeBowl*) (Ling, Martin, & Treeby, 2015). When a focused transducer is desired, TUSX performs beam forming by setting the pressure source to a spherical cap with a radius of curvature of the desired focal length. To improve focusing even further, the temporal delay of the sinusoidal pressure traces emitted from each source point are then adjusted to better match their aliased positioning on the orthogonal grid (k-Wave function: *focus*) (Eleanor Martin, Ling, & Treeby, 2016).

3.3.4 Validation: Water Tank

Pressure measurements were taken in an acrylic water tank filled with degassed deionized water. Measurements were made in a 3D volume surrounding the focus of the transducer pressure field. Measurements were done with two setups: with a skull analogue between the transducer and the hydrophone and with nothing between the transducer and the hydrophone (free water).

3.3.4.1 Ultrasound Equipment

A 500-kHz focused piezoelectric transducer (Blatek Industries, Inc., State College, PA) was used for all water tank measurements. The cylindrical transducer had a diameter of 3 cm and a focal point of 3 cm. The transducer was secured in a custom 3D-printed mount, which was affixed to the measurement rig. This transducer was chosen because it is representative of models used in various human transcranial ultrasound stimulation experiments (e.g. Legon et al., 2014; Heimbuch et al., 2021).

The transducer was driven by 500-kHz sine-wave voltage pulses from a waveform generator (33500B Series, Keysight Technologies, Santa Rosa, CA). Voltage pulses were amplified by a 50-dB radio

frequency amplifier (Model 5048, Ophir RF, Los Angeles, CA). A 3-dB fixed attenuator was attached in line following the amplifier.

3.3.4.2 Measurement Equipment

Time-varying pressure traces were recorded via a hydrophone placed orthogonal to the face of the transducer (1 mm, Precision Acoustics Ltd, Dorchester, UK). The pre-amplified signals were sampled at 10 MHz by a PCI oscilloscope device (PCI-5105, National Instruments, Austin, TX), which were recorded using LabVIEW (National Instruments). Pressures were sampled across a three-dimensional volume using a micromanipulator, with multiple pressure traces sampled at each point on the sampling grid. Duplicate pressure traces were averaged offline in MATLAB to get a single average pressure trace per grid point per setup.

3.3.4.3 Skull Analogue

The skull analogue was a 4.6-mm thick polytetrafluoroethylene (PTFE) sheet (ASTM D3308) (Figure 3-2). We chose to use a flat analogue to create a best-case scenario for a one-to-one match between the real-world setup and its representation in simulation space—in this case an orthogonal grid. Specifically, the representation of a curve (e.g. a plastic analogue with the radius of curvature of a typical cranium) would introduce aliasing artifacts (see Smoothing).

To counteract curling caused by the fabrication process, the PTFE sheet was clamped between two steel plates and placed in a laboratory oven overnight. The PTFE was then supported with steel brackets. The PTFE was placed 4.8 mm from the transducer face.

3.3.5 Validation: Simulation

3.3.5.1 Simulation Grid

For validation experiments, acoustic simulations were performed via TUSX that matched conditions present in the real-world water tank measurements (Validation: Water Tank). Simulations were

performed using a grid spacing of 0.2 by 0.2 by 0.2 mm, which matched the highest spatial resolution used for water tank measurements. A NIfTI mask volume (dimensions: 236 x 236 x 492 voxels) that matched the setup of each tank experiment was fed into TUSX in place of an MR or CT head volume (i.e. a 4.6-mm thick mask layer for the PTFE experiment and an empty volume for the water experiment). PML was set to 10 grid points, creating a final simulation grid of 256 by 256 by 512 grid points.

The pressure source for the validation experiment was set to mirror the transducer used in the water tank. This consisted of a focused source with a 32-mm focal length at 500 kHz (see Transducer Creation), with the face of the transducer oriented orthogonal with the computational grid. A focal length of 32 mm, rather than the manufacturer specification for the transducer of 30 mm, was chosen to better match the water tank data when measured in free water (Figure 3-8). Simulations were performed at a temporal interval of 285 temporal points per period (PPP) for a Courant-Friedreichs-Lewy (CFL) number of 0.0519, which is well within guidelines for accurate simulation using k-Wave's pseudospectral time domain scheme (J. L. B. Robertson et al., 2017).

3.3.5.2 Acoustic Properties for Validation

Speed of sound of the water in the tank at the time of each recording was calculated by the mean delay arrival time between sequential sample points in the Z axis (away from the transducer) (~1502 m/s), since the distance between sample points was known (0.4 mm for speed of sound measurements). These calculations were with mean pressure traces taken from multiple sequential samples, and delays were found using cross-correlation with the input voltage trace. Density and attenuation were set to referenced values (density: 998 kg/m^3; $2.50x10^{-5}$ dB/cm) (Duck, 1990).

Speed of sound of the PTFE was set using a referenced value: 1310 m/s (Ono, 2020). Density and attenuation of PTFE were set to manufacturer specifications and a referenced value, respectively (density: 2131 kg/m^3; 7.36 dB/cm) (Ono, 2020).

3.3.6 Validation: Comparison

3.3.6.1 Alignment

Comparison between volumes of measured water tank pressures and simulated pressures were enabled by aligning the two grids based on distance from the ultrasound transducer (real or simulated). Spatial calibration for the water tank measurement grid was performed by calculating the distance of central grid points from the delay between signal and pressure onset, since the speed of sound was known (see Acoustic Properties for Validation).

3.3.6.2 Error Metrics

In addition to visual inspection of aligned slices, comparisons between water tank and simulation results were aided with two error metrics: spatial deviation of the focus and the full width at half maximum (FWHM) of the focus. Specifically, we used the center of mass of the -3 dB focus area (i.e. center of mass above ~79% of the maximum of the 3D volume) and the FWHM in the X- and Y-planes averaged.

3.4 Results

3.4.1 Water Tank Validation

3.4.1.1 Free Water

We compared the results of a 3D acoustic simulation prepped through TUSX that matched the setup of a 3D pressure measurement tank in free water. Results show that the simulation produced a pressure field that closely matches the real-world pressure field (Figure 3-3). The center of mass of the -3 dB focus of the real-world transducer was at a depth of 29.6 mm, while the parameter-matched simulation

showed a center of mass at 30.1 mm (delta: 0.48 mm) (Figure 3-6). The FWHM of the real-world transducer focus was 4.6 mm, while the simulated focus had a FWHM of 4.0 mm.

3.4.1.2 Skull Analogue

We also compared a parameter-matched simulation to a water tank measurement in which a flat skull analogue (PTFE, 4.8 mm) was placed against the transducer. This comparison also showed a close match between simulated and measured pressure fields (Figure 3-4). The center of mass of the -3 dB focus of the 'transcranial' pressure field was at a depth of 30.5 mm, while the parameter-matched simulation showed a center of mass at 30.8 mm (delta: 0.29 mm) (Figure 3-7). FWHMs mirrored those in free water (water tank: 4.6 mm; simulation: 4.0 mm). In the water tank pressure field, we did observe some deviation of the pressure field from the Z axis. This is likely due to residual warping in the PTFE and/or imperfect alignment of the transducer by the 3D-printed mount.

3.5 Discussion

We have created a MATLAB toolbox, TUSX, that streamlines the process of performing acoustic ultrasound simulations with subject-specific medical images for transcranial ultrasound experiments. In addition to detailing the processing steps performed by TUSX to enable accurate simulations, we have validated the accuracy of TUSX (and the acoustic simulation package it uses, k-Wave) via real-world measurements in a water tank.

3.5.1 Advantages of TUSX

3.5.1.1 CT vs. MRI for Transcranial Ultrasound Simulation

The support for use of MRI for acoustic simulations, over simply CT, significantly broadens the accessibility of TUSX. CT is the standard for calculation of phase correction in high-intensity focused ultrasound (HIFU) for tissue ablation, but the desire to avoid radiation exposure for healthy volunteers makes the acquisition of MRI a more appealing option—though CT has been used for acoustic

simulation in two non-clinical tUS studies (Lee et al., 2015; Lee, Kim, et al., 2016). Beyond radiation considerations, MRI is more feasible to acquire, since many neuroscience labs have existing MRI access and experience. While MR cannot directly derive bone density as CT can, MRI has already been validated as an adequate reference for transcranial focusing of ultrasound (K. Hynynen & Sun, 1999; G. W. Miller et al., 2015; J. Robertson et al., 2017; Wintermark et al., 2014), with results approaching that of CT. Especially considering that the margin of error for tUS is likely higher than HIFU aiming to ablate precise tissue volumes (e.g. specific thalamic nuclei), we believe the use of MRI provides adequate accuracy for acoustic simulations for tUS studies.

3.5.1.2 Reorientation

The feature to realign the skull volume in TUSX such that the ultrasound trajectory is orthogonal to the computational grid should provide for improved, consistent results for tUS targets that necessitate trajectories at oblique angles. This is because reorientation of the volume, along with subsequent smoothing, avoids having the ultrasound pressures interface with the skull at aliased portions of its curvature, and such 'staircasing' has been noted as the most serious cause of error in previous investigations of acoustic simulation accuracy (J. L. B. Robertson et al., 2017). As an additional tangential benefit, reorientation to an orthogonal trajectory could also improve the performance of the PML, since the PML performs better on waves of low angle of incidence (J. L. B. Robertson et al., 2017).

3.5.1.3 3D Simulations

We chose to support 3D simulations with TUSX, compared to 2D simulations using slices through a 3D volume, for two reasons. First, simulating in 3D should provide a more accurate representation of the real pressures and exposures created during tUS. Second, the preparation of accurate 3D simulations has an additional degree of complexity compared to 2D. As such, a tool for 3D simulations should hopefully provide the most help to researchers.

3.5.1.4 Ease of Use

For a novel user performing simulations of transcranial ultrasound, TUSX greatly simplifies performing k-Wave acoustic simulations compared to k-Wave alone. It saves the user significant labor processing image volumes, placing ultrasound sources, and researching the necessary acoustic and k-Wave parameters for accurate transcranial simulations.

3.6 CONCLUSIONS

Since skull morphology varies highly between individuals, variations in skull thickness and shape result in equally varied intensity levels and foci location following skull transmission of ultrasound. As such, having access to estimations of in-tissue intensities in each research participant is helpful for both safety and interpretation of results. TUSX lowers the high barrier to entry for transcranial ultrasound researchers to include acoustic simulation in their projects.

tUS is still a novel field, and the field is still developing a collective understanding of what neural responses can consistently be elicited by tUS and what tUS parameters it takes to do so. This need to synthesize optimized tUS parameters has been increasingly brought forward by members of the field in the past few years. Our hope is that by enabling more frequent reporting of in-brain tUS pressures and locations, we can more rapidly move toward that goal.

3.7 FIGURES

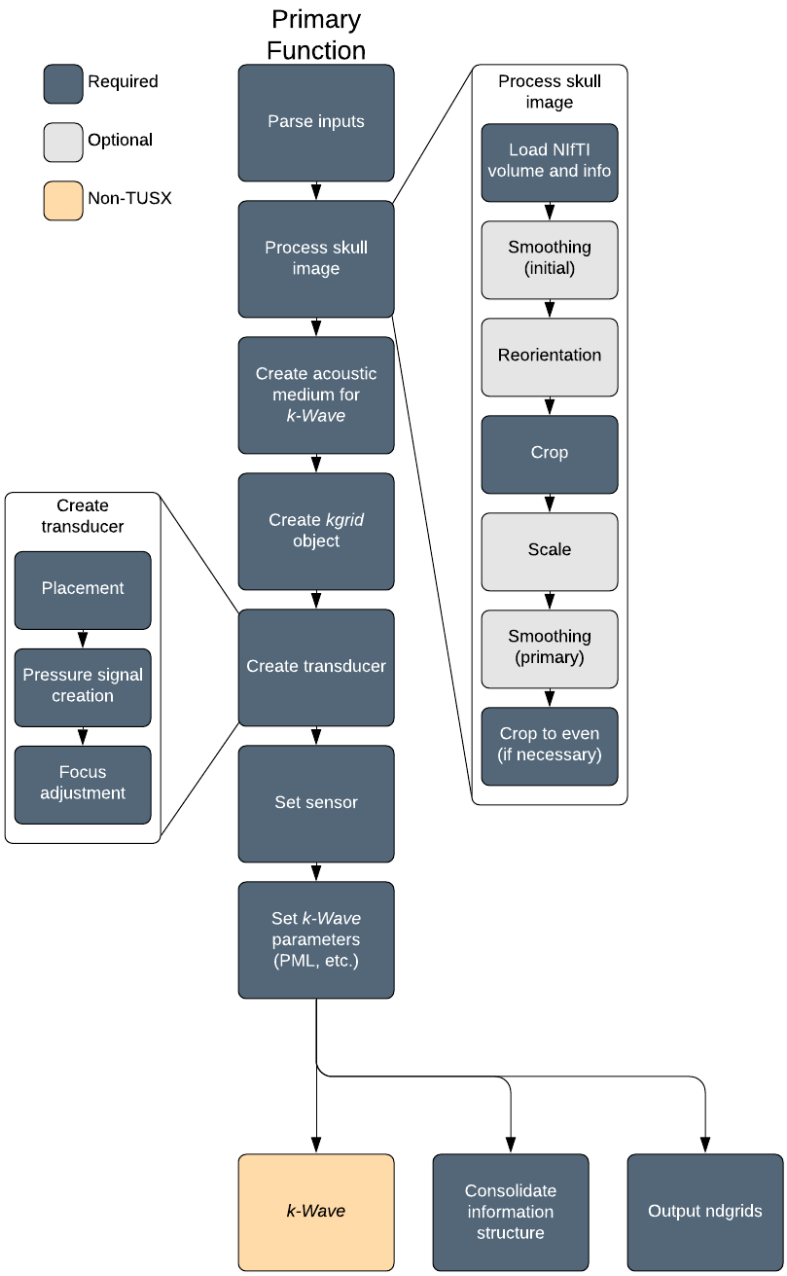

Figure 3-1. Diagram of primary TUSX pipeline. Primary Function) Major steps of the pipeline. Details for "Process skull image" and "Create transducer" steps are in breakout sections.

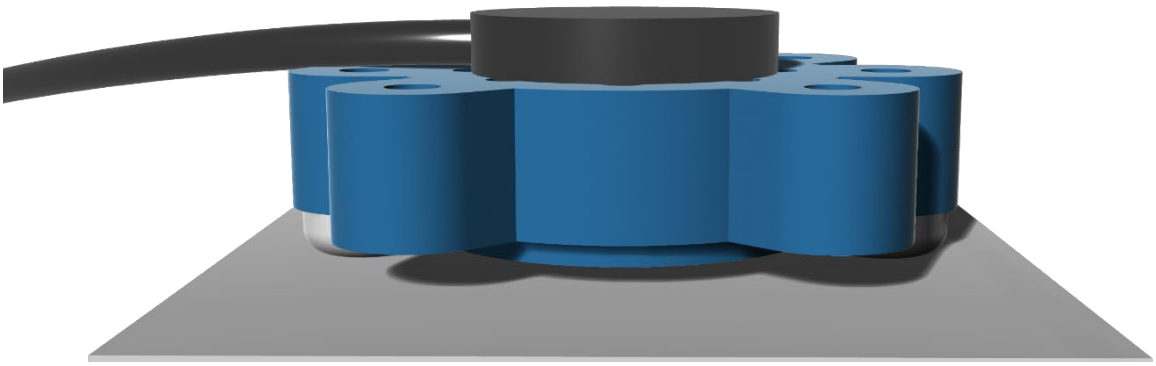

Figure 3-2. Render of transducer mount and skull analogue. The ultrasound transducer (black) sat in a 3D-printed housing (blue), which was mounted to a stereotaxic height control (not shown). For measurements with a skull analogue, the PTFE (white) was directly below the transducer mount, with a 4.8-mm gap between the transducer face and the PTFE. The PTFE was mounted to the same stereotaxic rig (not shown).

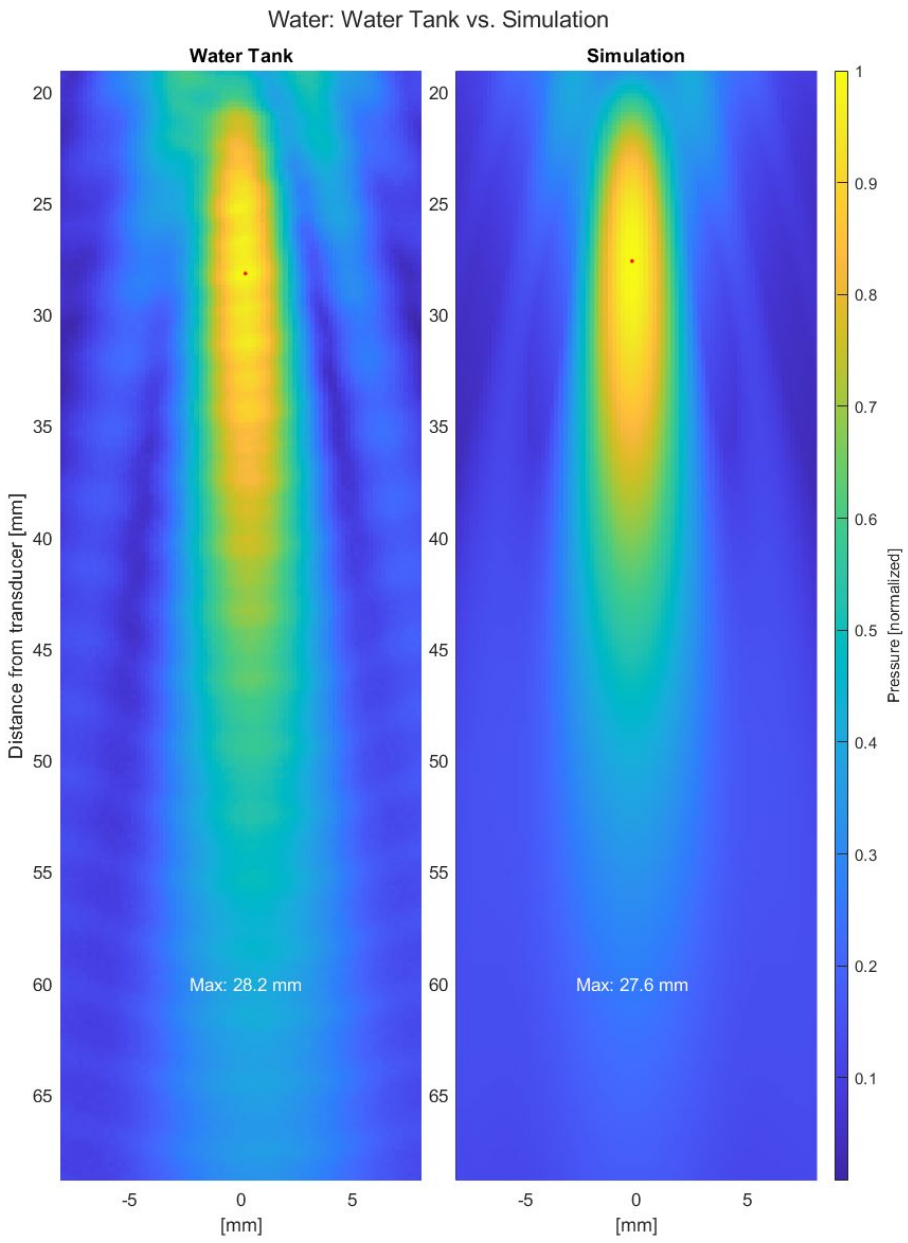

Figure 3-3. Real pressure distribution vs. simulated pressure distribution; free water. Left: A cross section of the pressure distribution of a focused ultrasound transducer in a water tank. No skull analogue.. Right: A cross section of the pressure distribution of a focused ultrasound source simulation using the same medium properties of the water used in the water tank recording (Left). Simulated pressure source had a focal length of 32 mm. Both were measured and simulated, respectively, with grids point widths of 0.2 by 0.2 by 0.2 mm.

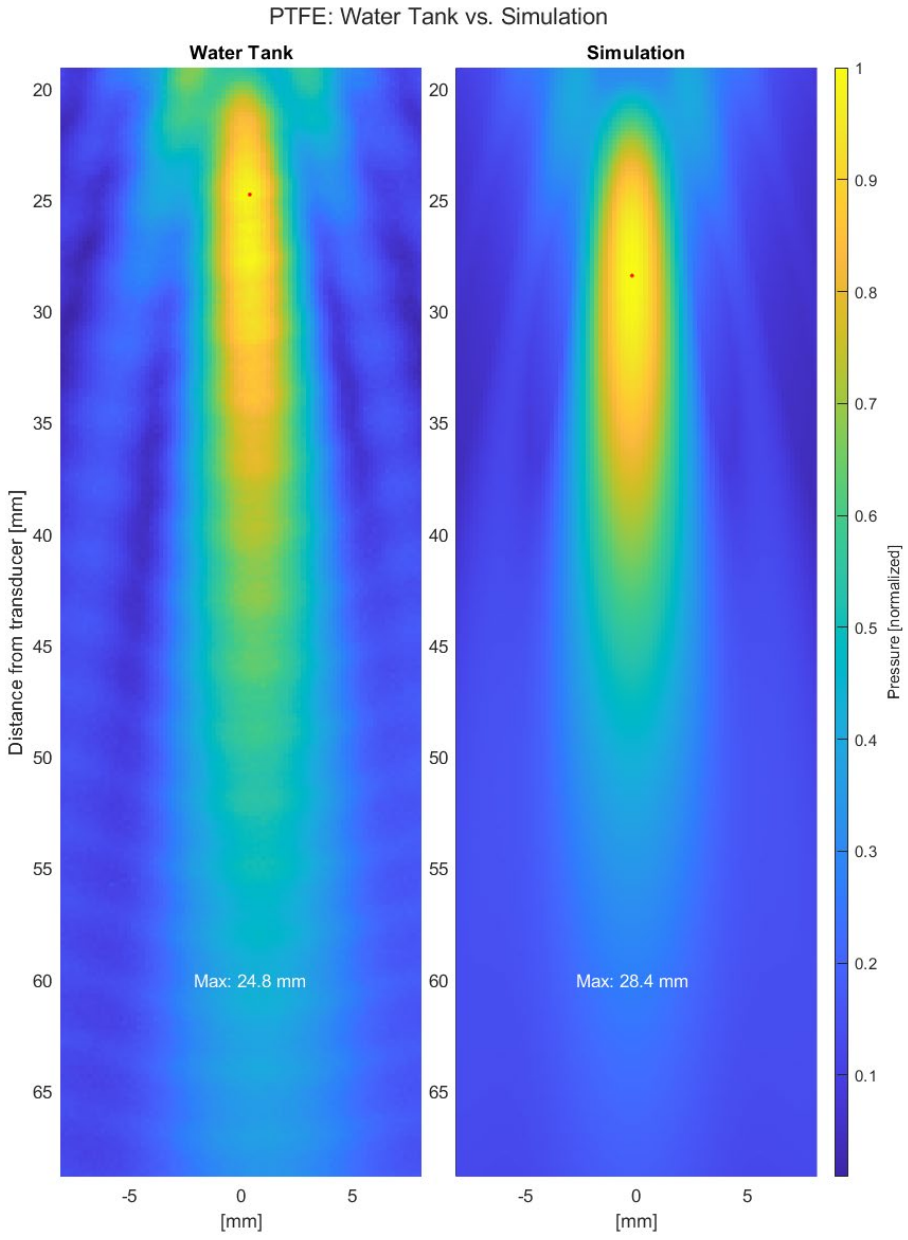

Figure 3-4. Real pressure distribution vs. simulated pressure distribution; PTFE. Left: A cross section of the pressure distribution of a focused ultrasound transducer in a water tank. PTFE skull analogue (4.6 mm thick) located below the tUS transducer. Right: A cross section of the pressure distribution of a focused ultrasound source simulation using the same medium properties of the water used in the water tank recording (Left) and the acoustic properties of PTFE. Simulated pressure source had a focal length of 32 mm. Both were measured and simulated, respectively, with grids point widths of 0.2 by 0.2 by 0.2 mm.

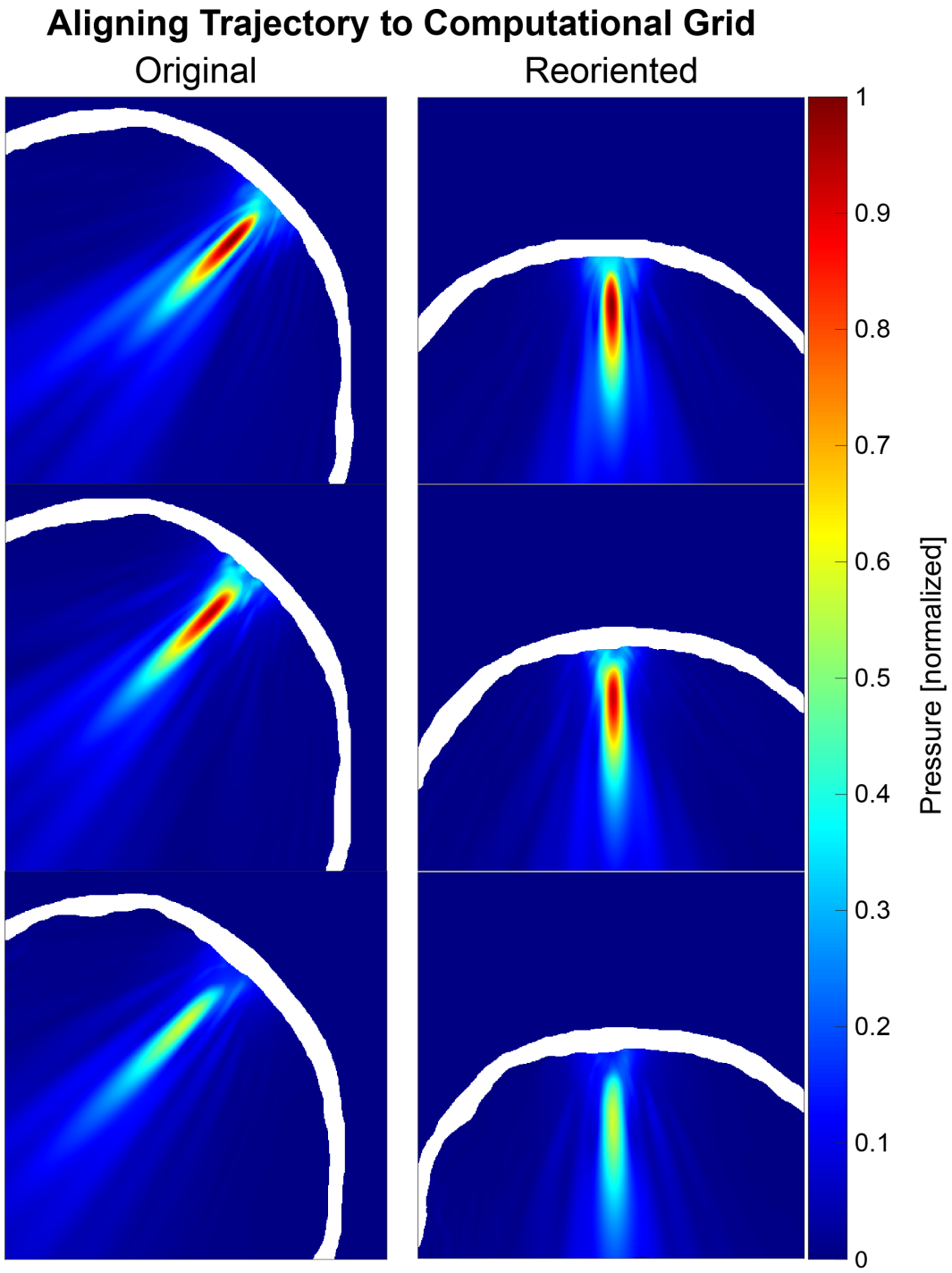

Figure 3-5. Simulation with and without alignment to computational grid. Three example parietal trajectories. Pressures are normalized to the maximum pressure for the respective simulation. Left: Original volume. Right: Volume reoriented before simulation. Trajectory of the emitted ultrasound is now orthogonal to the 3D grid used for simulation.

3.8 Additional Figures

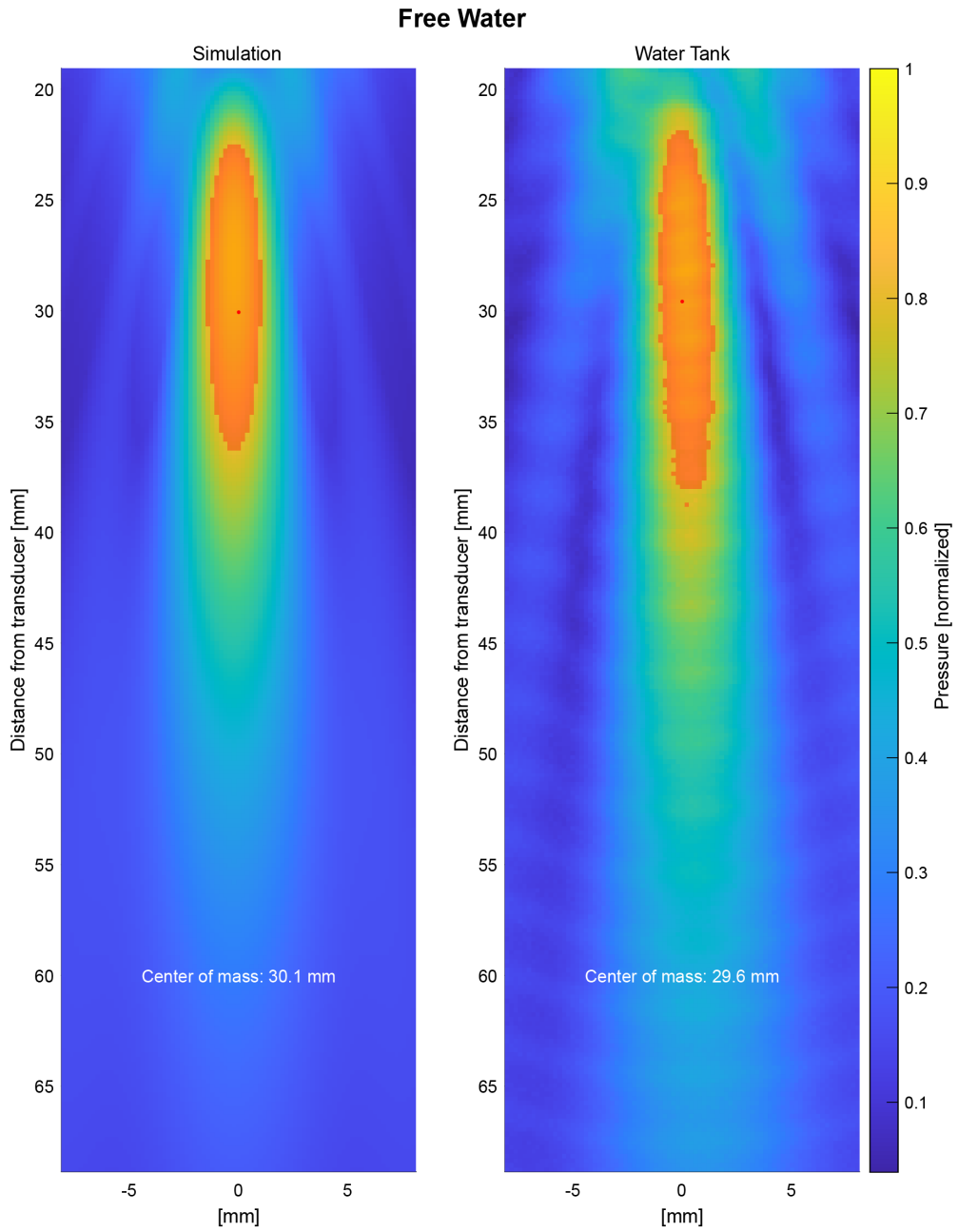

Figure 3-6. Real pressure distribution vs. simulated pressure distribution; free water; center of mass. Orange overlay: -3 dB focus area (i.e. volume above ~79% of the maximum of the 3D volume). Red dot: center of mass of the -3 dB focus area in 3D space. Left: A cross section of the pressure distribution of a focused ultrasound transducer in a water tank. Right: A cross section of the pressure distribution of a focused ultrasound source simulation using the same medium properties of the water used in the water tank recording (Left). Simulated pressure source had a focal length of 32 mm. Both were measured and simulated, respectively, with grids point widths of 0.2 by 0.2 by 0.2 mm.

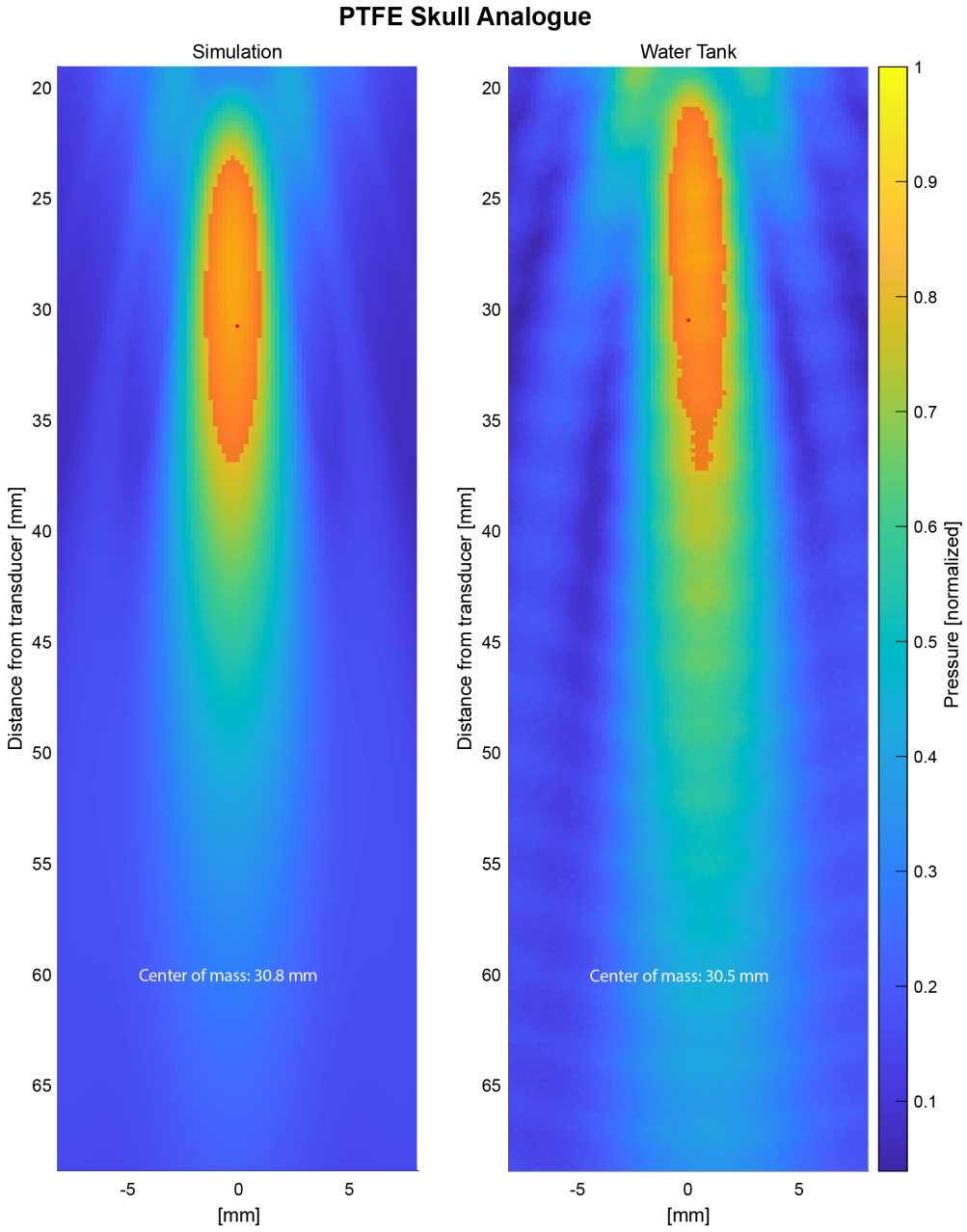

Figure 3-7. Real pressure distribution vs. simulated pressure distribution; PTFE; center of mass. Orange overlay: -3 dB focus area (i.e. volume above ~79% of the maximum of the 3D volume). Red dot: center of mass of the -3 dB focus area in 3D space. Left: A cross section of the pressure distribution of a focused ultrasound transducer in a water tank. PTFE skull analogue (4.6 mm thick) located below the tUS transducer. Right: A cross section of the pressure distribution of a focused ultrasound source simulation using the same medium properties of the water used in the water tank recording (Left) and the acoustic properties of PTFE. Simulated pressure source had a focal length of 32 mm. Both were measured and simulated, respectively, with grids point widths of 0.2 by 0.2 by 0.2 mm.

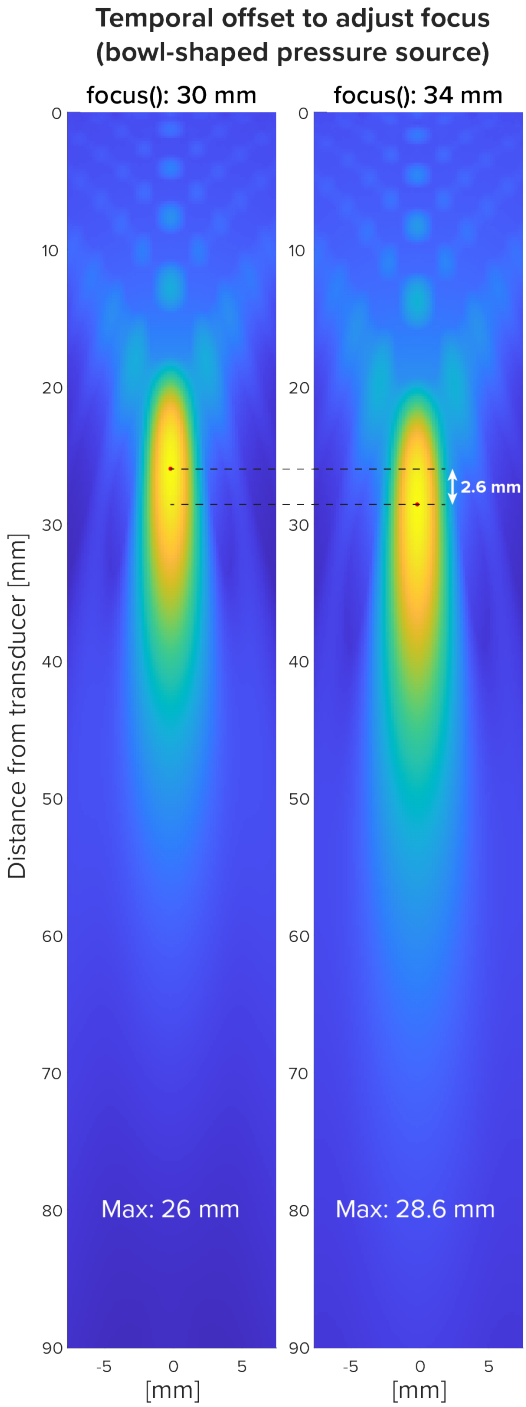

Figure 3-8. Adjusting focus with point-specific pressure trace delay. Comparison of two simulations in which the pressure source is a spherical cap with a 30-mm radius of curvature. Left: Same sine wave emitted from all points of spherical cap source (i.e. a pressure focus set to match the 30-mm radius of curvature). Right: Sine waves onset is based on the euclidean distance to focal point, now set to 34 mm. Distances [mm] are relative to the furthest point of the spherical cap (i.e. back). Temporal adjustment was made using the k-Wave function 'focus'. Acoustic values of medium for simulation were that of brain.

4 A Brief Discussion on Artifacts

Below are two brief topics regarding artifacts I encountered over the course of my dissertation work. These sections did not fit well into other chapters, so I include them here.

4.1 Insidious Artifacts

Signal processing and careful inspection of the data is always crucial when processing physiological data. In cases of novel techniques, such as those described in this document, there is arguably an increased need for care and skepticism, considering there may be less *a posteriori* knowledge regarding what the data should look like. I give an example of such a case in this section.

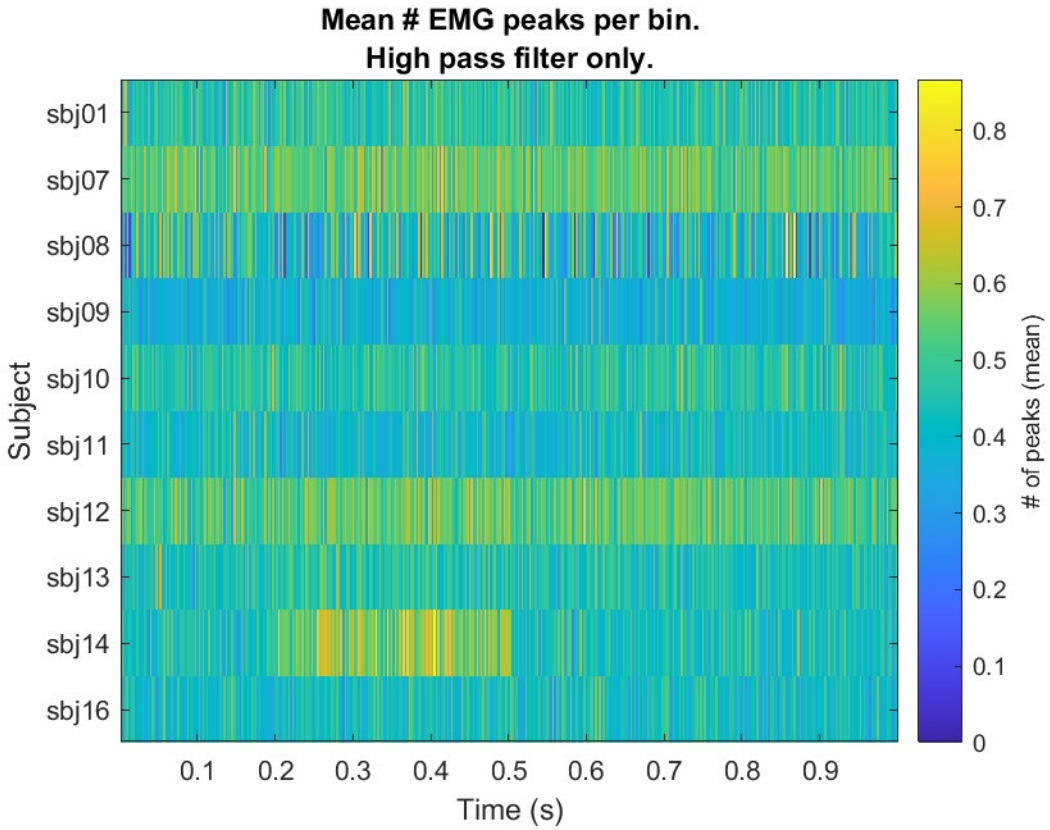

Figure 4-1. Mean spike rate using EMG data that has not been low pass filtered. For trials used in this figure, tUS was on during the 0.2 to 0.5 s time window.

From the data presented earlier in this dissertation in which tUS of M1 is performed during tonic muscle contraction, processing the EMG data to look for peaks in the EMG voltage trace reveals an apparent increase in the number of EMG peaks during tUS exposure of M1 in a single subject (Figure 4-1). As processed, this data might seem as though the subject's contractions were successfully modulated, while the other subjects showed no effect. Perhaps one could conjecture that the narrow focus of the ultrasound beam caused us to "miss" some physiologically relevant target, while the one subject showed a "hit", or this volunteer is simply a "responder", while the others were "non-responders". However, the apparent response during tUS disappears when you filter out the ~1000-Hz noise caused by the amplifier (Figure 4-2).

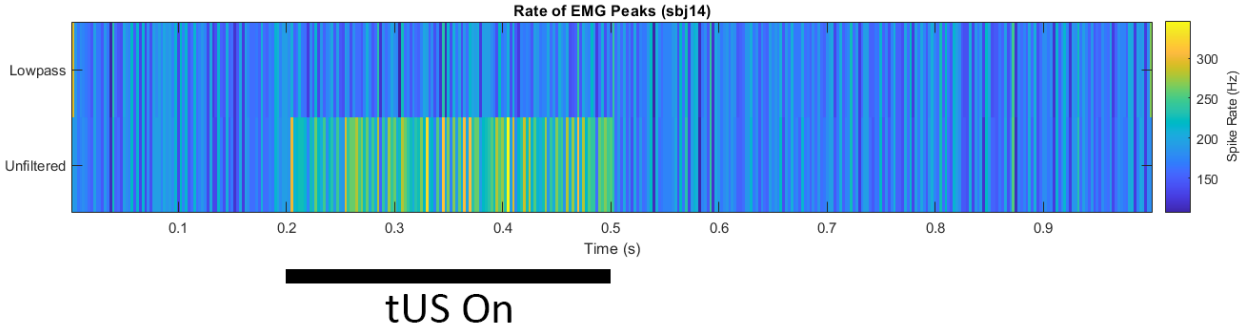

Figure 4-2. Mean spike rate per timepoint across all trials; single subject (sbj14). For trials used in this figure, tUS was on during the 0.2 to 0.5 s time window.

4.2 tUS AND MRI

tUS transducers can be fabricated to be MR safe (i.e. without ferrous metals). Therefore, tUS provides an exciting option for MR-compatible NIBS. Perhaps because of this advantage compared to other NIBS, a growing number of studies are choosing to perform tUS during fMRI (Ai et al., 2018, 2016; Khalighinejad et al., 2020; Lee, Kim, et al., 2016; Verhagen et al., 2019; Yoo et al., 2011).

I did encounter one hiccup for performing tUS inside an MR scanner. Placing the ultrasound transducer inside the bore of the MR scanner contaminated the signal with extraneous electromagnetic radiation. This noise was caused by the electrical connection introduced through the shielding of the MR scanner (Bungert, Chambers, Long, & Evans, 2012)—necessary to carry the amplified sinusoidal drive signal to the ultrasound transducer. Specifically, the equipment that drives the ultrasound transducer (i.e. waveform generator, amplifier, associated cables) is not MR safe and must stay outside the MR scanner room. The drive signal must instead be passed through an electrical panel to the transducer cable inside the scanner room. However, these series of cables undermine the radiofrequency (RF) shielding of the scanner room, allowing electromagnetic radiation to leak into the chamber. This extraneous electromagnetic radiation would contaminate the signal, creating MR-image artifacts (Bungert et al., 2012). But, placing a low-pass filter (70-MHz cutoff) in line on the coaxial cable of the transducer at the panel significantly reduced the amount of electromagnetic noise picked up by the MR scanner within the ~123-MHz RF range used by the scanner (Figure 4-3). At least one fMRI study has reported image artifacts surrounding the tUS transducer in an MR scanner (Ai et al., 2016), so it is possible the reported artifacts arose from RF noise introduced by the transducer setup. Given the risk of data contamination by RF leaks, it is important to test tUS-MRI protocols for signal quality before enrollment.

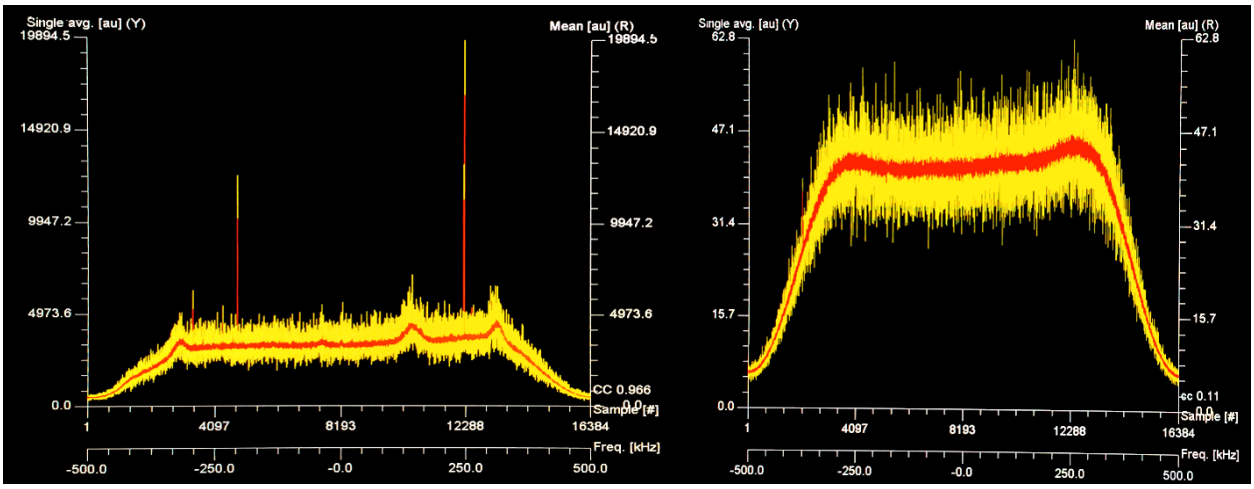

Figure 4-3. RF noise spectra: without and with lowpass filter. tUS transducers introduce noise into MRI if not addressed. RF leak tests with tUS transducer in Prisma 3T scanner, Brain Mapping Center, UCLA. Left) Without lowpass filter. Right) With lowpass filter. Note different Y-axis scales.

5 DISSERTATION DISCUSSION

The aim of my thesis work was to understand the strengths, weaknesses, and feasibility prospects of transcranial ultrasound as a non-invasive brain stimulation technique. In doing so, I wanted to investigate potential causes for, at times, lackluster or variable tUS results that have been published.

I started this investigation by comparing tUS to an established NIBS technique, TMS, in a cortical region with unclear tUS results but established TMS results: M1. First, I determined that single-trial tUS of $M1_{hand}$ could not recruit motor units at rest. Next, I found that single-trial tUS of $M1_{hand}$ had no concurrent effect on voluntary finger abduction. Lastly, I tested whether repeated tUS exposure used to test for tUS effects on motor activity had any lasting effect on motor cortex. To do this, I used single-pulse TMS to compare $M1_{hand}$ excitability before and after tUS exposure, but I found no group effect on cortical excitability from tUS exposure—at least with the parameters used here.

To understand what may have contributed to the null results from M1 ultrasound investigation, I performed 3D acoustic simulations to estimate the ultrasonic pressure field for each tUS placement used in the M1 experiment. To do this, I used T1-weighted head volumes for each participant to create an accurate representation of their head in simulation space. I placed the tUS pressure source in simulation space according to the neuronavigated coordinate used for the experiment. After running the simulations, real-world pressures were deduced from the simulated values by normalizing them to the pressure field emitted by the tUS transducer, as measured in a water tank.

Once I had estimates of intracranial pressure fields, I could tabulate indices of tUS exposure of neuroanatomical targets and tie these to physiological outcomes. Specifically, I calculated the cumulative exposure of $M1_{hand}$ for each participant and tied those exposure levels to the

aforementioned cortical excitability changes following tUS. While both $M1_{hand}$ exposure levels and $M1_{hand}$ excitability varied across participants, there was no clear correlation between the two measures.

Lastly, I leveraged the progress I had made with ultrasonic simulations to build an open-source MATLAB toolbox, TUSX, to allow tUS investigators to easily perform acoustic simulations for their tUS experiments. TUSX streamlines the same pipeline I used to perform acoustic simulations on the M1 data, in which medical head volumes and tUS transducer pressures are integrated into simulation space. I also validated output from the toolbox using water tank recordings of condition-matched tUS pressure fields.

5.1 tUS AND M1

When I started the M1 project, the prospects for tUS being effective in M1 were more promising than they are today. At the time, it was believed that ultrasound could stimulate M1 circuitry to induce muscle contractions, since there were multiple sources in animal models with such data (King et al., 2013; King, Brown, & Pauly, 2014; Tufail et al., 2010; Ye et al., 2017; Yoo et al., 2011). However, the 2018 tandem-published findings by *Sato et al.* and *Guo et al.* call the previous motor activity results into question by showing ultrasound of M1 caused muscle contraction of animal models through auditory mechanisms (Guo et al., 2018; Sato et al., 2018).

Before the auditory confound findings, the data suggested that tUS could robustly affect M1 activity in animal models, so it seemed likely that *some* form of neuromodulation in human M1 should be possible. The fact that I (and now others) could not replicate in humans the motor activations seen in animals seemed non-problematic—my reaction being that perhaps the lower intensity levels necessary for human safety measures precluded raising tUS intensity levels high enough to rise above threshold for motor activation. After all, sub-threshold TMS pulses can, when delivered repetitively, modulate M1 excitability even though the individual pulses do not perturb the circuitry enough to reach threshold for

motor activation. In combination with the fact that tUS has been proposed to preferentially stimulate inhibitory interneurons compared to TMS, it seemed fair that tUS could be stimulating 'sub-threshold' as well.

After the auditory confound findings, the cumulative evidence paints a different picture—one in which tUS-induced effects instead seem difficult to find in M1. In this dissertation, I showed that tUS of $M1_{hand}$ caused no concurrent change to finger muscle activity during voluntary muscle contraction. I also found no consistent effect of tUS M1 exposure on motor cortex excitability, as probed by single-pulse TMS of M1. As for work published by others during the course of my project, the two fMRI studies that performed tUS of M1 in humans showed no significant BOLD changes from tUS (Ai et al., 2018, 2016). Similarly, the studies that did find concurrent M1 modulation by tUS had to pair tUS with simultaneous, concentric TMS to probe any effects (Fomenko et al., 2020; Legon, Bansal, et al., 2018). Yet tUS has shown consistent results elsewhere in the brain.

One potential explanation for these different outcomes could lie in cytoarchitectural differences between brain regions. Crucially, motor cortex has significantly lower neuronal density compared to somatosensory and visual cortex (Atapour et al., 2019; Beaulieu & Colonnier, 1989; Collins, 2011; Collins et al., 2010). This means that for two perfectly matched pressure fields the pressure field within M1 would encompass fewer neurons than the same field in S1. This recruitment of inherently smaller cell populations in M1 could be contributing to the difficulty of eliciting results.

Similarly, differences in cortical structure and distribution of cell types between regions could underlie some of the variability. For example, the laminar cytoarchitecture of M1 is fairly distinct from that of sensory cortices. M1 lacks the layer IV spiny stellate cells that are integral to the input processes in layer 4 of some other cortical regions like S1 and V1 (García-Cabezas & Barbas, 2014; Yamawaki, Borges, Suter, Harris, & Shepherd, 2014). Also, layer V of M1 is thicker than S1 and V1 and contains the giant

pyramidal neurons, Betz cells (Betz, 1874; Geyer, Matelli, Luppino, & Zilles, 2000). Since variations in ion channel ultrasonic sensitivity should likely lead to varying cell type sensitivities, the cell type distributions of cortices alone could cause variability of response to tUS. When combined with structural circuitry differences, this could theoretically lead to significant differences in systems-level responses to ultrasound.

Lastly, the impact of neuronal size on ultrasound response has yet to be investigated. If size is a factor in individual neuron responses, cytoarchitecture-based differences in tUS response could occur. For example, perhaps larger neurons are more difficult to recruit or modulate with ultrasound, due to higher membrane resistance (Henneman, 1957; Henneman, Somjen, & Carpenter, 1965). This could explain why M1, with its higher prevalence of large pyramidal neurons including the giant Betz cells, is harder to perturb with tUS. In contrast, V1 is densely populated with small neurons, including stellate cells in layer IV (Blasdel & Fitzpatrick, 1984; Lund, 1973), which would match results of V1 responsivity to tUS. The cells of M1 could simply have a higher average membrane resistance, making any current introduced by tUS-mediated ion channel opening to have a smaller impact on the voltage potential of cells.

5.2 Acoustic Simulation in tUS Experiments

The idea for building TUSX was to address variability and interpretability of tUS experiments going forward. Skull morphology differences among participants can lead to variable intracranial pressures and spatial deviations as high as 16 cm (Lee, Kim, et al., 2016). By allowing more investigators to confidently quantify the magnitude and location of their tUS hotspots, i.e. through TUSX, reproducibility within the tUS field should improve.

The field has also yet to synthesize ultrasound protocols into a clear set of protocols known to provide desired modulatory effects. Setting intracranial intensity is a component of this goal. Making acoustic

simulation more ubiquitous, i.e. through TUSX, should accelerate the collection of high-confidence data on this front—allowing promising protocols to rise above the noise.

Lastly, performing acoustic simulations on my data reinforced how small the volume of effect can be with tUS. The spatial precision of tUS over alternatives like TMS or tDCS is one of the core reasons for the field's interest in the technique. However, it is investigating in the future wheter small-volume hotspots actually hamper tUS outcomes, since perhaps in certain structures small volumes of stimulation could prevent reaching threshold for effects at the systems level.

5.2.1 Safety

An additional benefit of performing acoustic simulations for tUS experiments is that it gives investigators a better understanding of protocol safety. For example, someone with a thinner skull will tend to experience higher intracranial ultrasound, given a constant transducer drive signal amplitude. Performing simulations, ideally before tUS sessions, can assure investigators and their respective safety review boards that volunteers are safe.

While the lack of serious side effects reported for experiments performed so far (Lee et al., 2015; Lee, Kim, et al., 2016; Lee, Lee, et al., 2016; Legon et al., 2014, 2020; J. Mueller et al., 2014; Tufail et al., 2010) suggests that the lack of acoustic simulation in all tUS experiments has likely not been a safety issue, this could change if investigators begin to push protocols into higher tUS intensities or more extended repetitive tUS sessions in search of more robust modulation.

6 CONCLUSION

Transcranial ultrasound stimulation is still a novel field, but it is one that is accelerating quickly. When I started graduate school, there were two tUS papers in humans. Now there are over fifteen. As such, even during the course of my work there emerged findings within the field that led to key insights for how I approached and interpreted this project. At this pace, the progress of the coming years could be substantial—potentially rounding a corner for our understand of tUS as a field.

My hope for this progress is that we will see improved understanding of the mechanobiological and cell type-specific effects of ultrasound in neural tissue, since having a stronger foundation on that front will facilitate more informed approaches to investigating systems-level questions with tUS—including structure-specific effects and inter-region variability. Beyond that, I hope an increased adoption of acoustic simulation in tUS projects does come to fruition. Based on recent trends in publications, we may already be making headway. With these shifts and others, perhaps we can finally begin to aggregate sets of tUS protocols with known efficacies. Having these set parameters for acoustic frequency, pulse protocols, protocol duration, focal volumes, focal intensities, and the regions they are applicable will allow for more confident, directed use of tUS to probe brain function and provide helpful, targeted neural interventions in clinical settings.

7 REFERENCES

Ai, L., Bansal, P., Mueller, J. K., & Legon, W. (2018). Effects of transcranial focused ultrasound on human primary motor cortex using 7T fMRI. *BMC Neuroscience*, *19*(1), 56. https://doi.org/10.1186/s12868-018-0456-6

Ai, L., Mueller, J. K., Grant, A., Eryaman, Y., & Legon, W. (2016). Transcranial focused ultrasound for BOLD fMRI signal modulation in humans. In *Proceedings of the Annual International Conference of the IEEE Engineering in Medicine and Biology Society, EMBS* (Vol. 2016–Octob, pp. 1758–1761). IEEE. https://doi.org/10.1109/EMBC.2016.7591057

Apfel, R. E., & Holland, C. K. (1991). Gauging the likelihood of cavitation from short-pulse, low-duty cycle diagnostic ultrasound. *Ultrasound in Medicine & Biology*, *17*(2), 179–185.

Atapour, N., Majka, P., Wolkowicz, I. H., Malamanova, D., Worthy, K. H., & Rosa, M. G. P. (2019). Neuronal Distribution across the Cerebral Cortex of the Marmoset Monkey (Callithrix jacchus). *Cerebral Cortex*, *29*(9), 3836–3863. https://doi.org/10.1093/cercor/bhy263

Bachtold, M. R., Rinaldi, P. C., Jones, J. P., Reines, F., & Price, L. R. (1998). Focused ultrasound modifications of neural circuit activity in a mammalian brain. *Ultrasound in Medicine and Biology*, *24*(4), 557–565. https://doi.org/10.1016/S0301-5629(98)00014-3

Baron, C., Aubry, J.-F., Tanter, M., Meairs, S., & Fink, M. (2009). Simulation of Intracranial Acoustic Fields in Clinical Trials of Sonothrombolysis. *Ultrasound in Medicine & Biology*, *35*(7), 1148–1158. https://doi.org/10.1016/J.ULTRASMEDBIO.2008.11.014

Baumgärtner, U., Greffrath, W., & Treede, R.-D. (2012). Contact heat and cold, mechanical, electrical and chemical stimuli to elicit small fiber-evoked potentials: Merits and limitations for basic science and clinical use. *Neurophysiologie Clinique/Clinical Neurophysiology*, *42*(5), 267–280. https://doi.org/10.1016/J.NEUCLI.2012.06.002

Beaulieu, C., & Colonnier, M. (1989). Number of neurons in individual laminae of areas 3B, 4γ, and 6aα of the cat cerebral cortex: A comparison with major visual areas. *Journal of Comparative Neurology*, *279*(2), 228–234. https://doi.org/10.1002/cne.902790206

Betz, W. (1874). Anatomischer nachweis zweier gehirncentra. *Zentralbl Med Wiss*, *12*(578,595).

Blackmore, J., Shrivastava, S., Sallet, J., Butler, C. R., & Cleveland, R. O. (2019, July 1). Ultrasound Neuromodulation: A Review of Results, Mechanisms and Safety. *Ultrasound in Medicine and Biology*. Elsevier USA. https://doi.org/10.1016/j.ultrasmedbio.2018.12.015

Blasdel, G. G., & Fitzpatrick, D. (1984). Physiological organization of layer 4 in macaque striate cortex. *Journal of Neuroscience*, *4*(3), 880–895. https://doi.org/10.1523/jneurosci.04-03-00880.1984

Borrelli, M. J., Bailey, K. I., & Dunn, F. (1981). Early ultrasonic effects upon mammalian CNS structures (chemical synapses). *The Journal of the Acoustical Society of America*, *69*(5), 1514. https://doi.org/10.1121/1.385791

Bowman, C. L., Ding, J. P., Sachs, F., & Sokabe, M. (1992). Mechanotransducing ion channels in astrocytes. *Brain Research*, *584*(1–2), 272–286. https://doi.org/10.1016/0006-8993(92)90906-P

Bungert, A., Chambers, C. D., Long, E., & Evans, C. J. (2012). On the importance of specialized radiofrequency filtering for concurrent TMS/MRI. *Journal of Neuroscience Methods*, *210*(2), 202–205. https://doi.org/10.1016/j.jneumeth.2012.07.023

Butler, J. E., Petersen, N. C., Herbert, R. D., Gandevia, S. C., & Taylor, J. L. (2012). Origin of the low-level EMG during the silent period following transcranial magnetic stimulation. *Clinical Neurophysiology*, *123*(7), 1409–1414. https://doi.org/https://doi.org/10.1016/j.clinph.2011.11.034

Cain, J. A., Spivak, N. M., Coetzee, J. P., Crone, J. S., Johnson, M. A., Lutkenhoff, E. S., … Monti, M. M. (2021, March 1). Ultrasonic thalamic stimulation in chronic disorders of consciousness. *Brain Stimulation*. Elsevier Inc. https://doi.org/10.1016/j.brs.2021.01.008

Cain, J. A., Visagan, S., Johnson, M. A., Crone, J., Blades, R., Spivak, N. M., … Monti, M. M. (2021). Real time and delayed effects of subcortical low intensity focused ultrasound. *Scientific Reports*, *11*(1), 6100. https://doi.org/10.1038/s41598-021-85504-y

Cantello, R., Gianelli, M., Civardi, C., & Mutani, R. (1992). Magnetic brain stimulation: the silent period after the motor evoked potential. *Neurology*, *42*(10), 1951–9. https://doi.org/10.1212/wnl.42.10.1951

Chapman, I. V., MacNally, N. A., & Tucker, S. (1980). Ultrasound-induced changes in rates of influx and efflux of potassium ions in rat thymocytes in vitro. *Ultrasound in Medicine & Biology*, *6*(1), 47–58. https://doi.org/10.1016/0301-5629(80)90063-0

Chen, R., Classen, J., Gerloff, C., Celnik, P., Wassermann, E. M., Hallett, M., & Cohen, L. G. (1997). Depression of motor cortex excitability by low-frequency transcranial magnetic stimulation. *Neurology*, *48*(5), 1398–1403. https://doi.org/10.1212/WNL.48.5.1398

Christov-Moore, L., Sugiyama, T., Grigaityte, K., & Iacoboni, M. (2016). Increasing generosity by disrupting prefrontal cortex. *Social Neuroscience*, *919*(June), 1–8. https://doi.org/10.1080/17470919.2016.1154105

Classen, J., & Benecke, R. (1995). Inhibitory phenomena in individual motor units induced by transcranial magnetic stimulation. *Electroencephalography and Clinical Neurophysiology/ Electromyography*, *97*(5), 264–274. https://doi.org/10.1016/0924-980X(95)00099-2

Collins, C. E. (2011). Variability in Neuron Densities across the Cortical Sheet in Primates. *Brain, Behavior and Evolution*, *78*(1), 37–50. https://doi.org/10.1159/000327319

Collins, C. E., Airey, D. C., Young, N. A., Leitch, D. B., & Kaas, J. H. (2010). Neuron densities vary across and within cortical areas in primates. *Proceedings of the National Academy of Sciences of the United States of America*, *107*(36), 15927–15932. https://doi.org/10.1073/pnas.1010356107

Connor, C. W., Clement, G. T., & Hynynen, K. (2002). A unified model for the speed of sound in cranial bone based on genetic algorithm optimization. *Physics in Medicine and Biology*, *47*(22), 3925–3944. https://doi.org/10.1088/0031-9155/47/22/302

Constans, C., Mateo, P., Tanter, M., & Aubry, J. F. (2018). Potential impact of thermal effects during ultrasonic neurostimulation: Retrospective numerical estimation of temperature elevation in seven rodent setups. *Physics in Medicine and Biology*, *63*(2), 25003. https://doi.org/10.1088/1361-6560/aaa15c

Cox, B. T., Kara, S., Arridge, S. R., & Beard, P. C. (2007). k-space propagation models for acoustically

heterogeneous media: Application to biomedical photoacoustics. *The Journal of the Acoustical Society of America*, *121*(6), 3453. https://doi.org/10.1121/1.2717409

Daffertshofer, M., Gass, A., Ringleb, P., Sitzer, M., Sliwka, U., Els, T., … Hennerici, M. G. (2005). Transcranial Low-Frequency Ultrasound-Mediated Thrombolysis in Brain Ischemia. *Stroke*, *36*(7), 1441–1446. https://doi.org/10.1161/01.STR.0000170707.86793.1a

Davey, N. J., Romaiguère, P., Maskill, D. W., & Ellaway, P. H. (1994). Suppression of voluntary motor activity revealed using transcranial magnetic stimulation of the motor cortex in man. *The Journal of Physiology*, *477*(2), 223–235. https://doi.org/10.1113/jphysiol.1994.sp020186

Deffieux, T., Younan, Y., Wattiez, N., Tanter, M., Pouget, P., & Aubry, J.-F. (2013). Low-Intensity Focused Ultrasound Modulates Monkey Visuomotor Behavior. *Current Biology*, *23*(23), 2430–2433. https://doi.org/http://dx.doi.org/10.1016/j.cub.2013.10.029

Desideri, D., Zrenner, C., Gordon, P. C., Ziemann, U., & Belardinelli, P. (2018). Nil effects of μ-rhythm phase-dependent burst-rTMS on cortical excitability in humans: A resting-state EEG and TMS-EEG study. *PLoS ONE*, *13*(12), e0208747. https://doi.org/10.1371/journal.pone.0208747

Duck, F. A. (1990). *Physical properties of tissue : a comprehensive reference book*. Academic Press.

Eames, M. D. C., Farnum, M., Khaled, M., Elias, W. J., Hananel, A., Snell, J. W., … Aubry, J.-F. (2015). Head phantoms for transcranial focused ultrasound. *Medical Physics*, *42*(4), 1518–27. https://doi.org/10.1118/1.4907959

Farrer, A. I., Odéen, H., de Bever, J., Coats, B., Parker, D. L., Payne, A., & Christensen, D. A. (2015). Characterization and evaluation of tissue-mimicking gelatin phantoms for use with MRgFUS. *Journal of Therapeutic Ultrasound*, *3*, 9. https://doi.org/10.1186/s40349-015-0030-y

Feynman, R. P., Leighton, R. B., Sands, M., & Hafner, E. M. (1965). The Feynman Lectures on Physics; Vol. I. *American Journal of Physics*, *33*(9), 750–752. https://doi.org/10.1119/1.1972241

Fitzgerald, P. B., Fountain, S., & Daskalakis, Z. J. (2006). A comprehensive review of the effects of rTMS on motor cortical excitability and inhibition. *Clinical Neurophysiology*, *117*(12), 2584–2596. https://doi.org/10.1016/j.clinph.2006.06.712

Folloni, D., Verhagen, L., Mars, R. B., Fouragnan, E., Constans, C., Aubry, J.-F., … Sallet, J. (2019). Manipulation of Subcortical and Deep Cortical Activity in the Primate Brain Using Transcranial Focused Ultrasound Stimulation. *Neuron*, *101*(6), 1109–1116.e5. https://doi.org/10.1016/J.NEURON.2019.01.019

Fomenko, A., Chen, K. H. S., Nankoo, J. F., Saravanamuttu, J., Wang, Y., El-Baba, M., … Chen, R. (2020). Systematic examination of low-intensity ultrasound parameters on human motor cortex excitability and behaviour. *eLife*, *9*, 1–68. https://doi.org/10.7554/eLife.54497

Friston, K. J., Ashburner, J. T., Kiebel, S. J., Nichols, T. E., & Penny, W. D. (2007). *Statistical parametric mapping: the analysis of functional brain images*. Academic Press. https://doi.org/10.1016/B978-0-12-372560-8.X5000-1

Frizzell, L. A. (1988). Threshold dosages for damage to mammalian liver by high intensity focused ultrasound. *IEEE Transactions on Ultrasonics, Ferroelectrics, and Frequency Control*, *35*(5), 578–581. https://doi.org/10.1109/58.8036

Fry, F. J., Ades, H. W., & Fry, W. J. (1958). Production of Reversible Changes in the Central Nervous System by Ultrasound. *Science*, *127*(3289), 83 LP-84. Retrieved from http://science.sciencemag.org/content/127/3289/83.abstract

García-Cabezas, M. Á., & Barbas, H. (2014). Area 4 has layer IV in adult primates. *European Journal of Neuroscience*, *39*(11), 1824–1834. https://doi.org/10.1111/ejn.12585

Gaur, P., Casey, K. M., Kubanek, J., Li, N., Mohammadjavadi, M., Saenz, Y., … Pauly, K. B. (2020). Histologic safety of transcranial focused ultrasound neuromodulation and magnetic resonance acoustic radiation force imaging in rhesus macaques and sheep. *Brain Stimulation*, *13*(3), 804–814. https://doi.org/https://doi.org/10.1016/j.brs.2020.02.017

Gavrilov, L. R., Gersuni, G. V, Ilyinsky, O. B., Sirotyuk, M. G., Tsirulnikov, E. M., & Shchekanov, E. E. (1976). The Effect of Focused Ultrasound on the Skin and Deep Nerve Structures of Man and Animal. In A. I. and O. B. I. B. T.-P. in B. Research (Ed.), *Somatosensory and Visceral Receptor MechanismsProceedings of an International Symposium held in Leningrad, U.S.S.R.* (Vol. Volume 43, pp. 279–292). Elsevier. https://doi.org/http://dx.doi.org/10.1016/S0079-6123(08)64360-5

Gavrilov, L. R., & Tsirulnikov, E. M. (2012). Focused ultrasound as a tool to input sensory information to humans (review). *Acoustical Physics*. https://doi.org/10.1134/S1063771012010083

Gavrilov, L. R., Tsirulnikov, E. M., & Davies, I. a. I. (1996). Application of focused ultrasound for the stimulation of neural structures. *Ultrasound in Medicine & Biology*, *22*(2), 179–192. https://doi.org/10.1016/0301-5629(96)83782-3

Geyer, S., Matelli, M., Luppino, G., & Zilles, K. (2000). Functional neuroanatomy of the primate isocortical motor system. *Anatomy and Embryology*, *202*(6), 443–474.

Gibson, B. C., Sanguinetti, J. L., Badran, B. W., Yu, A. B., Klein, E. P., Abbott, C. C., … Clark, V. P. (2018). Increased Excitability Induced in the Primary Motor Cortex by Transcranial Ultrasound Stimulation. *Frontiers in Neurology*, *9*, 1007. https://doi.org/10.3389/fneur.2018.01007

Gordon, P. C., Desideri, D., Belardinelli, P., Zrenner, C., & Ziemann, U. (2018). Comparison of cortical EEG responses to realistic sham versus real TMS of human motor cortex. *Brain Stimulation*, *11*(6), 1322–1330. https://doi.org/10.1016/j.brs.2018.08.003

Goss, S. A., Johnston, R. L., & Dunn, F. (1978). Comprehensive compilation of empirical ultrasonic properties of mammalian tissues. *The Journal of the Acoustical Society of America*, *64*(2), 423–457. https://doi.org/10.1121/1.384509

Greffrath, W., Baumgärtner, U., & Treede, R. D. (2007). Peripheral and central components of habituation of heat pain perception and evoked potentials in humans. *Pain*, *132*(3), 301–311. https://doi.org/10.1016/j.pain.2007.04.026

Guo, H., Hamilton, M., Offutt, S. J., Gloeckner, C. D., Li, T., Kim, Y., … Lim, H. H. (2018). Ultrasound Produces Extensive Brain Activation via a Cochlear Pathway. *Neuron*, *98*(5), 1020–1030.e4. https://doi.org/10.1016/j.neuron.2018.04.036

Hameroff, S., Trakas, M., Duffield, C., Annabi, E., Gerace, M. B., Boyle, P., … Badal, J. J. (2013). Transcranial Ultrasound (TUS) Effects on Mental States: A Pilot Study. *Brain Stimulation*, *6*(3), 409–415. https://doi.org/http://dx.doi.org/10.1016/j.brs.2012.05.002

Harvey, E. N. (1929). The effect of high frequency sound waves on heart muscle and other irritable

tissues. *American Journal of Physiology*, *91*(1), 284–290. https://doi.org/10.1016/S0002-8703(30)90343-2

Hayner, M., & Hynynen, K. (2001). Numerical analysis of ultrasonic transmission and absorption of oblique plane waves through the human skull. *The Journal of the Acoustical Society of America*, *110*(6), 3319–3330. https://doi.org/10.1121/1.1410964

Henneman, E. (1957). Relation between Size of Neurons and Their Susceptibility to Discharge. *Science*, *126*(3287), 1345–1347. Retrieved from http://www.jstor.org/stable/1752769

Henneman, E., Somjen, G., & Carpenter, D. O. (1965). Functional significance of cell size in spinal motoneurons. *Journal of Neurophysiology*, *28*(3), 560–580. https://doi.org/10.1152/jn.1965.28.3.560

Hervieu, G. J., Cluderay, J. E., Gray, C. W., Green, P. J., Ranson, J. L., Randall, A. D., & Meadows, H. J. (2001). Distribution and expression of TREK-1, a two-pore-domain potassium channel, in the adult rat CNS. *Neuroscience*, *103*(4), 899–919. https://doi.org/10.1016/S0306-4522(01)00030-6

Hess, C. W., Mills, K. R., & Murray, N. M. (1987). Responses in small hand muscles from magnetic stimulation of the human brain. *The Journal of Physiology*, *388*(1), 397–419. https://doi.org/10.1113/jphysiol.1987.sp016621

Hess, C. W., Mills, K. R., Murray, N. M. F., & Schriefer, T. N. (1987). Excitability of the human motor cortex is enhanced during REM sleep. *Neuroscience Letters*, *82*(1), 47–52. https://doi.org/10.1016/0304-3940(87)90169-8

Heureaux, J., Chen, D., Murray, V. L., Deng, C. X., & Liu, A. P. (2014). Activation of a bacterial mechanosensitive channel in mammalian cells by cytoskeletal stress. *Cellular and Molecular Bioengineering*, *7*(3), 307–319. https://doi.org/10.1007/s12195-014-0337-8

Holland, C. K., & Apfel, R. E. (1989). An improved theory for the prediction of microcavitation thresholds. *IEEE Transactions on Ultrasonics, Ferroelectrics, and Frequency Control*, *36*(2), 204–208. https://doi.org/10.1109/58.19152

Huang, Y.-Z., Edwards, M. J., Rounis, E., Bhatia, K. P., & Rothwell, J. C. (2005). Theta Burst Stimulation of the Human Motor Cortex. *Neuron*, *45*(2), 201–206. https://doi.org/10.1016/j.neuron.2004.12.033

Huang, Y., Datta, A., Bikson, M., & Parra, L. C. (2019). Realistic volumetric-approach to simulate transcranial electric stimulation - ROAST - a fully automated open-source pipeline. *Journal of Neural Engineering*, *16*(5). https://doi.org/10.1088/1741-2552/ab208d

Hupfeld, K. E., Swanson, C. W., Fling, B. W., & Seidler, R. D. (2020). TMS-induced silent periods: A review of methods and call for consistency. *Journal of Neuroscience Methods*, *346*, 108950. https://doi.org/https://doi.org/10.1016/j.jneumeth.2020.108950

Hynynen, G. T. C. and K. (2002). A non-invasive method for focusing ultrasound through the human skull. *Physics in Medicine and Biology*, *47*(8), 1219. Retrieved from http://stacks.iop.org/0031-9155/47/i=8/a=301

Hynynen, K., & Jolesz, F. A. (1998). Demonstration of Potential Noninvasive Ultrasound Brain Therapy Through an Intact Skull. *Ultrasound in Medicine & Biology*, *24*(2), 275–283. https://doi.org/http://dx.doi.org/10.1016/S0301-5629(97)00269-X

Hynynen, K., & Sun, J. (1999). Trans-skull ultrasound therapy: The feasibility of using image-derived skull thickness information to correct the phase distortion. *IEEE Transactions on Ultrasonics, Ferroelectrics, and Frequency Control*, *46*(3), 752–755. https://doi.org/10.1109/58.764862

Ibsen, S., Tong, A., Schutt, C., Esener, S., & Chalasani, S. H. (2015). Sonogenetics is a non-invasive approach to activating neurons in Caenorhabditis elegans. *Nature Communications*, *6*, 8264. https://doi.org/10.1038/ncomms9264

Jenkinson, M., Bannister, P., Brady, M., & Smith, S. (2002). Improved Optimization for the Robust and Accurate Linear Registration and Motion Correction of Brain Images. *NeuroImage*, *17*(2), 825–841. https://doi.org/https://doi.org/10.1006/nimg.2002.1132

Jenkinson, M., Beckmann, C. F., Behrens, T. E. J., Woolrich, M. W., & Smith, S. M. (2012). FSL. *NeuroImage*. https://doi.org/10.1016/j.neuroimage.2011.09.015

Jenkinson, M., & Smith, S. (2001). A global optimisation method for robust affine registration of brain images. *Medical Image Analysis*, *5*(2), 143–156. https://doi.org/https://doi.org/10.1016/S1361-8415(01)00036-6

Jones, R. M., & Hynynen, K. (2016). Comparison of analytical and numerical approaches for CT-based aberration correction in transcranial passive acoustic imaging. *Physics in Medicine and Biology*, *61*(1), 23–36. https://doi.org/10.1088/0031-9155/61/1/23

Kallioniemi, E., Säisänen, L., Pitkänen, M., Könönen, M., Karhu, J., & Julkunen, P. (2015). Input–Output Characteristics of Late Corticospinal Silent Period Induced by Transcranial Magnetic Stimulation. *Journal of Clinical Neurophysiology*, *32*(4). Retrieved from https://journals.lww.com/clinicalneurophys/Fulltext/2015/08000/Input_Output_Characteristics_of_Late_Corticospinal.11.aspx

Khalighinejad, N., Bongioanni, A., Verhagen, L., Folloni, D., Attali, D., Aubry, J.-F., … Rushworth, M. F. S. (2020). A Basal Forebrain-Cingulate Circuit in Macaques Decides It Is Time to Act. *Neuron*, *105*(2), 370–384.e8. https://doi.org/10.1016/j.neuron.2019.10.030

Kim, H., Chiu, A., Lee, S. D., Fischer, K., & Yoo, S.-S. (2014). Focused Ultrasound-mediated Non-invasive Brain Stimulation: Examination of Sonication Parameters. *Brain Stimulation*, *7*(5), 748–756. https://doi.org/10.1016/j.brs.2014.06.011

Kim, T., Park, C., Chhatbar, P. Y., Feld, J., Mac Grory, B., Nam, C. S., … Feng, W. (2021). Effect of Low Intensity Transcranial Ultrasound Stimulation on Neuromodulation in Animals and Humans: An Updated Systematic Review. *Frontiers in Neuroscience*, *15*, 620863. https://doi.org/10.3389/fnins.2021.620863

King, R. L., Brown, J. R., Newsome, W. T., & Pauly, K. B. (2013). Effective parameters for ultrasound-induced in vivo neurostimulation. *Ultrasound in Medicine & Biology*, *39*(2), 312–331. https://doi.org/10.1016/j.ultrasmedbio.2012.09.009

King, R. L., Brown, J. R., & Pauly, K. B. (2014). Localization of Ultrasound-Induced In Vivo Neurostimulation in the Mouse Model. *Ultrasound in Medicine & Biology*. https://doi.org/10.1016/j.ultrasmedbio.2014.01.020

Krasovitski, B., Frenkel, V., Shoham, S., & Kimmel, E. (2011). Intramembrane cavitation as a unifying mechanism for ultrasound-induced bioeffects. *Proceedings of the National Academy of Sciences of the United States of America*, *108*(8), 3258–63. https://doi.org/10.1073/pnas.1015771108

Kubanek, J. (2018). Neuromodulation with transcranial focused ultrasound. *Neurosurgical Focus*, *44*(2), 14. https://doi.org/10.3171/2017.11.FOCUS17621

Kubanek, J., Shi, J., Marsh, J., Chen, D., Deng, C., & Cui, J. (2016). Ultrasound modulates ion channel currents. *Scientific Reports*, *6*. https://doi.org/10.1038/srep24170

Kubanek, J., Shukla, P., Das, A., Baccus, S. A., & Goodman, M. B. (2018). Ultrasound elicits behavioral responses through mechanical effects on neurons and ion channels in a simple nervous system. *Journal of Neuroscience*, *38*(12), 3081–3091. https://doi.org/10.1523/JNEUROSCI.1458-17.2018

Kwon, J.-H., Kim, J. S., Kang, D.-W., Bae, K.-S., & Kwon, S. U. (2006). The Thickness and Texture of Temporal Bone in Brain CT Predict Acoustic Window Failure of Transcranial Doppler. *Journal of Neuroimaging*, *16*(4), 347–352. https://doi.org/10.1111/j.1552-6569.2006.00064.x

Kyriakou, A., Neufeld, E., Werner, B., Paulides, M. M., Szekely, G., & Kuster, N. (2014). A review of numerical and experimental compensation techniques for skull-induced phase aberrations in transcranial focused ultrasound. *International Journal of Hyperthermia*, *30*(1), 36–46. https://doi.org/10.3109/02656736.2013.861519

Lazzaro, V. Di, Ziemann, U., & Lemon, R. N. (2008). State of the art: Physiology of transcranial motor cortex stimulation. *Brain Stimulation*, *1*(4), 345–362. https://doi.org/https://doi.org/10.1016/j.brs.2008.07.004

Lee, W., Kim, H.-C., Jung, Y., Chung, Y. A., Song, I.-U., Lee, J.-H., & Yoo, S.-S. (2016). Transcranial focused ultrasound stimulation of human primary visual cortex. *Scientific Reports*, *6*, 34026. Retrieved from http://dx.doi.org/10.1038/srep34026

Lee, W., Kim, H., Jung, Y., Song, I.-U., Chung, Y. A., & Yoo, S.-S. (2015). Image-guided transcranial focused ultrasound stimulates human primary somatosensory cortex. *Scientific Reports*, *5*, 8743. https://doi.org/10.1038/srep08743

Lee, W., Kim, S., Kim, B., Lee, C., Chung, Y. A., Kim, L., & Yoo, S. S. (2017). Non-invasive transmission of sensorimotor information in humans using an EEG/focused ultrasound brain-to-brain interface. *PLoS ONE*, *12*(6), e0178476. https://doi.org/10.1371/journal.pone.0178476

Lee, W., Lee, S. D., Park, M. Y., Foley, L., Purcell-Estabrook, E., Kim, H., … Yoo, S. S. (2016). Image-Guided Focused Ultrasound-Mediated Regional Brain Stimulation in Sheep. *Ultrasound in Medicine and Biology*, *42*(2). https://doi.org/10.1016/j.ultrasmedbio.2015.10.001

Lefaucheur, J.-P., André-Obadia, N., Antal, A., Ayache, S. S., Baeken, C., Benninger, D. H., … Garcia-Larrea, L. (2014). Evidence-based guidelines on the therapeutic use of repetitive transcranial magnetic stimulation (rTMS). *Clinical Neurophysiology*, *125*(11), 2150–2206. https://doi.org/https://doi.org/10.1016/j.clinph.2014.05.021

Legon, W., Adams, S., Bansal, P., Patel, P. D., Hobbs, L., Ai, L., … Gillick, B. T. (2020). A retrospective qualitative report of symptoms and safety from transcranial focused ultrasound for neuromodulation in humans. *Scientific Reports*, *10*(1), 5573. https://doi.org/10.1038/s41598-020-62265-8

Legon, W., Ai, L., Bansal, P., & Mueller, J. K. (2018). Neuromodulation with single-element transcranial focused ultrasound in human thalamus. *Human Brain Mapping*, *39*(5), 1995–2006. https://doi.org/10.1002/hbm.23981

Legon, W., Bansal, P., Tyshynsky, R., Ai, L., & Mueller, J. K. (2018). Transcranial focused ultrasound neuromodulation of the human primary motor cortex. *Scientific Reports*, *8*(1), 10007. https://doi.org/10.1038/s41598-018-28320-1

Legon, W., Sato, T. F., Opitz, A., Mueller, J., Barbour, A., Williams, A., & Tyler, W. J. (2014). Transcranial focused ultrasound modulates the activity of primary somatosensory cortex in humans. *Nature Neuroscience*, *17*(2), 322–9. https://doi.org/10.1038/nn.3620

Liebetanz, D., Fauser, S., Michaelis, T., Czéh, B., Watanabe, T., Paulus, W., … Fuchs, E. (2003). Safety aspects of chronic low-frequency transcranial magnetic stimulation based on localized proton magnetic resonance spectroscopy and histology of the rat brain. *Journal of Psychiatric Research*, *37*(4), 277–286. https://doi.org/10.1016/S0022-3956(03)00017-7

Ling, Y. T., Martin, E., & Treeby, B. (2015). *A Discrete Source Model for Simulating Bowl-Shaped Focused Ultrasound Transducers on Regular Grids: Design and Experimental Validation*. https://doi.org/10.1109/ULTSYM.2015.0281

Lund, J. S. (1973). Organization of neurons in the visual cortex, area 17, of the monkey (Macaca mulatta). *Journal of Comparative Neurology*, *147*(4), 455–495. https://doi.org/10.1002/cne.901470404

Lutkenhoff, E. S., Rosenberg, M., Chiang, J., Zhang, K., Pickard, J. D., Owen, A. M., & Monti, M. M. (2014). Optimized Brain Extraction for Pathological Brains (optiBET). *PLoS ONE*, *9*(12), e115551. https://doi.org/10.1371/journal.pone.0115551

Mahinda, H. A. M., & Murty, O. P. (2009). Variability in thickness of human skull bones and sternum - An autopsy experience. *Journal of Forensic Medicine and Toxicology*, *26*(2), 26–31.

Maingret, F., Patel, A. J., Lesage, F., Lazdunski, M., & Honoré, E. (1999). Mechano- or acid stimulation, two interactive modes of activation of the TREK-1 potassium channel. *Journal of Biological Chemistry*, *274*(38), 26691–26696. https://doi.org/10.1074/jbc.274.38.26691

Martin, E., Jeanmonod, D., Morel, A., Zadicario, E., & Werner, B. (2009). High-intensity focused ultrasound for noninvasive functional neurosurgery. *Annals of Neurology*, *66*(6), 858–61. https://doi.org/10.1002/ana.21801

Martin, E., Ling, Y. T., & Treeby, B. E. (2016). Simulating Focused Ultrasound Transducers Using Discrete Sources on Regular Cartesian Grids. *IEEE Transactions on Ultrasonics, Ferroelectrics, and Frequency Control*, *63*(10), 1535–1542. https://doi.org/10.1109/TUFFC.2016.2600862

Mayka, M. A., Corcos, D. M., Leurgans, S. E., & Vaillancourt, D. E. (2006). Three-dimensional locations and boundaries of motor and premotor cortices as defined by functional brain imaging: A meta-analysis. *NeuroImage*, *31*(4), 1453–1474. https://doi.org/10.1016/j.neuroimage.2006.02.004

McIntyre, C. C., & Grill, W. M. (2002). Extracellular Stimulation of Central Neurons: Influence of Stimulus Waveform and Frequency on Neuronal Output. *Journal of Neurophysiology*, *88*(4), 1592–1604. https://doi.org/10.1152/jn.2002.88.4.1592

Mehić, E., Xu, J. M., Caler, C. J., Coulson, N. K., Moritz, C. T., & Mourad, P. D. (2014). Increased Anatomical Specificity of Neuromodulation via Modulated Focused Ultrasound. *PLoS ONE*, *9*(2), e86939. Retrieved from http://dx.doi.org/10.1371%2Fjournal.pone.0086939

Menz, M. D., Oralkan, Ö., Khuri-Yakub, P. T., & Baccus, S. A. (2013). Precise Neural Stimulation in the

Retina Using Focused Ultrasound. *The Journal of Neuroscience*, *33*(10), 4550–4560. https://doi.org/10.1523/JNEUROSCI.3521-12.2013

Miller, G. W., Eames, M., Snell, J., & Aubry, J.-F. (2015). Ultrashort echo-time MRI versus CT for skull aberration correction in MR-guided transcranial focused ultrasound: In vitro comparison on human calvaria. *Medical Physics*, *42*(5), 2223–2233. https://doi.org/10.1118/1.4916656

Miller, M. W., Miller, D. L., & Brayman, A. A. (1996). A review of in vitro bioeffects of inertial ultrasonic cavitation from a mechanistic perspective. *Ultrasound in Medicine & Biology*, *22*(9), 1131–1154. https://doi.org/10.1016/S0301-5629(96)00089-0

Min, B.-K., Bystritsky, A., Jung, K.-I., Fischer, K., Zhang, Y., Maeng, L.-S., … Yoo, S.-S. (2011). Focused ultrasound-mediated suppression of chemically-induced acute epileptic EEG activity. *BMC Neuroscience*, *12*(1), 1–12. https://doi.org/10.1186/1471-2202-12-23

Möller, C., Arai, N., Lücke, J., & Ziemann, U. (2009). Hysteresis effects on the input–output curve of motor evoked potentials. *Clinical Neurophysiology*, *120*(5), 1003–1008. https://doi.org/https://doi.org/10.1016/j.clinph.2009.03.001

Monti, M. M., Schnakers, C., Korb, A. S., Bystritsky, A., & Vespa, P. M. (2016). Non-Invasive Ultrasonic Thalamic Stimulation in Disorders of Consciousness after Severe Brain Injury: A First-in-Man Report. *Brain Stimulation*, *9*(6), 940–941. https://doi.org/10.1016/j.brs.2016.07.008

Morris, C. E. (2011). Voltage-Gated Channel Mechanosensitivity: Fact or Friction? *Frontiers in Physiology*, *2*, 25. https://doi.org/10.3389/fphys.2011.00025

Mortimer, A. J., & Dyson, M. (1988). The effect of therapeutic ultrasound on calcium uptake in fibroblasts. *Ultrasound in Medicine & Biology*, *14*(6), 499–506.

Mueller, J. K., Ai, L., Bansal, P., & Legon, W. (2016). Computational exploration of wave propagation and heating from transcranial focused ultrasound for neuromodulation. *Journal of Neural Engineering*, *13*(5). https://doi.org/10.1088/1741-2560/13/5/056002

Mueller, J., Legon, W., Opitz, A., Sato, T. F., & Tyler, W. J. (2014). Transcranial focused ultrasound modulates intrinsic and evoked EEG dynamics. *Brain Stimulation*, *7*(6), 900–908. https://doi.org/10.1016/j.brs.2014.08.008

Naor, O., Krupa, S., & Shoham, S. (2016). Ultrasonic neuromodulation. *Journal of Neural Engineering*. https://doi.org/10.1088/1741-2560/13/3/031003

Nguyen, D. T., Berisha, D., Konofagou, E., & Dmochowski, J. P. (2020). Differential effects of amplitude-modulated transcranial focused ultrasound on excitatory and inhibitory neurons. *bioRxiv*, 2020.11.26.400580. https://doi.org/10.1101/2020.11.26.400580

Nowak, L. G., & Bullier, J. (1998). Axons, but not cell bodies, are activated by electrical stimulation in cortical gray matter. I. Evidence from chronaxie measurements. *Experimental Brain Research*, *118*(4), 477–488. https://doi.org/10.1007/s002210050304

O'Brien, W. D. (2007). Ultrasound-biophysics mechanisms. *Progress in Biophysics and Molecular Biology*, *93*(1–3), 212–255. https://doi.org/10.1016/j.pbiomolbio.2006.07.010

Oberman, L., Edwards, D., Eldaief, M., & Pascual-Leone, A. (2011). Safety of Theta Burst Transcranial Magnetic Stimulation: A systematic review of the literature. *Journal of Clinical Neurophysiology*,

28(1), 67–74. https://doi.org/10.1097/WNP.0b013e318205135f

Ono, K. (2020). A Comprehensive Report on Ultrasonic Attenuation of Engineering Materials, Including Metals, Ceramics, Polymers, Fiber-Reinforced Composites, Wood, and Rocks. *Applied Sciences*. https://doi.org/10.3390/app10072230

Ostrow, L. W., & Sachs, F. (2005). Mechanosensation and endothelin in astrocytes—hypothetical roles in CNS pathophysiology. *Brain Research Reviews*, *48*(3), 488–508. https://doi.org/http://dx.doi.org/10.1016/j.brainresrev.2004.09.005

Ostrow, L. W., Suchyna, T. M., & Sachs, F. (2011). *Stretch induced endothelin-1 secretion by adult rat astrocytes involves calcium influx via stretch-activated ion channels (SACs)*. *Biochemical and Biophysical Research Communications* (Vol. 410). https://doi.org/10.1016/j.bbrc.2011.05.109

Pichardo, S., Sin, V. W., & Hynynen, K. (2010). Multi-frequency characterization of speed of sound for longitudinal transmission on freshly excised human skulls. *AIP Conference Proceedings*, *1215*, 282–286. https://doi.org/10.1063/1.3367161

Pinton, G., Aubry, J.-F., Bossy, E., Muller, M., Pernot, M., & Tanter, M. (2012). Attenuation, scattering, and absorption of ultrasound in the skull bone. *Medical Physics*, *39*(1), 299–307. https://doi.org/10.1118/1.3668316

Plaksin, M., Kimmel, E., & Shoham, S. (2016). Cell-Type-Selective Effects of Intramembrane Cavitation as a Unifying Theoretical Framework for Ultrasonic Neuromodulation. *Eneuro*, *3*(3). Retrieved from http://eneuro.org/content/3/3/ENEURO.0136-15.2016.abstract

Prieto, M. L., Firouzi, K., Khuri-Yakub, B. T., & Maduke, M. (2018). Activation of Piezo1 but Not NaV1.2 Channels by Ultrasound at 43 MHz. *Ultrasound in Medicine and Biology*, *44*(6), 1217–1232. https://doi.org/10.1016/j.ultrasmedbio.2017.12.020

Priori, A., Berardelli, A., Rona, S., Accornero, N., & Manfredi, M. (1998). Polarization of the human motor cortex through the scalp. *NeuroReport*, *9*(10). Retrieved from http://journals.lww.com/neuroreport/Fulltext/1998/07130/Polarization_of_the_human_motor_cortex_through_the.20.aspx

R Core Team. (2021). R: A Language and Environment for Statistical Computing. Vienna, Austria: R Foundation for Statistical Computing. Retrieved from https://www.r-project.org/

Rinaldi, P. C., Jones, J. P., Reines, F., & Price, L. R. (1991). Modification by focused ultrasound pulses of electrically evoked responses from an in vitro hippocampal preparation. *Brain Research*, *558*(1), 36–42. https://doi.org/http://dx.doi.org/10.1016/0006-8993(91)90711-4

Robertson, J. L. B., Cox, B. T., Jaros, J., & Treeby, B. E. (2017). Accurate simulation of transcranial ultrasound propagation for ultrasonic neuromodulation and stimulation. *The Journal of the Acoustical Society of America*, *141*(3), 1726–1738. https://doi.org/10.1121/1.4976339

Robertson, J., Martin, E., Cox, B., & Treeby, B. E. (2017). Sensitivity of simulated transcranial ultrasound fields to acoustic medium property maps. *Physics in Medicine and Biology*, *62*(7), 2559–2580. https://doi.org/10.1088/1361-6560/aa5e98

Roth, Y., Amir, A., Levkovitz, Y., & Zangen, A. (2007). Three-dimensional distribution of the electric field induced in the brain by transcranial magnetic stimulation using figure-8 and deep H-coils. *Journal of Clinical Neurophysiology*, *24*(1), 31–38. https://doi.org/10.1097/WNP.0b013e31802fa393

Sato, T., Shapiro, M. G., & Tsao, D. Y. (2018). Ultrasonic Neuromodulation Causes Widespread Cortical Activation via an Indirect Auditory Mechanism. *Neuron*, *98*(5), 1031–1041.e5. https://doi.org/10.1016/j.neuron.2018.05.009

Şen, T., Tüfekçioğlu, O., & Koza, Y. (2015). Mechanical index. *Anatolian Journal of Cardiology*, *15*(4), 334–336. https://doi.org/10.5152/akd.2015.6061

Shattuck, D. W., & Leahy, R. M. (2002). BrainSuite: An automated cortical surface identification tool. *Medical Image Analysis*, *6*(2), 129–142. https://doi.org/10.1016/S1361-8415(02)00054-3

Sukharev, S., & Corey, D. P. (2004). Mechanosensitive Channels: Multiplicity of Families and Gating Paradigms. *Science's STKE*, *2004*(219), re4 LP-re4. Retrieved from http://stke.sciencemag.org/content/2004/219/re4.abstract

ter Haar, G., Shaw, A., Pye, S., Ward, B., Bottomley, F., Nolan, R., & Coady, A.-M. (2011). Guidance on Reporting Ultrasound Exposure Conditions for Bio-Effects Studies. *Ultrasound in Medicine & Biology*, *37*(2), 177–183. https://doi.org/http://dx.doi.org/10.1016/j.ultrasmedbio.2010.10.021

The Safe Use of Ultrasound in Medical Diagnosis. (2012).

Thut, G., & Miniussi, C. (2009). New insights into rhythmic brain activity from TMS–EEG studies. *Trends in Cognitive Sciences*, *13*(4), 182–189. https://doi.org/10.1016/j.tics.2009.01.004

Treeby, B. E., & Cox, B. T. (2009). Fast tissue-realistic models of photoacoustic wave propagation for homogeneous attenuating media. In A. A. Oraevsky & L. V. Wang (Eds.), *Photons Plus Ultrasound: Imaging and Sensing 2009* (Vol. 7177, p. 717716). SPIE. https://doi.org/10.1117/12.806794

Treeby, B. E., & Cox, B. T. (2010). k-Wave: MATLAB toolbox for the simulation and reconstruction of photoacoustic wave fields, *15*, 21312–21314. Retrieved from https://doi.org/10.1117/1.3360308

Treeby, B. E., & Cox, B. T. (2014). Modeling power law absorption and dispersion in viscoelastic solids using a split-field and the fractional Laplacian. *The Journal of the Acoustical Society of America*, *136*(4), 1499–1510. https://doi.org/10.1121/1.4894790

Treeby, B. E., Jaros, J., Rendell, A. P., & Cox, B. T. (2012). Modeling nonlinear ultrasound propagation in heterogeneous media with power law absorption using a k-space pseudospectral method. *The Journal of the Acoustical Society of America*, *131*(6), 4324–4336. https://doi.org/10.1121/1.4712021

Tufail, Y., Matyushov, A., Baldwin, N., Tauchmann, M. L., Georges, J., Yoshihiro, A., … Tyler, W. J. (2010). Transcranial Pulsed Ultrasound Stimulates Intact Brain Circuits. *Neuron*, *66*(5), 681–694. https://doi.org/10.1016/j.neuron.2010.05.008

Tufail, Y., Yoshihiro, A., Pati, S., Li, M. M., & Tyler, W. J. (2011). Ultrasonic neuromodulation by brain stimulation with transcranial ultrasound. *Nat. Protocols*, *6*(9), 1453–1470. Retrieved from http://dx.doi.org/10.1038/nprot.2011.371

Tyler, W. J. (2011). Noninvasive Neuromodulation with Ultrasound? A Continuum Mechanics Hypothesis. *The Neuroscientist*, *17*(1), 25–36. https://doi.org/10.1177/1073858409348066

Tyler, W. J. (2012). The mechanobiology of brain function. *Nature Reviews Neuroscience*, *13*(12), 867–878. https://doi.org/10.1038/nrn3383

Tyler, W. J., Lani, S. W., & Hwang, G. M. (2018, June 1). Ultrasonic modulation of neural circuit activity.

Current Opinion in Neurobiology. Elsevier Ltd. https://doi.org/10.1016/j.conb.2018.04.011

Tyler, W. J., Tufail, Y., Finsterwald, M., Tauchmann, M. L., Olson, E. J., & Majestic, C. (2008). Remote excitation of neuronal circuits using low-intensity, low-frequency ultrasound. *PLoS ONE*, *3*(10). https://doi.org/10.1371/journal.pone.0003511

Vance, J., Wulf, G., Töllner, T., McNevin, N., & Mercer, J. (2004). EMG Activity as a Function of the Performer's Focus of Attention. *Journal of Motor Behavior*, *36*(4), 450–459. https://doi.org/10.3200/JMBR.36.4.450-459

Verhagen, L., Gallea, C., Folloni, D., Constans, C., Jensen, D. E., Ahnine, H., … Sallet, J. (2019). Offline impact of transcranial focused ultrasound on cortical activation in primates. *eLife*, *8*. https://doi.org/10.7554/eLife.40541

Wagner, T., Valero-Cabre, A., & Pascual-Leone, A. (2007). Noninvasive Human Brain Stimulation. *Annual Review of Biomedical Engineering*, *9*(1), 527–565. https://doi.org/10.1146/annurev.bioeng.9.061206.133100

Wahab, R. A., Choi, M., Liu, Y., Krauthamer, V., Zderic, V., & Myers, M. R. (2012). Mechanical bioeffects of pulsed high intensity focused ultrasound on a simple neural model. *Medical Physics*, *39*(7), 4274–4283. https://doi.org/10.1118/1.4729712

Wang, P., Zhang, J., Yu, J., Smith, C., & Feng, W. (2019, July 24). Brain modulatory effects by low-intensity Transcranial Ultrasound Stimulation (TUS): A systematic review on both animal and human studies. *Frontiers in Neuroscience*. Frontiers Media S.A. https://doi.org/10.3389/fnins.2019.00696

Warbrick, T., Derbyshire, S. W. G., & Bagshaw, A. P. (2009). Optimizing the measurement of contact heat evoked potentials. *Journal of Clinical Neurophysiology*, *26*(2), 117–122. https://doi.org/10.1097/WNP.0b013e31819d8016

Wassermann, E. M., Pascual-Leone, A., Valls-Solé, J., Toro, C., Cohen, L. G., & Hallett, M. (1993). Topography of the inhibitory and excitatory responses to transcranial magnetic stimulation in a hand muscle. *Electroencephalography and Clinical Neurophysiology/Evoked Potentials Section*, *89*(6), 424–433. https://doi.org/10.1016/0168-5597(93)90116-7

Werhahn, K. J., Kunesch, E., Noachtar, S., Benecke, R., & Classen, J. (1999). Differential effects on motorcortical inhibition induced by blockade of GABA uptake in humans. *The Journal of Physiology*, *517*(2), 591–597. https://doi.org/10.1111/j.1469-7793.1999.0591t.x

White, P. J., Clement, G. T., & Hynynen, K. (2006). Local frequency dependence in transcranial ultrasound transmission. *Physics in Medicine and Biology*, *51*(9), 2293–2305. https://doi.org/10.1088/0031-9155/51/9/013

White, P. J. J. (2006). Transcranial focused ultrasound surgery. *Topics in Magnetic Resonance Imaging : TMRI*, *17*(3), 165–172. https://doi.org/10.1097/RMR.0b013e31803774a3

Wilson, S. A., Thickbroom, G. W., & Mastaglia, F. L. (1995). An investigation of the late excitatory potential in the hand following magnetic stimulation of the motor cortex. *Electroencephalography and Clinical Neurophysiology/Electromyography and Motor Control*, *97*(1), 55–62. https://doi.org/https://doi.org/10.1016/0924-980X(94)00274-B

Wintermark, M., Tustison, N. J., Elias, W. J., Patrie, J. T., Xin, W., Demartini, N., … Aubry, J.-F. (2014). T1-

weighted MRI as a substitute to CT for refocusing planning in MR-guided focused ultrasound. *Physics in Medicine and Biology*, *59*(13), 3599–3614. https://doi.org/10.1088/0031-9155/59/13/3599

Wise, E. S., Cox, B. T., Jaros, J., & Treeby, B. E. (2019). Representing arbitrary acoustic source and sensor distributions in Fourier collocation methods. *The Journal of the Acoustical Society of America*, *146*(1), 278–288. https://doi.org/10.1121/1.5116132

Wolters, A., Ziemann, U., & Benecke, R. (2012). The cortical silent period. In *Oxford Handbook of Transcranial Stimulation*. https://doi.org/10.1093/oxfordhb/9780198568926.013.0010

Yamawaki, N., Borges, K., Suter, B. A., Harris, K. D., & Shepherd, G. M. G. (2014). A genuine layer 4 in motor cortex with prototypical synaptic circuit connectivity. *eLife*, *3*, e05422. https://doi.org/10.7554/eLife.05422

Yang, P. F., Phipps, M. A., Newton, A. T., Chaplin, V., Gore, J. C., Caskey, C. F., & Chen, L. M. (2018). Neuromodulation of sensory networks in monkey brain by focused ultrasound with MRI guidance and detection. *Scientific Reports*, *8*(1), 1–9. https://doi.org/10.1038/s41598-018-26287-7

Ye, P. P., Brown, J. R., & Pauly, K. B. (2017). Frequency Dependence of Ultrasound Neurostimulation in the Mouse Brain. *Ultrasound in Medicine and Biology*, *42*(7), 1512–1530. https://doi.org/10.1016/j.ultrasmedbio.2016.02.012

Yoo, S. S., Bystritsky, A., Lee, J. H., Zhang, Y., Fischer, K., Min, B. K., … Jolesz, F. A. (2011). Focused ultrasound modulates region-specific brain activity. *NeuroImage*, *56*(3), 1267–1275. https://doi.org/10.1016/j.neuroimage.2011.02.058

Yousry, T. A., Schmid, U. D., Alkadhi, H., Schmidt, D., Peraud, A., Buettner, A., & Winkler, P. (1997). Localization of the motor hand area to a knob on the precentral gyrus. A new landmark. *Brain*, *120*(1), 141–157. https://doi.org/10.1093/brain/120.1.141

Zachry, T., Wulf, G., Mercer, J., & Bezodis, N. (2005). Increased movement accuracy and reduced EMG activity as the result of adopting an external focus of attention. *Brain Research Bulletin*, *67*(4), 304–309. https://doi.org/10.1016/J.BRAINRESBULL.2005.06.035

Ziemann, U., Reis, J., Schwenkreis, P., Rosanova, M., Strafella, A., Badawy, R., & Müller-Dahlhaus, F. (2015). TMS and drugs revisited 2014. *Clinical Neurophysiology*, *126*(10), 1847–1868. https://doi.org/https://doi.org/10.1016/j.clinph.2014.08.028